THE UNIVERSITY OF CHICAGO

SOLID-LIQUID TRANSITION IN POLYELECTROLYTE COMPLEXES

A DISSERTATION SUBMITTED TO

THE FACULTY OF THE PRITZKER SCHOOL OF MOLECULAR ENGINEERING

IN CANDIDACY FOR THE DEGREE OF

DOCTOR OF PHILOSOPHY

BY

SIQI MENG

CHICAGO, ILLINOIS

MARCH 2021

Table of Contents

List of Figures

List of Tables

Acknowledgement

First and foremost, I would like to thank my Ph.D. advisor Professor Matthew V. Tirrell for all the trust, guidance and support throughout my doctorate study. With his encouragement and belief in me, I have achieved many seemingly improbable goals I have never imaged during the past few years. He has always been my source of inspiration whenever I encounter problems in my projects. I have learned a lot from his continuous curiosity, profound knowledge, and unlimited enthusiasm in science. In addition to all the constructive instructions in academic research, he has also provided me with very precious and insightful advice for my career development. I feel very grateful for having Professor Tirrell as an exemplary professor, mentor and individual. I would also like to thank my thesis committee members, Prof. Shrayesh Patel and Prof. Sihong Wang for the important suggestions on my dissertation and defense. It is a great honor for me to present my work to these excellent scientists.

Next, I would like express my gratitude to the amazing cohort of graduate students and postdocs in the Tirrell group. I want to give my special thanks to Dr. Jeffrey M. Ting. He has been an amazing mentor and collaborator for me from my day one in Tirrell group. He has generously and patiently assisted me in designing experiments, analyzing data, writing papers, delivering presentations and many other aspects in research. He also showed me the qualities of an excellent researcher and a great mentor. I would like to thank Dr. Hao Wu, Dr. Lu Li and Professor Amanda Marciel for all the important suggestions and inputs in my research, which helped me greatly in my projects. I would like to thank Kaden Stevens, Dr. Alexander Marras, Dr. Angelika Neitzel and Dr. Jelena Dinic for all the valuable discussions about my research. I would like to thank Jihyeon Yeo and Yueming Liu, two undergraduate researchers I have worked with, for their

contribution to the research. I also would like to thank Whitney Fowler, Ge Zhang, Yu Tian, Harrison Paul, Matthew Schnorenberg and Dr. Dean Mastropietro for being incredible colleagues.

Additionally, I would like to thank many other scientists who have provided significant help to my research. I would like to thank Professor Kenneth S. Schweizer from University of Illinois Urbana-Champaign for his valuable comments and ideas to my first research projects. His unique advice from the perspective of a theorist really promoted my understanding in the research area. I would like to thank Dr. Philip Griffin at the Soft Matter Characterization Facility (SMCF) in PME for training me how to use many important facilities and helping me out whenever I encountered technical difficulties during the measurement. I would like to thank Dr. Justin Juller at the Materials Research Science and Engineering Center for the assistance in the physical characterization of my samples and Dr. Tera Lavoie at the microbiome center for helping me acquire the electron microscopy images. I would like to thank Dr. Xiaobing Zuo and Dr. Soenke Seifert in the Advanced Photo Source of the Argonne National Laboratory, and Dr. Thomas M. Weiss and Dr. Ivan Rajkovia at the Stanford National Accelerator Laboratory for the help in X-ray scattering measurements.

Last but not least, I would like to thank my family. There are no words to express my deep love and gratitude to them. My parents Xin Meng and Guohong Li, and my grandparents Zhaoxun Meng and Bingjie Li have always trusted and loved me unconditionally throughout my life. I can never become who I am without any of them. I also thank my husband Zhuofu Ni, who understands me the best as a graduate student himself, and has been my best friend and great companion.

Abstract

Polyelectrolyte complexes (PECs) can be formed when mixing together two oppositely charged polyelectrolyte solutions. These ionic assemblies have received numerous interests not only because of the critical role they play in natural systems, but also due to their broad utilization in many industrial areas. Chapter 1 of this dissertation summarized important applications of PECs and highlighted recent advances in understanding the physical behaviors of PECs.

The physical states of PECs can range from glassy solids to low viscosity liquids, controlled by the nature of their polyelectrolyte components and the external environmental conditions. For strongly interacting PECs that start as solids under the salt-free condition, salt addition can drive the phase transition from solid into liquid. However, the molecular details of this transition still remain poorly understood. In Chapter 2, we comprehensively explored the solid-liquid transition of a model PEC system formed by two symmetric styrenic polyelectrolytes, from the aspects of dynamics, phase behavior, and internal structures. Rheological measurements revealed an unexpected salt-stiffening trend in the solid states, which was later attributed to dehydration in the complex indicative of osmotic deswelling. From small-angle X-ray scattering and cryogenic TEM images, we also proposed a structural evolution model of this model PEC system. In the solid state, polyelectrolyte chains formed tightly coiled spherical clusters that loosened and expanded upon salt doping. As the PEC transformed into a viscoelastic liquid, polyelectrolyte chains rearranged into ladder-like structures.

Even though strongly interacting PECs display exceptional versatility upon salt doping, they have an obvious shortcoming. They usually demonstrate high salt stability to common monovalent salts, causing huge difficulties in accessing the entire solid-liquid-solution spectrum.

Chapter 3 introduced a novel approach of decreasing the amount of salt needed to drive this PEC through phase transitions by adjusting solvent quality. We switched the solvent from pure water into binary mixtures of ethylene glycol/water or ethanol/water, enabling the systematic control of solvent hydrophobicity by tuning the ratios between the two solvent components. We discovered that significantly less NaBr was needed to drive this PEC through phase transitions when solvent hydrophobicity increased.

Chapter 4 continued to probe the mutual effect of salt and solvent on the behaviors of the model PEC system across the complex-coacervate continuum. We systematically prepared this PEC in two types of salt and four organic cosolvents. Through monitoring the physical states of this PEC with microscopy and cross-comparing the amount of salt needed to drive phase transitions, we developed a general correlation between this salt threshold and the solubility of salt in solvent. Interestingly, at high salt and high organic solvent conditions, an unexpected reverse phase transition occurs from liquid back to solid was captured in selective cosolvent systems, which was traced to the collapse of single polyelectrolyte chains as its origin. These findings provide useful new strategies for controlling the interplay between salinity and solvent quality, and thus enriching potential applications for both bulk macroscale PEC and multilayer complex assemblies.

Chapter 1. Introduction

This chapter will be published in the future as a book chapter.

1.1 Introduction of Polyelectrolyte Complexation

1.1.1 General Introduction of Polyelectrolyte Complexes

Polyelectrolytes are polymeric molecules whose repeating units carry electrolyte groups and can dissociate in aqueous solution to form either positively or negatively charged polymers. When two aqueous solutions of oppositely charged polyelectrolytes are mixed together, polyelectrolyte complexation occurs, resulting in a polymer-poor supernatant phase separated from a polymer-rich phase termed as polyelectrolyte complexes (PECs). (Figure 1) It is generally believed that this process is driven by electrostatic attraction forces, as well as the entropic gain from the release of counterions that are initially attached to the polyelectrolyte chains.[1-7] The first polyelectrolyte complexation behavior was reported nearly a century ago in 1929 by Bungenberg de Jong and Kryut, with observations of complexation between two biomacromolecules, gelatin and gum arabic.[8] Ever since then, this class of material has received continuous scientific interests due to its presence in plentiful biological scenarios, as well as its wide utility in various industrial applications.

Figure 1. 1: Schematic that demonstrates complexation behavior between oppositely charged polyelectrolytes.

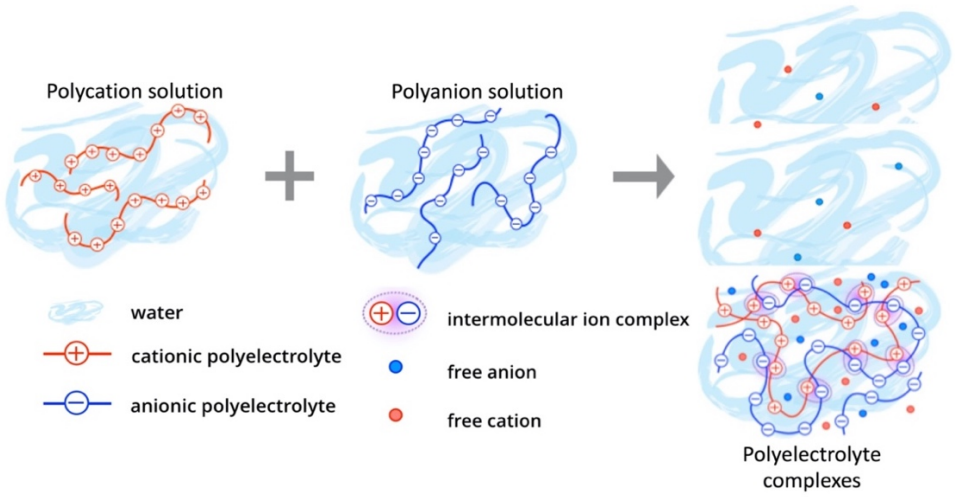

1.1.2 Factors Influencing Polyelectrolyte Complexation Behaviors

Complex coacervation process is an intricate balance of numerous parameters. One of the most essential factors that dominates this process is the molecular features of polyelectrolyte chains, including chain length,[9] charge density,[10] ionic strength,[11] chemical structure,[12] and so on. For example, through inspecting the phase behaviors of a complex formed by poly(L-lysine hydrochloride) (PLK) and poly(D,L-glutamic acid) (PRE) with varying degrees of polymerization, Li et al.[13] found that the final phase boundary is strongly dependent on the polymer chain lengths. The complexes were observed to be denser in polymer and more salt resistant with increasing chain length. (Figure 1.2a) Huang et al.[10] explored an array of acrylamide copolymers with changing charge density. Using optical turbidity and small-amplitude oscillatory shear rheology, they found that decreasing charge density resulted in a decrease in transition salt concentration, a decrease in the polymer concentration in the coacervate phase, and faster relaxation dynamics.

Figure 1. 2: PEC behaviors and physical states influenced by polymer chain length and chirality.

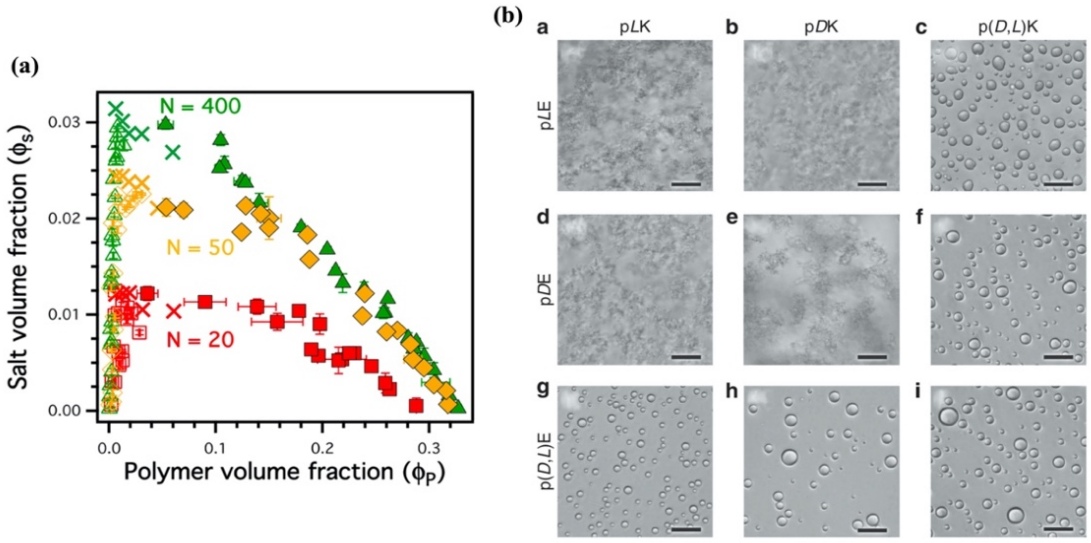

(a) Polyelectrolyte complexation phase diagrams for PLK_{20}+PRE_{20} (red), PLK_{50}+PRE_{50} (yellow), and PLK_{400}+PRE_{400} (green).[13] Reprinted (adapted) with permission from (Reference 13). Copyright (2018) American Chemical Society. (b) Optical micrographs of PECs formed by poly(lysine) and poly(glutamic acid).[14] Copyright 2015, Nature Communications.

Even though the main driving force that defines the phase separation process is electrostatic association, a number of other non-covalent intermolecular interactions may also play a role in the formation of the final product, such as hydrogen bonding,[15–17] chirality,[18–20] hydrophobicity,[10,21] π-π stacking,[22,23] cation-π interaction,[24] etc. Many studies have explored these secondary interactions in great detail. For instance, Sadman et al.[21] examined the effects of hydrophobicity on PECs using poly(styrene sulfonate) (PSS) paired with a series of systematically quaternized poly(4-vinylpyridine) (QVP) that governed hydrophobicity with increasing side chain length. They showed that complexes with more hydrophobic QVP chains exhibited stronger salt resistance, thus demonstrating that hydrophobicity can be adopted as an important parameter to tune PEC stability towards salt doping. Perry et al.[14] discovered that chirality determines the physical states

(solid or liquid) of PECs. By systematically pairing poly(lysine) and poly(glutamic acid) with different chirality, they showed that mixing purely chiral polypeptides resulted in rigid solids by forming β-sheet structure. However, liquid coacervates will form when at least one of the polypeptide components is racemic due to the disruption of the hydrogen-bonding networks in the backbone. (Figure 1.2b)

In addition to the molecular details in polymer chains and the resultant non-covalent interactions, external conditions in the environment can also dominate the properties of PECs. As a class of stimuli-responsive material, PECs can vary their physical attributes based on the adjustment in their external environments. The most commonly introduced stimulus to drive changes in PECs is salt. PECs associated through forming ionic pairings between oppositely charged chains. Adding salt can compensate and break these pairings, thereby dissociating the internal structures of PECs. Many recent studies have also investigated how PEC states and properties can be influenced by other parameters in the environment, such as temperature,[25,26] pH,[27,28] solvent quality,[29,30] etc. All of these factors can become exploitable tools for controlling the properties of PECs during their design and application.

1.1.3 Emerging Applications of Polyelectrolyte Complexes

Because of the versatility, responsivity and excellent material properties, PECs have been adopted for many industrial applications for many decades. One of the most widely applied usage is underwater adhesive for applications such as underwater coating and biomedical fixing. The development of PECs into underwater adhesive is inspired from marine organisms such as sandcastle worm and mussel. PECs in the coacervate form have low surface tension and strong

interfacial adhesion strength, which enable them to endure underwater conditions and be easily applied on surfaces and cracks. Research on PEC-based underwater adhesives can be categorized into two types. The first type imitates natural adhesives in marine organisms and incorporates catechol group into the polymer chains since catechol group is found to be capable of forming bidentate hydrogen bonding and crosslinking with each other to achieve adhesion.[31–34] The second category of research utilizes other chemical reactions or non-covalent physical interactions to obtain strong adhesion force and mechanical robustness.[35–37] Aside from underwater adhesive, another common application for PECs is the treatment of industrial and agricultural water to remove contaminants.[38–40] As an example, Chiappisi et al.[41] investigated a pH-sensitive chitosan-based PEC system capable of selectively binding specific types of surfactants through pH-triggered electrostatic complexation. PECs have also been broadly used in food industry due to their protective functions through encapsulation.[42–44] Coacervates formed by oppositely charged proteins and polysaccharides are generally chosen as the shell material to protect the food or flavor in the core, for the purpose of transport, mask of unpleasant smell, extension of life, etc.[45]

In the biological and biomedical fields, PECs have plentiful essential applications as well. Liquid coacervates have been broadly fabricated into drug delivery platforms. Due to the stimuli-responsive nature and versatile structures with both hydrophilic and hydrophobic components on the polyelectrolyte chains, liquid PEC coacervates display advantages over many other existing systems that are based on hydrogels, liposomes and nanoparticles. They are capable of stably and efficiently encapsulating a wide range of solutes with different hydrophobicity in a controllable manner.[46–48] As an example, Silva et al.[49] developed a coacervate delivery platform composed of poly(allylamine hydrochloride) (PAH) and tripolyphosphate (TPP). They showed that their system

was able to encapsulate an amphiphilic anionic drug with exceptionally high load capacity and could keep releasing drug in over 6 months' time period. Another reason that PECs have gained great attraction in biological area is that it can be exploited as the subcellular membrane-less compartment to serve as abiotic cellular analog.[50–54] Cellular process can be mimicked and even enhanced in these coacervate-based compartments, as compartmentalization displays various advantages over intracellular process.[45,55–57]

1.2 Recent Advances in the Research of Polyelectrolyte Complexation

1.2.1 Dynamics of Polyelectrolyte Complexes

The dynamics of polyelectrolyte complexes is an essential area in the research of polymer physics, as it can provide important message about the thermodynamics, structures, physical states, and mechanical properties of the studied material. Small-amplitude oscillatory shear (SAOS) is the most commonly utilized method to probe the dynamic responses of PECs over a wide range of timescales. Researchers have exploited SAOS to measure important parameters that describe PEC mechanical properties, determine the physical states of PECs, investigate the nature of solid-liquid transition,[58,59] examine the effect of salt on dissociating PECs, and develop molecular models and theories for PECs.[60,61] SAOS measurements are limited to situations where the material conditions are independent of the applied strain amplitude. Therefore, before conducting SAOS measurements, researchers usually carry out an amplitude sweep test first to make sure the strain amplitude applied in the following SAOS is within the linear regime. In SAOS, the properties of the materials are described in terms of storage modulus (G') and loss modulus (G''), which indicate

the "in-phase" and "out-of-phase" responses of the measured materials, respectively. Through analyzing and comparing the values of G' and G'', researchers are able to characterize material properties and physical states over a wide range of timescales. For most of the PEC systems investigated so far, their electrostatic pairings are able to constantly break and form again so viscoelasticity responses were usually observed in the SAOS measurements.

Figure 1. 3: PEC dynamics and the time-salt superposition.

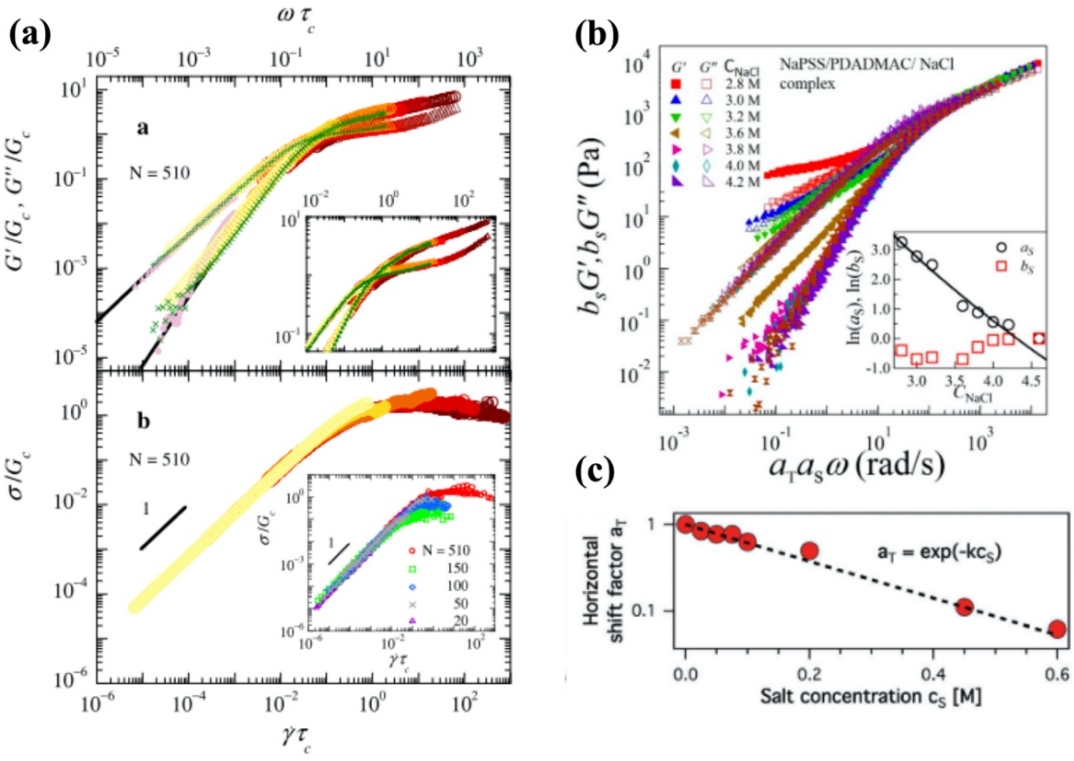

(a) Rescaled frequency sweep measurements and flow curves. The inset of the bottom figure shows the rescaled flow curve for PECs with different molecular weights.[60] Copyright 2010, Physical Review Letter. (b) Time-temperature-salt superposition of frequency sweep data acquired in a PEC under different salt concentrations.[62] Copy right 2018, Gels. (c)The dependence of the horizontal shift factor as a function of added salt concentration.[63] Copy right 2018, Soft Matter. Reproduced from Ref. 63 with permission from The Royal Society of Chemistry.

Single SAOS measurement is only capable of accessing a narrow range of timescale due to limitations in equipment. Superposition, as a powerful tool in rheology, overcomes this issue and allows the access of a wide range of frequency. Spruijt et al.[9,60] integrated superposition into the study of PEC and introduced the idea of time-salt superposition, which utilized salt as the reference variable to generate master curves. After obtaining a series frequency sweep measurement data of PECs under different salt conditions, they found that master curves can be achieved by shifting the data horizontally and vertically. (Figure 1.3a) The vertical shift factor corrects the variations in moduli across different samples and the horizontal shift factor dictates the relaxation dynamics, which is dependent upon the amount of existing electrostatic pairings between oppositely charged chains. Through detailed and quantitative analysis of the horizontal shift factors, Spruijt et al. found that the relaxation behaviors of PECs can be well described by the sticky Rouse model,[61] which describes electrostatic pairings as "sticky points" that hinder the movement of polyelectrolyte chains and slow down their relaxation. Based on the sticky Rouse model[61] and Debye–Hückel approximation, they proposed that the horizontal shift factor should be proportional to $\exp\left(-A\sqrt{c_{Salt}}+B\right)$, where c_{Salt} represents the added salt concentration and A and B are constants. Later, Hamad et al.[64] further expanded on this correlation by assuming that salt screening electrostatic interactions rely on the Debye screening length and also incorporating the number of individual ionic interactions involved in one sticky point. They proposed a more explicit correlation that the horizontal shift factor should be proportional to $\exp\left(\frac{1}{\sigma}-\sqrt{8\pi * l_B * C_S * N_A}\right)$, where $\sigma, l_B, C_S, and\ N_A$ are bond length, Bjerrum length, salt concentration and Avogadro's number, respectively.

Using time-salt superposition strategy, many other studies have also observed the sticky Rouse correlations between horizontal shift factors and salt concentrations in multiple different systems.[62,65,66] A few study have even expanded upon the time-superposition. For example, Yang et al.[66] and Ali et al.[62] have combined time-temperature superposition and time-salt superposition to achieve time-temperature-salt-superposition. Ali et al.[62] found that time-salt superposition can be applied to all salt concentrations, while time-temperature-salt-superposition only applies for limited salt concentrations and frequency range. (Figure 1.3b) A recent study by Vaqar et al.[67] found that accounting small counterions on polyelectrolyte chains allows the superposition of PECs with varying initial polyelectrolyte concentrations onto a single universal master curve. This method was named as time-ionic strength superposition. Even though the sticky Rouse model has been found applicable to most of the PEC tested so far, there are also exceptions. The proportional correlation between horizontal shift factors and the exponent of $\sqrt{c_{Salt}}$ could not be well applied to all the systems. Marciel et al.[63] discovered that for the PECs composed of poly(lysine) (PLK) and poly(glutamic acid) (PRE), the horizontal shift factors are proportional to the exponent of c_{Salt}, instead of $\sqrt{c_{Salt}}$. (Figure 1.3c) They attributed the disagreement between their findings and the sticky Rouse model to a relatively low salt range investigated in their study. Their findings implied that the sticky Rouse model is still incomplete and future works are needed to improve the model.

1.2.2 Effect of Water on the Physical Behaviors of Polyelectrolyte Complexes

Water content within PECs is another very important factor that controls the behaviors of PECs both at atomic level and at macroscopic level. Figure 1.4a[68] illustrates the typical structure of a PEC, where the charge groups on polyelectrolyte chains exist in two forms. Some associate

with charged groups on the oppositely charged polyelectrolyte chains to form intrinsic ion pairs. Other unbound groups are compensated by small counterions to form extrinsic ion pairs. Adding salt in PECs will break the intrinsic ion pairs and increase the amount of extrinsic ion pairs on polyelectrolyte chains. At the same time, water molecules will be introduced as salt is increasing. In other words, the level of hydration is governed by the extent of intrinsic ion pairs. Therefore, salt and water are usually analyzed together when discussing the plasticization of PEC. Ion paring and hydration level can affect many physical properties of PECs. Among them, the topic that has been discussed the most is a glass-transition-like thermal transition. Lutkenhaus and coworkers[68–74] have extensively studied this thermal transition in bulk polyelectrolyte complexes as well as polyelectrolyte multilayers using a combination of differential scanning calorimetry (DSC), dynamic mechanical testing (DMA), and electrochemical impedance spectroscopy (EIS). They also collaborated with Sammalkorpi and coworkers to compare experimental results with molecular dynamics simulation.[15,72,73,75] For example, through inspecting the trend of the thermal transition under controlled hydration and salt, they unveiled the effect of salt and water on the plasticization of PECs formed by poly(diallyldimethylammonium chloride) (PDAC) and poly(sodium 4-styrenesulfonate).[73] Water is known to be a plasticizer for PEC, while salt can have opposite plasticizing effect. It promotes plasticization through dissociating bindings and enhancing chain movements, but reducing plasticization by restricting the mobility of water molecules. In a more recent study,[68] they quantitively described the effect of water on PEC relaxation on the molecular scale. They revealed that the correlation between the glass transition temperature (T_g) and the number of water molecules surrounding an intrinsic ion pair ($n_{H_2O}/n_{intrisic\ ion\ pair}$) should follow $\frac{1}{T_g} \sim ln\left(\frac{n_{H_2O}}{n_{intrisic\ ion\ pair}}\right)$. This relationship was demonstrated to be general, as it can be very

well applied to two totally different types of PEC systems (PDADMA/PSS and PAH/ PAA) and also for two formats of electrostatic assemblies (PECs and PEMS). (Figure 1.4b)

In addition to thermal transition, the dynamics of PECs can also be significantly influenced by the amount of water in PEC. The role that water plays in the dynamic mechanical and rheological properties of PECs has been carefully examined in a few recent studies. Suarez-Martinez et al.[74] studied PEC precipitates assembled from poly(allylamine hydrochloride) (PAH) and poly(acrylic acid) (PAA) and were able to utilize water content within PEC as the variable to perform time-water superposition for the first time. (Figure 1.4c) They found that the modulus decreases with increasing water and the horizontal shift factor in the time-water superposition follows a log-linear correlation with the water content in the complex phase. Lyu et al.[76] investigated how humidity history influenced the properties of PECs composed of poly(diallydimethylammonium chloride) (PDADMAC) and poly(sodium 4-styrenesulfonate) (PSS) by exposing dried PECs under different humidity conditions. They found that unlike the hydrated PECs, the dried complexes became stiffer through humidity tempering. Their explanation for such unexpected behavior is that water from humid air facilitates the reorganization of polyelectrolyte chains, which increases the extend of intrinsic pairings and results in higher moduli. From these findings, they proposed that humidity can be exploited as a very novel and mild approach to control the structure and mechanical properties of dried PECs.

Figure 1. 4: Effect of water on PEC behaviors.

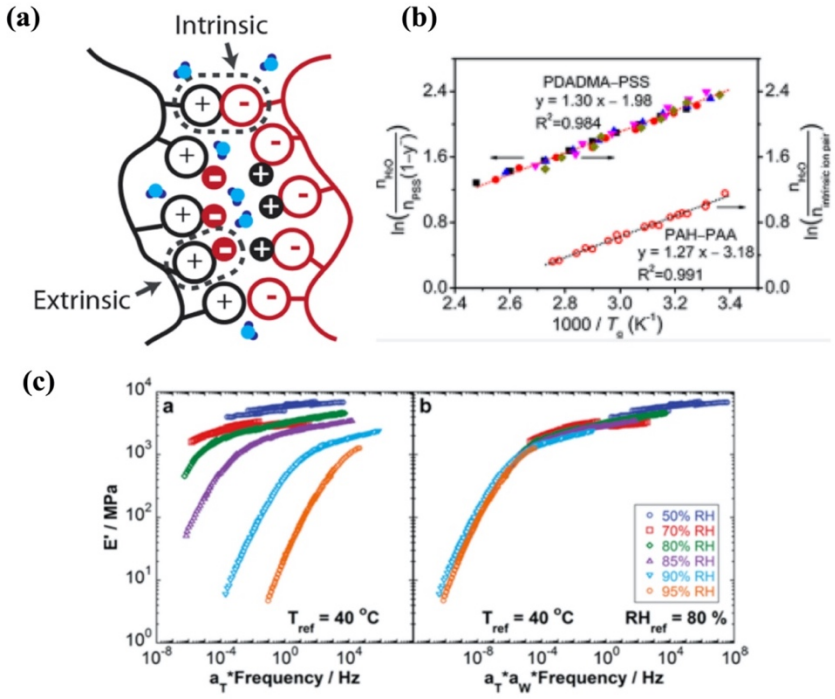

(a) Schematic of charged polyelectrolyte assembly.[68] Copyright 2018, ACS Central Science. (b) $ln\left(\frac{n_{H_2O}}{n_{intrisic\ ion\ pair}}\right)$ vs $\frac{1000}{T_g}$ for PDADMA/PSS and PAH/PAA.[68] Copyright 2018, ACS Central Science. (c) Application of time-water superposition principle for PAA/PAH complexes. Left figure shows time-temperature superposition master curves at different relative humidity (RH) and right figure is the time-water super master curve from the time-temperature superposition curves.[74] Reprinted (adapted) with permission from (Reference 74). Copyright (2019) American Chemical Society.

As mentioned above, for PEC system, the effects of water and salt are inseparable in terms of the plasticization effect, as salt doping can induce change in water component at the same time. Both salt and water are believed to cause swelling in PECs. Quartz crystal microbalance (QCM) is a powerful tool to explore the role that different factors play in PEC swelling. The unique feature of QCM lies in its capability to measure the swelling behavior and viscoelastic phase angle simultaneously, enabling researchers to directly correlate these two physical properties. For example, Sadman et al.[21] utilized QCM technique to characterize mechanical properties in PEC.

Under its help, they discovered that the mechanical properties of their PEC films are dependent only on the degree of swelling, not on the identity of the salt. (Figure 1.5a) Furthermore, through analyzing a spectrum of PEC systems with different hydrophobicity in the polycation chains using QCM, they found that the rheological behaviors of different films rely only on the swelling ratio, not on the hydrophobicity of the chains. Universal swelling-modulus master curves were achieved by superposing density-shear modulus product curves from various PEC systems with different hydrophobicity. (Figure 1.5b)

Figure 1. 5: Relationship between swelling and mechanical properties of PECs.

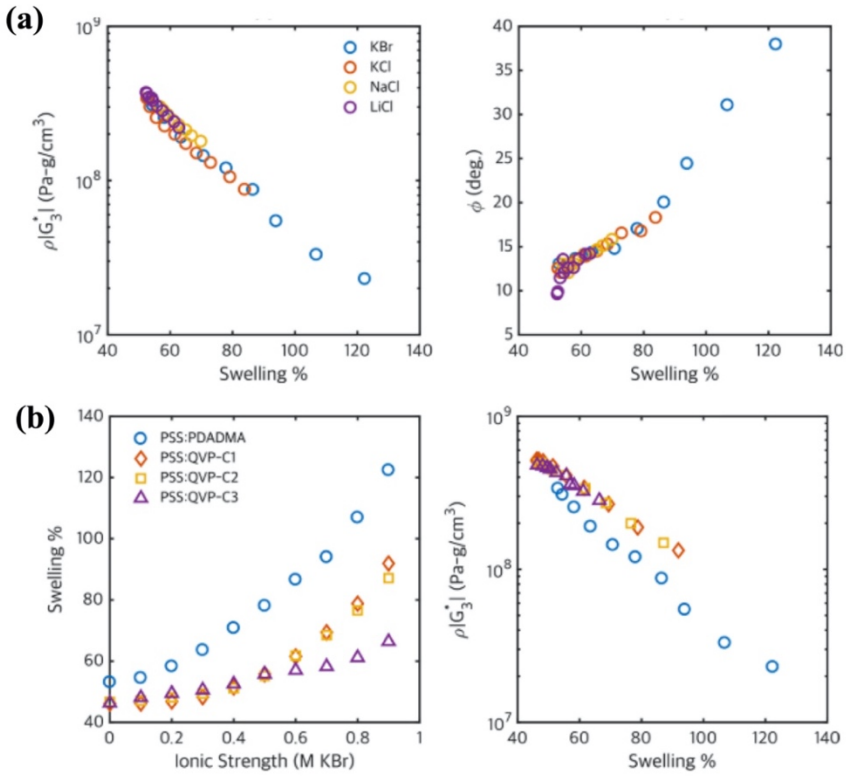

Reprinted (adapted) with permission from (Reference 21). Copyright (2017) American Chemical Society. (a) Swelling-modulus (left figure) and swelling-phase angle (right figure) master curves for PSS/PDADMA films in different salts with up to 1.0 M Salt concentrations.[21] (b) Swelling behavior of QVP complexes compared with PSS/PDADMA (left figure) and swelling-modulus master curves for PSS/PDADMA and PSS/QVP complexes (right figure).[21]

1.2.3 Structural Analysis in Polyelectrolyte Complexes

As early as 1965, Alan S. Michaels[1] mentioned two possible molecular architecture models for polyelectrolyte complexes. The first one is a ladder-like conformation, where extended polyelectrolyte chains with opposite charges zipper together. The second model suggests that the complexes are composed of completely random and ionically interlinked chains, which result in a scrambled salt or glassy ionic solid structure. Even though the prediction on PEC structures has been proposed for a few decades, not a lot of studies have directly tested these models. Among the studies on PEC internal structures, most of them investigated natural protein-based PECs.[77–80] These natural polymers have many shortcomings, including a high polydispersity in chain length and huge variations in the chemical structure. Recently, with the rapid progress in polyelectrolyte synthesis techniques, a few studies that examined the structure of PECs composed of synthetic chains with more controlled molecular structures emerged.[63,81–84] For example, Spruijt et al.[81] investigated the structure of PEC composed of poly(acrylic acid) (PAA) and poly(N,N-dimethylaminoethyl methacrylate) (PDMAEMA) using a combination of neutrons, X-rays, and light scattering. They revealed that the polyelectrolyte chains, both polycations and polyanions, follow ideal Gaussian chain conformation. The overall structure is akin to a semidilute polymer solution, with strongly overlapping polycations and polyanions to form a network. The mesh size of the network was found to decrease with decreasing salt concentration. Marciel et al. [59] observed a different conformation model by studying PECs formed by poly(lysine) and poly(glutamic acid) with small-angle X-ray scattering (SAXS). They discovered that the chain conformations are dependent upon the chirality of these polypeptides. When at least one of the polypeptide components is racemic, liquid coacervates will form and the conformations of their structures are

similar to semidilute polyelectrolyte solutions. (Figure 1.6a) However, for solid precipitates with the formation of hydrogen-bonded beta sheet structures, stiff and ladder-like conformations were observed from SAXS data. Fare et al.[83] explored the trend of PSS chain conformation in PDADMA/PSS with small-angle neutron scattering (SANS) as the PEC transitions from solid to liquid upon salt doping. They found that as salt concentration increases, the radius of gyration of PSS remained constant when the PEC was in solid phase, but started to decrease after entering liquid regime. (Figure 1.6b)

Over the decades, many efforts have dedicated to the theoretical developments in PEC structures as well. For example, in 1993, Srivastava et al.[85] studied the aggregates composed of oppositely charged chains with the same length and charge density through dynamic Monte Carlo algorithm. They proposed that the radii of gyration of the chains scale as $N^{1/2}$, where N is the polyelectrolyte chain length. In recent years, theories on polyelectrolyte chain conformation have been refined and specified to incorporate PECs composed of polyelectrolyte chains with diverse polyelectrolyte chain structures and properties. For example, a recent work with theoretical study combined with molecular dynamic simulations predicted a structural model for asymmetric coacervates, whose polycation and polyanion chain components are different in charge density and the number of charges per chain.[86] They proposed that those coacervates are interpenetrating solutions by nature with two different conformations and two correlations lengths. The lower charge density domain is similar to quasi-neutral solutions, while the higher charge density regime is analogous to polyelectrolyte solutions. As shown in Figure 1.6(c), chains with weaker charges formed a screening coat surrounding the stronger charged polyelectrolytes.

Figure 1. 6: Studies on the structures of PECs.

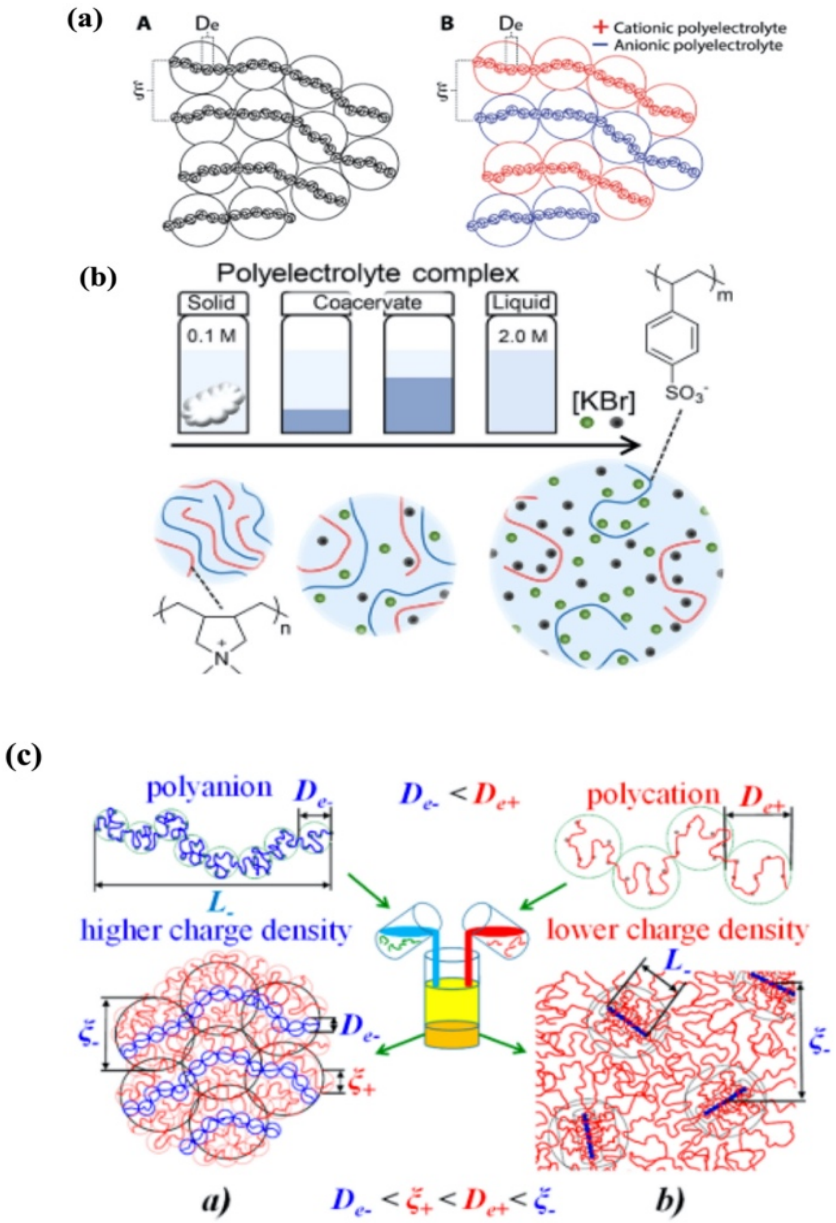

(a) Schematics that illustrate the similarity in the structures of A. salt free semidilute polyelectrolyte solutions and B. polyelectrolyte complex coacervates with oppositely charged chains.[63] Copyright 2018, Soft Matter. Reproduced from Ref. 63 with permission from The Royal Society of Chemistry. (b) Schematic depicting the conformation evolution of PSS in PDADMA/PSS PEC upon salt doping.[83] Reprinted (adapted) with permission from (Reference 83). Copyright (2018) American Chemical Society. (c) Conformations of a polyanion and a polyanion in a mixture of asymmetric oppositely charged polyelectrolytes.[86] Reprinted (adapted) with permission from (Reference 86). Copyright (2018) American Chemical Society.

1.2.4 Phase Behavior of Polyelectrolyte Complexes

Phase behavior has been a main focus area in the research of polyelectrolyte complexes, as it serves as a crucial guidance for the material design and application of PEC. The earliest theory on complex coacervation was proposed by Voorn and Overbeek.[4,87] In their theory, the total free energy of mixing was described as the sum of two terms: a Flory-Huggins theory term that calculates the entropy gain from the mixing of polymer solutions,[88–90] and a Debye-Hückel theory expression that accounts for the electrostatic interactions. Many assumptions were made in this original model. For example, the oppositely charged polyelectrolyte chains were considered to be symmetric and the coacervation was assumed to occur under low salt concentrations. Because of these assumptions, the Voorn-Overbeek model has many inherent limitations, as illustrtated in Figure 1.7(b). First of all, in the Voorn-Overbeek theory, the charge units on polyelectrolyte chains are considered as unconnected electrolyte particles so the salt ions and polymer charges cannot be distinguished from each other. Secondly, the Debye-Hückel theory can only be applied to weak and dilute polyelectrolytes so it is only suitable for low salt concentration situation. Thirdly, the existence of water is only represented by the dielectric constant parameter in the expression of Bjerrum length. Thus, many roles that water molecules play in the thermodynamics of PECs have been ignored. Also, the excluded volume effect in the electrostatic interactions and the volumes of the salt and polymers were ignored in Voorn-Overbeek theory.

Despite the above-mentioned shortcomings in the Voorn-Overbeek model, it has been widely exploited and referred to in early studies on the phase behaviors of polyelectrolyte complexation.[89,91–93] For example, Spruijt et al.[89] depicted the phase diagram of the PEC system formed by poly(N,N-dimethylaminoethyl methacrylate) (PDMAEMA) and poly(acrylic acid)

(PAA), in which the PAA chains were fluorescein-labeled so that the polymer concentrations can be measured by fluorescence spectroscopy, based on the assumption that the concentrations of PDMAEMA and PAA are the same. Another assumption they made in this study is that the salt concentration is the same in the complex phase and supernatant phase. Using mean-field model of Voorn and Overbeek to interpret their results on binodal compositions, water content, and critical salt concentrations, they observed good agreement between their results and the Voorn-Overbeek theory, as shown in Figure 1.7(c). Even though this experimental study can be improved in many aspects, for example the data points on the binodal curve have very large error bars due to the nature of the spectroscopy technique, and the assumption on equal salt amount in the supernatant and complex phase neglects salt partitioning behavior, this work stimulated many later efforts in investigating the phase behaviors of PECs.

In recent years, plentiful experimental and theoretical studies have been dedicated to refining and improving the Voorn-Overbeek theory. Many molecular details have been incorporated into the model to construct a more complete theoretical picture to describe the behaviors of PEC. Salt partitioning is an important aspect that has been shown by recent studies to be at odds with the original Voorn-Overbeek theory. In the phase diagram, salt partitioning is reflected by the slope of tie line connecting a point in the supernatant phase and its corresponding data point in the complex phase. A negatively slope tie-line implies that salt prefers the supernatant phase and has higher salt concentration in the supernatant than in the complex. Voorn-Overbeek theory and many recent works have predicted and reported positively sloped tie lines, suggesting a preferential partitioning of salt in the complex phase.[92,94,95] In 2004, Kudlay et al.[96,97] first reported an opposite salt partitioning trend in their prediction by including the excluded volume in

the calculation. Following these works, Sing and Perry[98] exploited PRISM theory to incorporate hard-core interactions and an obvious partitioning to the supernatant phase was observed. Same trend was also reported by many other theoretical,[73,98–101] experimental,[13,98,102,103] and computational works as well.[98,102–104] An important example is the work by Li et al.,[13] which combined experimental and simulation methods to quantitively and comprehensively describe the phase behaviors of a model PEC system, formed by poly(L-lysine) (PLK) and poly(D,L-glutamic acid) (PRE), as seen in Figure 1.7(d). To carefully scrutinize the phase behaviors of PECs, they not only measured the exact concentrations of each components under the same condition for multiple times using thermogravimetric analysis, but also followed up with turbidity and conductivity measurements to ensure the accuracy of their TGA results. Their experimental results from multiple experimental techniques and simulation calculations excellently agreed with each other. In their study, the salt molecules were also found to partition preferentially in the supernatant phase. The Voorn-Overbeek theory has also been enhanced and completed in different other aspects, such as polymer connectivity, polymer chemical structures, architecture, hydrophobicity, etc. Recent progress on these aspects can be found in many excellent review papers.[2,105,106]

Figure 1. 7: Phase behavior of polyelectrolyte complexes.

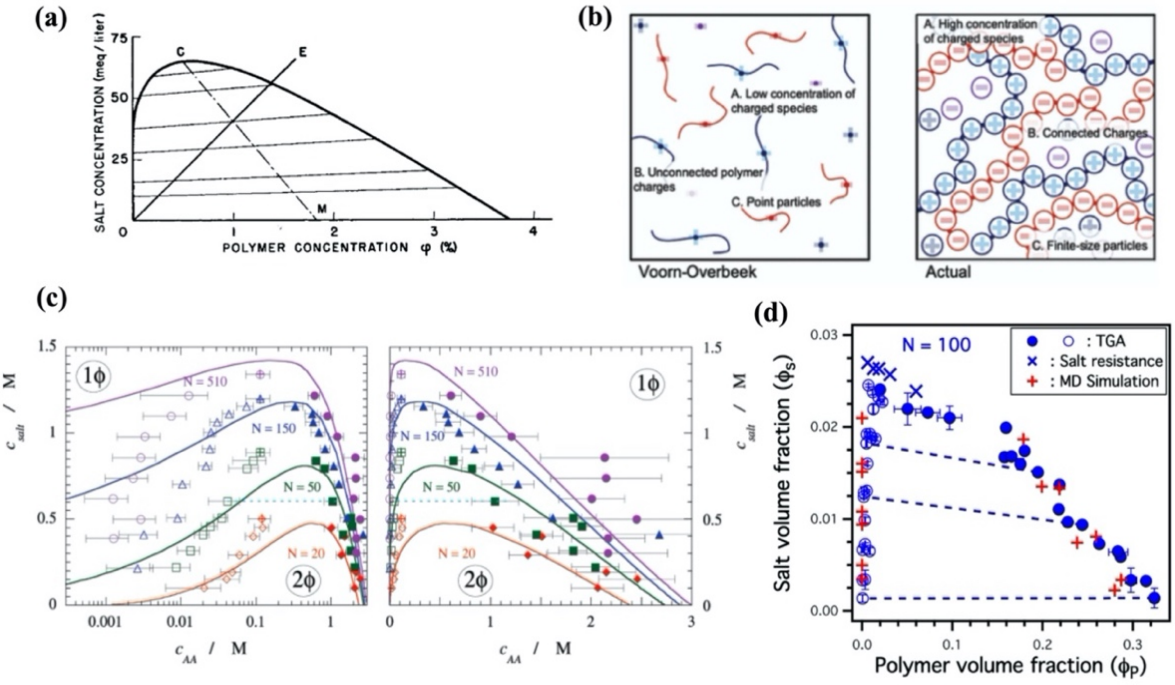

(a) Phase diagram for complex coacervation predicted by Voorn and Overbeek.[4] Copyright 1957, Journal of Cellular and Comparative Physiology. (b) Schematics demonstrating the key assumptions in Voorn-Overbeek theory. The left figure illustrates what Voorm-Overbeek theory predicts, while the right figure dictates a few major aspects that the model neglects.[105] Copyright 2020, Soft Matter. Reproduced from Ref. 105 with permission from The Royal Society of Chemistry. (c) Phase diagrams for the PAA/PDMAEMA system at pH 6.5 on the logarithmic scale (left) and linear scale (right). The lines are theoretical predictions and the symbols are from experimental results.[89] Reprinted (adapted) with permission from (Reference 89). Copyright (2010) American Chemical Society. (d) Phase diagram from the PLK_{100} and PRK_{100} system. Blue circles are the results from TGA, blue "X" symbols represent salt resistance results, and red symbols are from simulation calculations.[13] Reprinted (adapted) with permission from (Reference 13). Copyright (2018) American Chemical Society.

1.3 Solid-Liquid Transition in Polyelectrolyte Complexes

The physical states of polyelectrolyte complexes can range from glassy solids to low viscosity liquids. Whether the final self-assembled material exists as a solid or liquid is dependent upon many different parameters. In terms of the features of polyelectrolyte chains, chain length, ionic strength, chemical structures, charge density, chirality for peptides,[14] hybridization of nucleic acids[107] etc. can all govern the final physical state. The external condition, such as temperature, salt concentration, and pH, also plays a critical role. Over the years, liquid coacervates have received numerous attention because of their broad utility in underwater adhesives, food industry, drug and gene delivery, etc. In contrast to the systematic studies on multiple physical aspects of liquid coacervates, the investigations on polyelectrolyte complexes in the form of solid precipitates have been very scattered, mostly due to the intractable nature of the solid PECs. Even fewer studies have explored the transitions between these two states. The characterizations of solid precipitates and liquid coacervates had followed parallel paths. A recent study by Wang et al.[103] broke the boundaries between these two states and demonstrated how salt, as a plasticizer, can be used to drive the PECs to continuously phase change from solid into liquid and eventually into a homogenous polyelectrolyte solution in one phase. The polyelectrolyte complex system they studied, poly(diallymethylammonium) (PDADMA) and poly(styrene sulfonate) (PSS), started as a solid in the salt-free state. As illustrated in Figure 1.8(b), the addition of salt breaks the ionic pairings between oppositely charged polyelectrolytes and brings in additional water into the complex. At a certain salt threshold, solid is transformed into liquid, with the boundary between these two states determined by the emergence of cross-over points between G’ and G’’ through rheology measurements. Eventually, when every ion pairing is broken, the polyelectrolyte chains dissociate completely and PECs dissolve into homogenous solution.

The important work by Wang et al.[103] has introduced a simple method to access the entire solid-liquid-solution spectrum and achieve the transformation between solid and liquid states in an easy way. It has also spurred many interests in probing the mechanisms behind the phase transition from many perspectives. For example, Fares et al.[83] followed the study by Wang et al.[103] and investigated the same system they studied, PDADMA/PSS. They deuterated PSS chain and used small-angle neutron scattering (SANS) to track the change in PSS coil size as the complex was evolving from solid into liquid and eventually into solution with the addition of salt. Two hypotheses were proposed to illustrate the morphologies of the polymer chains from solid to liquid. (Figure 1.8c) For the first hypothesis (A to B in Figure 1.8c), polymer chains swell with the addition of salt, causing polymers to expand. In comparison, in the second hypothesis (A to C in Figure 1.8c), polymer chains remain to be compacted and the extra volume from water and salt enter the supernatant phase. Through analyzing the Guinier region of the SANS profiles shown in Figure 1.8 (e) and approximating the form factor using the Debye function, they were able to extract the radius of gyration (R_g) that is directly related to the form factor. As shown in Figure 1.8 (d), R_g remains constant in the solid phase upon salt doping but starts to decrease as the complex transforms into coacervate. Based on the trend in R_g, they were able to conclude that the second hypothesis (A to C in Figure 1.8c) is closer to the real scenario. The chains remain to be coiled until the salt concentration reaches a threshold, where the complex changes from solid into liquid state.

Another important study in the solid-liquid transitions of PECs is from Liu et al., where this phenomenon was explained by rheological characterization of the same PDADMAC/PSS system.[58] Using the small amplitude oscillatory shear (SAOS) linear viscoelasticity measurements

and facilitated by the time-salt superposition strategy to expand the probed frequency space, they were able to identify the mechanism of the liquid-to-solid transition in their PEC system driven by decreasing salt concentration as gelation. The first evidence suggesting a gelation-type transition is the tanδ vs frequency plot, where the curve becomes more horizontal and frequency-invariant as the sample approaches solid state. (Figure 1.8f) The gelation mechanism can also be supported by the so-called Winter plot that captures the difference in material response between solid and liquid sample at the critical gel point (Figure 1.8g).[59,108] Further analysis in the relaxation spectra also implies a gelation mechanism, where the suggestion of a plateau in the solid samples was observed as a sign for gelation, as seen in Figure 1.8h. Figure 1.8i illustrates the structural mechanism behind the salt induced liquid-to-solid gelation. At high salt concentration, the extrinsic ion pairs formed by added salt and polyelectrolyte chains facilitate the rearrangement of polyelectrolyte chains. As salt concentration decreases, intrinsic ion pairs between oppositely charged chains restrain chain movement and trigger the formation of crosslinks, which later percolate the sample and initiate gelation. Despite the recent efforts in investigating the structural evolution and the dynamical responses during solid-liquid transitions in PECs, further studies on examining other PEC systems, exploring the effect of different parameters, controlling various secondary interactions, etc. are definitely needed to achieve a more universal understanding in this phenomenon.

Figure 1. 8: Solid-to-Liquid transitions in polyelectrolyte complexes.

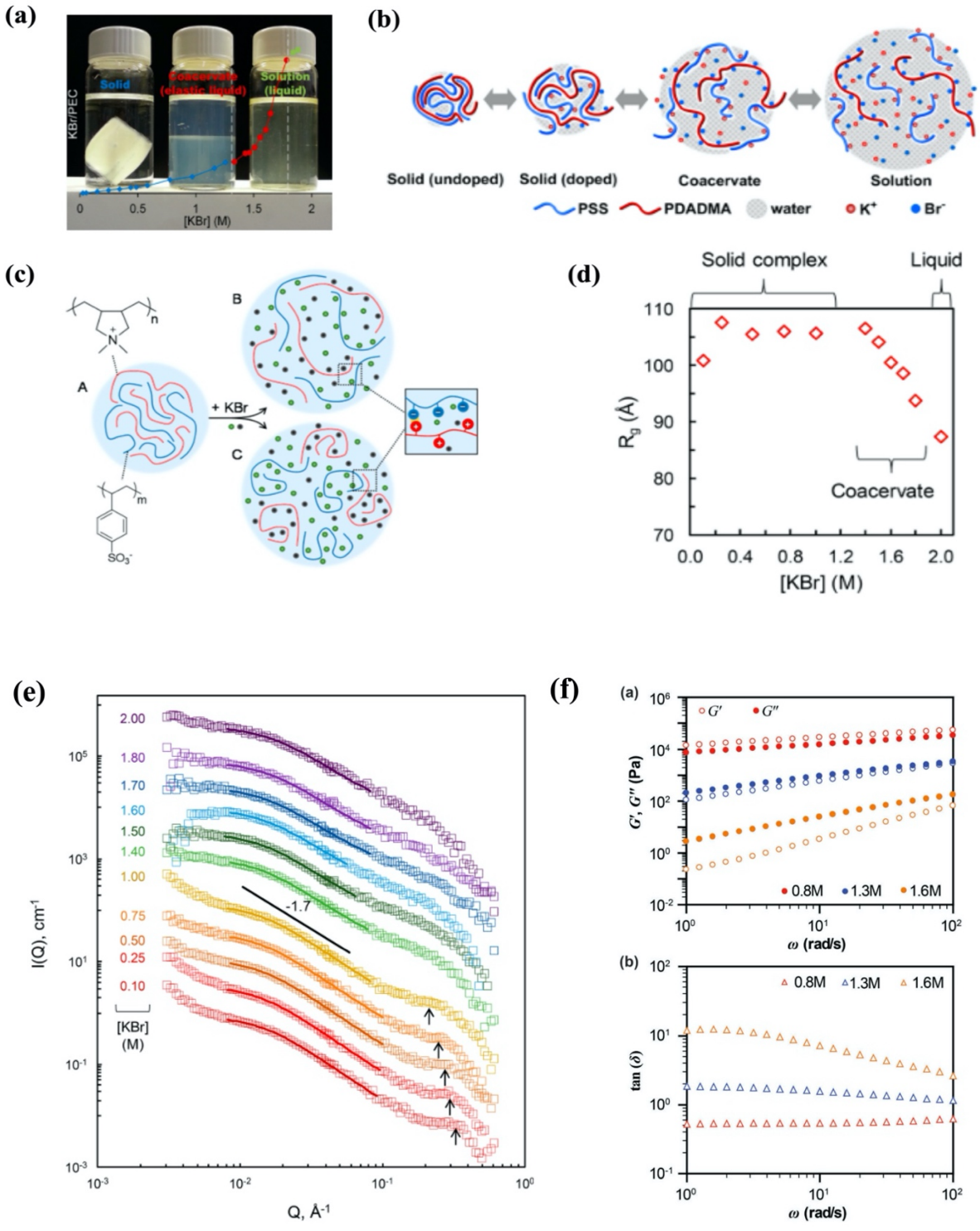

Figure 1.8 (Continued)

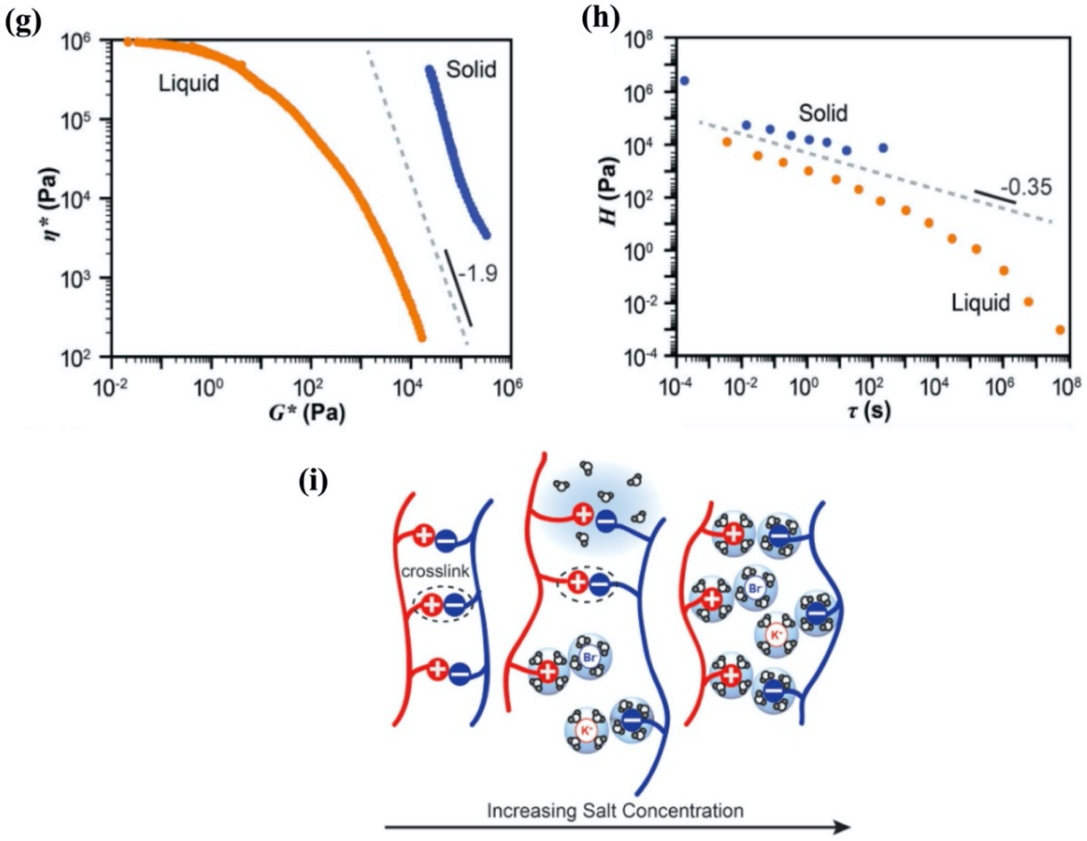

(a) PDADMA/PSS transferred from solid into liquid and eventually to solution with the addition of KBr.[103] (b) Schematic describing the effect of added salt on the microstructures of PECs.[103] (a)-(b) Copyright 2014, Macromolecules. (c) Two proposed structural models (A to B) or (A to C) of the PDADMA/PSS as it transitioned into coacervates through adding KBr.[83] (d) Radius of gyration of PSS in the PDADMA/PSS complex.[83] (e) Small-angle neutron scattering profiles for the PDADMA/PSS complex from 0.1 M to 2.0 M KBr.[83] (c)-(e) Reprinted (adapted) with permission from (Reference 83). Copyright (2018) American Chemical Society. (f) Frequency sweep data for PDADMA/PSS under 0.8M, 1.3M, and 1.6M KBr.[58] (g) Complex viscosity as a function of complex modulus.[58] (h) Relaxation spectrum as a function of relaxation time.[58] (i) Schematic demonstrating the salt-driven gelation in PEC.[58] (f)-(i) Copyright 2017, Soft Matter. Reproduced from Ref. 58 with permission from The Royal Society of Chemistry.

1.4 Effects of Solvents on Polyelectrolyte Complexes

Solvent can have significant influence on the properties of polyelectrolyte complexes. However, over the decades, most of the efforts have been committed to investigating the effect of salt. Solvent effect was only explored in a few studies. For example, Zhang et al.[30] characterized a weakly interacting PEC composed of branched poly(ethylene imine) (BPEI) and PAA and altered its solvent condition. Employing rheology to determine the states and characterize the mechanical properties of PECs, they showed that salt-free BPEI/PAA in ethanol/water shifted from liquid to solid and the modulus increased by almost four orders of magnitude as the percentage of ethanol component increased from 0% to 40%. (Figure 1.9a) They ascribed such behaviors to the hydration layers surrounding ionized groups of polyelectrolytes. These hydration layers composed of water molecules served as plasticizers that weakened interactions between oppositely charged polyelectrolytes. Introducing ethanol removed these hydration layers, thus strengthening the associations between BPEI and PAA. They also investigated the salt responses of this system in the co-solvent condition and found that BPEI/PAA dissociated a few times slower in both 10 mM NaCl and 10 mM $MgCl_2$ when ethanol content in the ethanol/water co-solvent increased from 0% to 40%, suggesting that its resistance to NaCl was highly enhanced when the organic solvent composition increased. (Figure 1.9b) They pointed out that this strengthened salt resistance was caused by the lowering of dielectric constant when introducing ethanol, which reduced the interactions between salts and coacervate. Aside from this systematic study by Zhang et al,[30] the effect of solvent was also briefly mentioned in a few other studies. In the studies by Chang et al.[109] and Sun et al.[110] on polypeptide-based and polysaccharide-based PECs, respectively, salt resistance increase with increasing organic solvent content was also reported. The effect of solvent

quality was examined in systems of polyelectrolyte multilayers (PEM) as well.[111–116] Despite the progress in figuring out the role of solvent in the behaviors of PECs and PEMs, more systematic and comprehensive efforts are needed to achieve a universal understanding and to utilize solvent to enhance applications of these materials.

Figure 1. 9: Effect of solvents on polyelectrolyte complexes and polyelectrolyte multilayers.

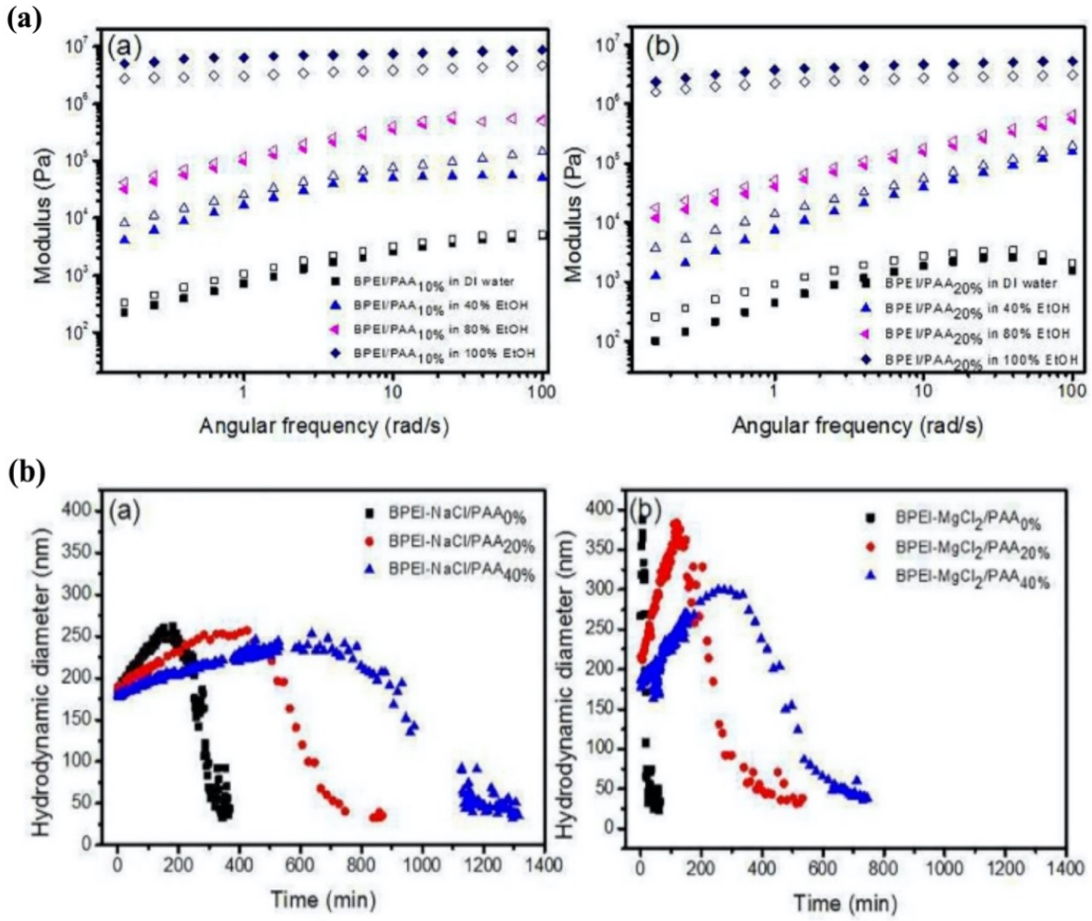

Figure 1.9 (Continued)

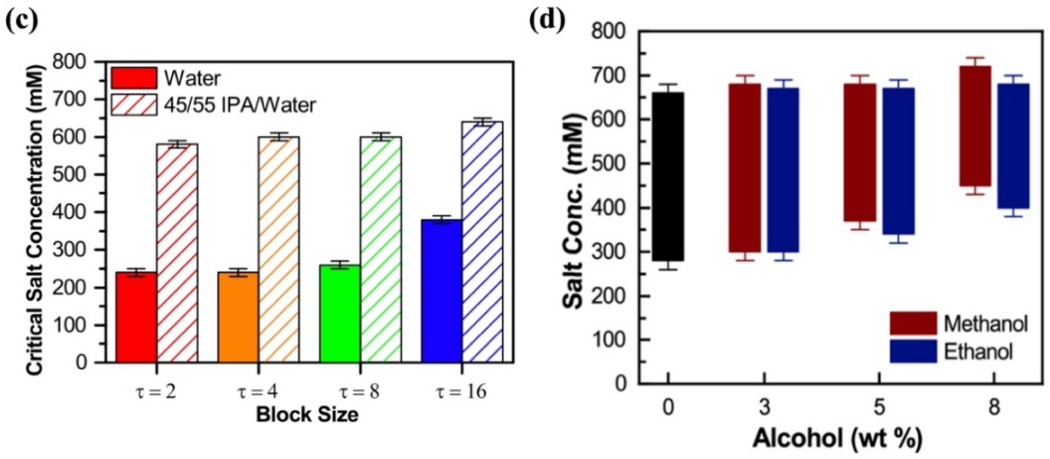

(a) Rheological behaviors of BPEI/PAA in water/ethanol mixture.[30] (b) Kinetic behaviors of BPEI/PAA in 10mM NaCl and 10mM $MgCl_2$[30] (a)-(b) Copyright 2018, The University of Akron. (c) The critical salt concentration for the sequence defined coacervates in water and in 45/55 v/v% mixture of isopropanol and water.[109] Copyright 2017, Nature communications. (d) The range of salt concentration over which the complex formed by chitosan and hyaluronic acid exist as liquid coacervate.[110] Reprinted (adapted) with permission from (Reference 110). Copyright (2019) American Chemical Society.

1.5 Reference

(1) Michaels, A. S. Polyelectrolyte Complexes. *Ind. Eng. Chem.* **1965**, *57*, 32–40. https://doi.org/10.1021/ie50670a007.

(2) Srivastava, S.; Tirrell, M. V. Polyelectrolyte Complexation. *Adv. Chem. Phys.* **2016**, *161*, 499–544. https://doi.org/10.1002/9781119324560.

(3) Veis, A. A Review of the Early Development of the Thermodynamics of the Complex Coacervation Phase Separation. *Adv. Colloid Interface Sci.* **2011**, *167*, 2–11. https://doi.org/10.1016/j.cis.2011.01.007.

(4) Overbeek, J. T. G.; Voorn, M. J. Phase Separation In Polyelectrolyte Solutions. Theory Of Complex Coacervation. *J. Cell. Comp. Physiol.* **1957**, *49*, 7–26. https://doi.org/10.1002/jcp.1030490404.

(5) Ghostine, R. A.; Shamoun, R. F.; Schlenoff, J. B. Doping and Diffusion in an Extruded Saloplastic Polyelectrolyte Complex. *Macromolecules* **2013**, *46*, 4089–4094. https://doi.org/10.1021/ma4004083.

(6) Priftis, D.; Laugel, N.; Tirrell, M. Thermodynamic Characterization of Polypeptide Complex Coacervation. *Langmuir* **2012**, *28*, 15947–15957. https://doi.org/10.1021/la302729r.

(7) Philipp, B.; Dautzenberg, H.; Linow, K. J.; Kötz, J.; Dawydoff, W. Polyelectrolyte Complexes - Recent Developments and Open Problems. *Prog. Polym. Sci.* **1989**, *14*, 91–172. https://doi.org/10.1016/0079-6700(89)90018-X.

(8) Bungenberg de Jong, H. G.; Kruyt, H. R. Coacervation. (Partial Miscibility in Colloid Systems). (Preliminary Communication). *Proc. K. Ned. Akad. Wet.* **1929**, *131*, 849–856.

(9) Spruijt, E.; Cohen Stuart, M. A.; Van Der Gucht, J. Linear Viscoelasticity of Polyelectrolyte Complex Coacervates. *Macromolecules* **2013**, *46*, 1633–1641. https://doi.org/10.1021/ma301730n.

(10) Huang, J.; Morin, F. J.; Laaser, J. E. Charge-Density-Dominated Phase Behavior and Viscoelasticity of Polyelectrolyte Complex Coacervates. *Macromolecules* **2019**, *52*, 4957–4967. https://doi.org/10.1021/acs.macromol.9b00036.

(11) Fu, J.; Fares, H. M. Ion-Pairing Strength in Polyelectrolyte Complexes. *Macromolecules* **2017**, *50*, 1066–1074. https://doi.org/10.1021/acs.macromol.6b02445.

(12) Lou, J.; Friedowitz, S.; Qin, J.; Xia, Y. Tunable Coacervation of Well-Defined Homologous Polyanions and Polycations by Local Polarity. *ACS Cent. Sci.* **2019**, *5*, 549–557. https://doi.org/10.1021/acscentsci.8b00964.

(13) Li, L.; Srivastava, S.; Andreev, M.; Marciel, A. B.; De Pablo, J. J.; Tirrell, M. V. Phase Behavior and Salt Partitioning in Polyelectrolyte Complex Coacervates. *Macromolecules* **2018**, *51*, 2988–2995. https://doi.org/10.1021/acs.macromol.8b00238.

(14) Perry, S. L.; Leon, L.; Hoffmann, K. Q.; Kade, M. J.; Priftis, D.; Black, K. A.; Wong, D.; Klein, R. A.; Pierce, C. F.; Margossian, K. O.; et al. Chirality-Selected Phase Behaviour in Ionic Polypeptide Complexes. *Nat. Commun.* **2015**, *6*, 6052.

https://doi.org/10.1038/ncomms7052.

(15) Batys, P.; Kivistö, S.; Lalwani, S. M.; Lutkenhaus, J. L.; Sammalkorpi, M. Comparing Water-Mediated Hydrogen-Bonding in Different Polyelectrolyte Complexes. *Soft Matter* **2019**, *15*, 7823–7831. https://doi.org/10.1039/c9sm01193e.

(16) Tabandeh, S.; Leon, L. Engineering Peptide-Based Polyelectrolyte Complexes with Increased Hydrophobicity. *Molecules* **2019**, *24*, 868. https://doi.org/10.3390/molecules24050868.

(17) Suarez-Martinez, P. C.; Batys, P.; Sammalkorpi, M.; Lutkenhaus, J. L. Time-Temperature and Time-Water Superposition Principles Applied to Poly(Allylamine)/Poly(Acrylic Acid) Complexes. *Macromolecules* **2019**, *52*, 3066–3074. https://doi.org/10.1021/acs.macromol.8b02512.

(18) Perry, S. L.; Leon, L.; Hoffmann, K. Q.; Kade, M. J.; Priftis, D.; Black, K. A.; Wong, D.; Klein, R. A.; Pierce, C. F.; Margossian, K. O.; et al. Chirality-Selected Phase Behaviour in Ionic Polypeptide Complexes. *Nat. Commun.* **2015**, *6*, 6052. https://doi.org/10.1038/ncomms7052.

(19) Hoffmann, K. Q.; Perry, S. L.; Leon, L.; Priftis, D.; Tirrell, M.; De Pablo, J. J. A Molecular View of the Role of Chirality in Charge-Driven Polypeptide Complexation. *Soft Matter* **2015**, *11*, 1525–1538. https://doi.org/10.1039/c4sm02336f.

(20) Pacalin, N. M.; Leon, L.; Tirrell, M. Directing the Phase Behavior of Polyelectrolyte Complexes Using Chiral Patterned Peptides. *Eur. Phys. J. Spec. Top.* **2016**, *225*, 1805–1815. https://doi.org/10.1140/epjst/e2016-60149-6.

(21) Sadman, K.; Wang, Q.; Chen, Y.; Keshavarz, B.; Jiang, Z.; Shull, K. R. Influence of Hydrophobicity on Polyelectrolyte Complexation. *Macromolecules* **2017**, *50*, 9417–9426. https://doi.org/10.1021/acs.macromol.7b02031.

(22) Zhao, M.; Zacharia, N. S. Sequestration of Methylene Blue into Polyelectrolyte Complex Coacervates. *Macromol. Rapid Commun.* **2016**, *37*, 1249–1255. https://doi.org/10.1002/marc.201600244.

(23) Zhou, K.; Zang, J.; Chen, H.; Wang, W.; Wang, H.; Zhao, G. On-Axis Alignment of Protein Nanocage Assemblies from 2D to 3D through the Aromatic Stacking Interactions of Amino Acid Residues. *ACS Nano* **2018**, *12*, 11323–11332. https://doi.org/10.1021/acsnano.8b06091.

(24) Kim, S.; Huang, J.; Lee, Y.; Dutta, S.; Young Yoo, H.; Mee Jung, Y.; Jho, Y.; Zeng, H.; Hwang, D. S. Complexation and Coacervation of Like-Charged Polyelectrolytes Inspired by Mussels. *Proc. Natl. Acad. Sci. U. S. A.* **2016**, *113*, E847–E853. https://doi.org/10.1073/pnas.1521521113.

(25) Adhikari, S.; Prabhu, V. M.; Muthukumar, M. Lower Critical Solution Temperature Behavior in Polyelectrolyte Complex Coacervates. *Macromolecules* **2019**, *52* (18), 6998–7004. https://doi.org/10.1021/acs.macromol.9b01201.

(26) Ali, S.; Prabhu, V. M. Characterization of the Ultralow Interfacial Tension in Liquid-Liquid Phase Separated Polyelectrolyte Complex Coacervates by the Deformed Drop Retraction Method. *Macromolecules* **2019**, *52* (19), 7495–7502.

https://doi.org/10.1021/acs.macromol.9b01491.

(27) Nichols, M. K.; Kumar, R. K.; Bassindale, P. G.; Tian, L.; Barnes, A. C.; Drinkwater, B. W.; Patil, A. J.; Mann, S. Fabrication of Micropatterned Dipeptide Hydrogels by Acoustic Trapping of Stimulus-Responsive Coacervate Droplets. *small* **2018**, *14* (26), 1800739. https://doi.org/10.1002/smll.201800739.

(28) Kayitmazer, A. B.; Koksal, A. F.; Kilic Iyilik, E. Complex Coacervation of Hyaluronic Acid and Chitosan: Effects of PH, Ionic Strength, Charge Density, Chain Length and the Charge Ratio. *Soft Matter* **2015**, *11* (44), 8605–8612. https://doi.org/10.1039/c5sm01829c.

(29) Meng, S.; Liu, Y.; Yeo, J.; Ting, J. M.; Tirrell, M. V; Tirrell, M. V. Effect of Mixed Solvents on Polyelectrolyte Complexes with Salt. *Colloid Polym Sci* **2020**, *298*, 887–894. https://doi.org/10.1007/s00396-020-04637-0.

(30) Zhang, H. Effects of Solution Composition (Salts, PH, Dielectric Constant) on Polyelectrolyte Complex (PEC) Formation and Their Properties, The University of Akron, 2018.

(31) Brennan, M. J.; Kilbride, B. F.; Wilker, J. J.; Liu, J. C. A Bioinspired Elastin-Based Protein for a Cytocompatible Underwater Adhesive. *Biomaterials* **2017**, *124*, 116–125. https://doi.org/10.1016/j.biomaterials.2017.01.034.

(32) Cui, C.; Fan, C.; Wu, Y.; Xiao, M.; Wu, T.; Zhang, D.; Chen, X.; Liu, B.; Xu, Z.; Qu, B.; et al. Water-Triggered Hyperbranched Polymer Universal Adhesives: From Strong Underwater Adhesion to Rapid Sealing Hemostasis. *Adv. Mater.* **2019**, *31* (49), 1–9. https://doi.org/10.1002/adma.201905761.

(33) Zhao, Q.; Lee, D. W.; Ahn, B. K.; Seo, S.; Kaufman, Y.; Israelachvili, J. N.; Waite, J. H. Underwater Contact Adhesion and Microarchitecture in Polyelectrolyte Complexes Actuated by Solvent Exchange. *Nat. Mater.* **2016**, *15*, 407–412. https://doi.org/10.1111/mec.13536.Application.

(34) Wang, W.; Xu, Y.; Li, A.; Li, T.; Liu, M.; Von Klitzing, R.; Ober, C. K.; Kayitmazer, A. B.; Li, L.; Guo, X. Zinc Induced Polyelectrolyte Coacervate Bioadhesive and Its Transition to a Self-Healing Hydrogel. *RSC Adv.* **2015**, *5* (82), 66871–66878. https://doi.org/10.1039/c5ra11915d.

(35) Vahdati, M.; Cedano-Serrano, F. J.; Creton, C.; Hourdet, D. Coacervate-Based Underwater Adhesives in Physiological Conditions. *ACS Appl. Polym. Mater.* **2020**, *2* (8), 3397–3410. https://doi.org/10.1021/acsapm.0c00479.

(36) Dompé, M.; Cedano-Serrano, F. J.; Heckert, O.; van den Heuvel, N.; van der Gucht, J.; Tran, Y.; Hourdet, D.; Creton, C.; Kamperman, M. Thermoresponsive Complex Coacervate-Based Underwater Adhesive. *Adv. Mater.* **2019**, *31* (21), 1808179. https://doi.org/10.1002/adma.201808179.

(37) Kim, H. J.; Choi, B. H.; Jun, S. H.; Cha, H. J. Sandcastle Worm-Inspired Blood-Resistant Bone Graft Binder Using a Sticky Mussel Protein for Augmented In Vivo Bone Regeneration. *Adv. Healthc. Mater.* **2016**, *5* (24), 3191–3202. https://doi.org/10.1002/adhm.201601169.

(38) Zhao, W.; Fan, Y.; Wang, H.; Wang, Y. Coacervate of Polyacrylamide and Cationic

Gemini Surfactant for the Extraction of Methyl Orange from Aqueous Solution. *Langmuir* **2017**, *33* (27), 6846–6856. https://doi.org/10.1021/acs.langmuir.7b01421.

(39) Zhang, Z.; Liu, Q.; Sun, Z.; Phillips, B. K.; Wang, Z.; Al-Hashimi, M.; Fang, L.; Olson, M. A. Poly-Lipoic Ester-Based Coacervates for the Efficient Removal of Organic Pollutants from Water and Increased Point-of-Use Versatility. *Chem. Mater.* **2019**, *31* (12), 4405–4417. https://doi.org/10.1021/acs.chemmater.9b00725.

(40) Valley, B.; Jing, B.; Ferreira, M.; Zhu, Y. Rapid and Efficient Coacervate Extraction of Cationic Industrial Dyes from Wastewater. *ACS Appl. Mater. Interfaces* **2019**, *11* (7), 7472–7478. https://doi.org/10.1021/acsami.8b21674.

(41) Chiappisi, L.; Simon, M.; Gradzielski, M. Toward Bioderived Intelligent Nanocarriers for Controlled Pollutant Recovery and PH-Sensitive Binding. *ACS Appl. Mater. Interfaces* **2015**, *7* (11), 6139–6145. https://doi.org/10.1021/am508846r.

(42) Hasanvand, E.; Rafe, A. Development of Vanillin/β-Cyclodexterin Inclusion Microcapsules Using Flax Seed Gum-Rice Bran Protein Complex Coacervates. *Int. J. Biol. Macromol.* **2019**, *131*, 60–66. https://doi.org/10.1016/j.ijbiomac.2019.03.066.

(43) Bosnea, L. A.; Moschakis, T.; Biliaderis, C. G. Microencapsulated Cells of Lactobacillus Paracasei Subsp. Paracasei in Biopolymer Complex Coacervates and Their Function in a Yogurt Matrix. *Food Funct.* **2017**, *8* (2), 554–562. https://doi.org/10.1039/c6fo01019a.

(44) Rocha-Selmi, G. A.; Bozza, F. T.; Thomazini, M.; Bolini, H. M. A.; Fávaro-Trindade, C. S. Microencapsulation of Aspartame by Double Emulsion Followed by Complex Coacervation to Provide Protection and Prolong Sweetness. *Food Chem.* **2013**, *139* (1–4), 72–78. https://doi.org/10.1016/j.foodchem.2013.01.114.

(45) Zhou, L.; Shi, H.; Li, Z.; He, C. Recent Advances in Complex Coacervation Design from Macromolecular Assemblies and Emerging Applications. *Macromol. Rapid Commun.* **2020**, *41* (21), 2000149. https://doi.org/10.1002/marc.202000149.

(46) Blocher, W. C.; Perry, S. L. Complex Coacervate-Based Materials for Biomedicine. *Wiley Interdiscip. Rev. Nanomedicine Nanobiotechnology* **2017**, *9* (4), 76–78. https://doi.org/10.1002/wnan.1442.

(47) Awada, H. K.; Hwang, M. P.; Wang, Y. Towards Comprehensive Cardiac Repair and Regeneration after Myocardial Infarction: Aspects to Consider and Proteins to Deliver. *Biomaterials* **2016**, *82*, 94–112. https://doi.org/10.1016/j.biomaterials.2015.12.025.

(48) Johnson, N. R.; Kruger, M.; Goetsch, K. P.; Zilla, P.; Bezuidenhout, D.; Wang, Y.; Davies, N. H. Coacervate Delivery of Growth Factors Combined with a Degradable Hydrogel Preserves Heart Function after Myocardial Infarction. *ACS Biomater. Sci. Eng.* **2015**, *1* (9), 753–759. https://doi.org/10.1021/acsbiomaterials.5b00077.

(49) De Silva, U. K.; Brown, J. L.; Lapitsky, Y. Poly(Allylamine)/Tripolyphosphate Coacervates Enable High Loading and Multiple-Month Release of Weakly Amphiphilic Anionic Drugs: An: In Vitro Study with Ibuprofen. *RSC Adv.* **2018**, *8* (35), 19409–19419. https://doi.org/10.1039/c8ra02588f.

(50) Drobot, B.; Iglesias-Artola, J. M.; Le Vay, K.; Mayr, V.; Kar, M.; Kreysing, M.; Mutschler, H.; Tang, T. Y. D. Compartmentalised RNA Catalysis in Membrane-Free

Coacervate Protocells. *Nat. Commun.* **2018**, *9* (1), 3643. https://doi.org/10.1038/s41467-018-06072-w.

(51) Martin, N.; Tian, L.; Spencer, D.; Coutable-Pennarun, A.; Anderson, J. L. R.; Mann, S. Photoswitchable Phase Separation and Oligonucleotide Trafficking in DNA Coacervate Microdroplets. *Angew. Chemie - Int. Ed.* **2019**, *58* (41), 14594–14598. https://doi.org/10.1002/anie.201909228.

(52) Banerjee, P. R.; Milin, A. N.; Moosa, M. M.; Onuchic, P. L.; Deniz, A. A. Reentrant Phase Transition Drives Dynamic Substructure Formation in Ribonucleoprotein Droplets. *Angew. Chemie - Int. Ed.* **2017**, *56* (38), 11354–11359. https://doi.org/10.1002/anie.201703191.

(53) Schuster, B. S.; Reed, E. H.; Parthasarathy, R.; Jahnke, C. N.; Caldwell, R. M.; Bermudez, J. G.; Ramage, H.; Good, M. C.; Hammer, D. A. Controllable Protein Phase Separation and Modular Recruitment to Form Responsive Membraneless Organelles. *Nat. Commun.* **2018**, *9* (1), 2985. https://doi.org/10.1038/s41467-018-05403-1.

(54) Aumiller, W. M.; Keating, C. D. Phosphorylation-Mediated RNA/Peptide Complex Coacervation as a Model for Intracellular Liquid Organelles. *Nat. Chem.* **2016**, *8* (2), 129–137. https://doi.org/10.1038/nchem.2414.

(55) Crowe, C. D.; Keating, C. D. Liquid–Liquid Phase Separation in Artificial Cells. *Interface Focus* **2018**, *8* (5), 20180032. https://doi.org/10.1098/rsfs.2018.0032.

(56) Banani, S. F.; Lee, H. O.; Hyman, A. A.; Rosen, M. K. Biomolecular Condensates: Organizers of Cellular Biochemistry. *Nat. Rev. Mol. Cell Biol.* **2017**, *18* (5), 285–298. https://doi.org/10.1038/nrm.2017.7.

(57) Deng, N. N.; Huck, W. T. S. Microfluidic Formation of Monodisperse Coacervate Organelles in Liposomes. *Angew. Chemie - Int. Ed.* **2017**, *56* (33), 9736–9740. https://doi.org/10.1002/anie.201703145.

(58) Liu, Y.; Momani, B.; Winter, H. H.; Perry, S. L. Rheological Characterization of Liquid-to-Solid Transitions in Bulk Polyelectrolyte Complexes. *Soft Matter* **2017**, *13*, 7332–7340. https://doi.org/10.1039/c7sm01285c.

(59) Winter, H. H. Glass Transition as the Rheological Inverse of Gelation. *Macromolecules* **2013**, *46*, 2425–2432. https://doi.org/10.1021/ma400086v.

(60) Spruijt, E.; Sprakel, J.; Lemmers, M.; Stuart, M. A. C.; Van Der Gucht, J. Relaxation Dynamics at Different Time Scales in Electrostatic Complexes: Time-Salt Superposition. *Phys. Rev. Lett.* **2010**, *105*, 208301. https://doi.org/10.1103/PhysRevLett.105.208301.

(61) Rubinstein, M.; Semenov, A. N. Dynamics of Entangled Solutions of Associating Polymers. *Macromolecules* **2001**, *34*, 1058–1068. https://doi.org/10.1021/ma0013049.

(62) Ali, S.; Prabhu, V. M. Relaxation Behavior by Time-Salt and Time-Temperature Superpositions of Polyelectrolyte Complexes from Coacervate to Precipitate. *Gels* **2018**, *4*, 11. https://doi.org/10.3390/gels4010011.

(63) Marciel, A. B.; Srivastava, S.; Tirrell, M. V. Structure and Rheology of Polyelectrolyte Complex Coacervates. *Soft Matter* **2018**, *14*, 2454–2464.

https://doi.org/10.1039/C7SM02041D.

(64) Hamad, F. G.; Chen, Q.; Colby, R. H. Linear Viscoelasticity and Swelling of Polyelectrolyte Complex Coacervates. *Macromolecules* **2018**, *51*, 5547–5555. https://doi.org/10.1021/acs.macromol.8b00401.

(65) Morin, F. J. Testing the Sticky Rouse Model for Polyelectrolyte Complex Coacervates, University of Pittsburgh, 2019.

(66) Yang, M.; Shi, J.; Schlenoff, J. B. Control of Dynamics in Polyelectrolyte Complexes by Temperature and Salt. *Macromolecules* **2019**, *52*, 1930–1941. https://doi.org/10.1021/acs.macromol.8b02577.

(67) Syed, V. M. S.; Srivastava, S. Time-Ionic Strength Superposition: A Unified Description of Chain Relaxation Dynamics in Polyelectrolyte Complexes. *ACS Macro Lett.* **2020**, *9* (7), 1067–1073. https://doi.org/10.1021/acsmacrolett.0c00252.

(68) Zhang, Y.; Batys, P.; O'Neal, J. T.; Li, F.; Sammalkorpi, M.; Lutkenhaus, J. L. Molecular Origin of the Glass Transition in Polyelectrolyte Assemblies. *ACS Cent. Sci.* **2018**, *4*, 638–644. https://doi.org/10.1021/acscentsci.8b00137.

(69) Sung, C.; Hearn, K.; Lutkenhaus, J. Thermal Transitions in Hydrated Layer-by-Layer Assemblies Observed Using Electrochemical Impedance Spectroscopy. *Soft Matter* **2014**, *10* (34), 6467–6476. https://doi.org/10.1039/c4sm01269k.

(70) Vidyasagar, A.; Sung, C.; Gamble, R.; Lutkenhaus, J. L. Thermal Transitions in Dry and Hydrated Layer-by-Layer Assemblies Exhibiting Linear and Exponential Growth. *ACS Nano* **2012**, *6* (7), 6174–6184. https://doi.org/10.1021/nn301526b.

(71) O'Neal, J. T.; Wilcox, K. G.; Zhang, Y.; George, I. M.; Lutkenhaus, J. L. Comparison of KBr and NaCl Effects on the Glass Transition Temperature of Hydrated Layer-by-Layer Assemblies. *J. Chem. Phys.* **2018**, *149* (16), 163319. https://doi.org/10.1063/1.5037491.

(72) Zhang, Y.; Li, F.; Valenzuela, L. D.; Sammalkorpi, M.; Lutkenhaus, J. L. Effect of Water on the Thermal Transition Observed in Poly(Allylamine Hydrochloride)-Poly(Acrylic Acid) Complexes. *Macromolecules* **2016**, *49*, 7563–7570. https://doi.org/10.1021/acs.macromol.6b00742.

(73) Zhang, R.; Zhang, Y.; Antila, H. S.; Lutkenhaus, J. L.; Sammalkorpi, M. Role of Salt and Water in the Plasticization of PDAC/PSS Polyelectrolyte Assemblies. **2017**. https://doi.org/10.1021/acs.jpcb.6b12315.

(74) Suarez-martinez, P. C.; Batys, P.; Sammalkorpi, M.; Lutkenhaus, J. L. Time–Temperature and Time–Water Superposition Principles Applied to Poly(Allylamine)/Poly(Acrylic Acid) Complexes. *Macromolecules* **2019**, *52*, 3066–3074. https://doi.org/10.1021/acs.macromol.8b02512.

(75) Yildirim, E.; Zhang, Y.; Lutkenhaus, J. L.; Sammalkorpi, M. Thermal Transitions in Polyelectrolyte Assemblies Occur via a Dehydration Mechanism. *ACS Macro Lett.* **2015**, *4*, 1017–1021. https://doi.org/10.1021/acsmacrolett.5b00351.

(76) Lyu, X.; Peterson, A. M. Humidity Tempering of Polyelectrolyte Complexes. *Macromolecules* **2018**, *51*, 10003–10010. https://doi.org/10.1021/acs.macromol.8b01367.

(77) Weinbreck, F.; Rollema, H. S.; Tromp, R. H.; De Kruif, C. G. Diffusivity of Whey Protein and Gum Arabic in Their Coacervates. *Langmuir* **2004**, *20* (15), 6389–6395. https://doi.org/10.1021/la049908j.

(78) Kayitmazer, A. B.; Strand, S. P.; Tribet, C.; Jaeger, W.; Dubin, P. L. Effect of Polyelectrolyte Structure on Protein - Polyelectrolyte Coacervates: Coacervates of Bovine Serum Albumin with Poly(Diallyldimethylammonium Chloride) versus Chitosan. *Biomacromolecules* **2007**, *8* (11), 3568–3577. https://doi.org/10.1021/bm700645t.

(79) Chodankar, S.; Aswal, V. K.; Kohlbrecher, J.; Vavrin, R.; Wagh, A. G. Structural Study of Coacervation in Protein-Polyelectrolyte Complexes. **2008**, No. July, 1–8. https://doi.org/10.1103/PhysRevE.78.031913.

(80) Chodankar, S.; Aswal, V. K.; Kohlbrecher, J.; Vavrin, R.; Wagh, A. G. Structural Evolution during Protein Denaturation as Induced by Different Methods. *Phys. Rev. E - Stat. Nonlinear, Soft Matter Phys.* **2008**, *77*, 031901. https://doi.org/10.1103/PhysRevE.77.031901.

(81) Spruijt, E.; Leermakers, F. A. M.; Fokkink, R.; Schweins, R.; Van Well, A. A.; Cohen Stuart, M. A.; Van Der Gucht, J. Structure and Dynamics of Polyelectrolyte Complex Coacervates Studied by Scattering of Neutrons, X-Rays, and Light. *Macromolecules* **2013**, *46* (11), 4596–4605. https://doi.org/10.1021/ma400132s.

(82) Markarian, M. Z.; Hariri, H. H.; Reisch, A.; Urban, V. S.; Schlenoff, J. B. A Small-Angle Neutron Scattering Study of the Equilibrium Conformation of Polyelectrolytes in Stoichiometric Saloplastic Polyelectrolyte Complexes. *Macromolecules* **2012**, *45* (2), 1016–1024. https://doi.org/10.1021/ma2022666.

(83) Fares, H. M.; Ghoussoub, Y. E.; Delgado, J. D.; Fu, J.; Urban, V. S.; Schlenoff, J. B. Scattering Neutrons along the Polyelectrolyte Complex/Coacervate Continuum. *Macromolecules* **2018**, *51*, 4945–4955. https://doi.org/10.1021/acs.macromol.8b00699.

(84) Vieregg, R.; Lueckheide, M.; Marciel, A. B.; Leon, L.; Bologna, A. J.; Rivera, J. R.; Tirrell, M. V. Oligonucleotide − Peptide Complexes: Phase Control by Hybridization. **2018**. https://doi.org/10.1021/jacs.7b03567.

(85) Srivastava, D.; Muthukumar, M. Interpenetration of Interacting Polyelectrolytes. *Macromolecules* **1994**, *27* (6), 1461–1465. https://doi.org/10.1021/ma00084a028.

(86) Rubinstein, M.; Liao, Q.; Panyukov, S. Structure of Liquid Coacervates Formed by Oppositely Charged Polyelectrolytes. *Macromolecules* **2018**, *51* (23), 9572–9588. https://doi.org/10.1021/acs.macromol.8b02059.

(87) Voorn, M. J. Complex Coacervation, 1956. https://doi.org/10.1002/jcp.1030490404.

(88) Tainaka, K. Effect of Counterions on Complex Coacervation. *Biopolymers* **1980**, *19* (7), 1289–1298. https://doi.org/10.1002/bip.1980.360190705.

(89) Spruijt, E.; Westphal, A. H.; Borst, J. W.; Stuart, M. A. C. Binodal Compositions of Polyelectrolyte Complexes. *Macromolecules* **2010**, *43*, 6476–6484. https://doi.org/10.1021/ma101031t.

(90) Jha, P. K.; Desai, P. S.; Li, J.; Larson, R. G. PH and Salt Effects on the Associative Phase

Separation of Oppositely Charged Polyelectrolytes. *Polymers (Basel).* **2014**, *6* (5), 1414–1436. https://doi.org/10.3390/polym6051414.

(91) Veis, A.; Bodor, E.; Mussell, S. Molecular Weight Fractionation and the Self-suppression of Complex Coacervation. *Biopolymers* **1967**, *5*, 37–59. https://doi.org/10.1002/bip.1967.360050106.

(92) Qin, J.; Priftis, D.; Farina, R.; Perry, S. L.; Leon, L.; Whitmer, J.; Hoffmann, K.; Tirrell, M.; De Pablo, J. J. Interfacial Tension of Polyelectrolyte Complex Coacervate Phases. *ACS Macro Lett.* **2014**, *3* (6), 565–568. https://doi.org/10.1021/mz500190w.

(93) Spruijt, E.; Sprakel, J.; Cohen Stuart, M. A.; Van Der Gucht, J. Interfacial Tension between a Complex Coacervate Phase and Its Coexisting Aqueous Phase. *Soft Matter* **2009**, *6*, 172–178. https://doi.org/10.1039/b911541b.

(94) Salehi, A.; Larson, R. G. A Molecular Thermodynamic Model of Complexation in Mixtures of Oppositely Charged Polyelectrolytes with Explicit Account of Charge Association/Dissociation. *Macromolecules* **2016**, *49* (24), 9706–9719. https://doi.org/10.1021/acs.macromol.6b01464.

(95) Danielsen, S. P. O.; McCarty, J.; Shea, J. E.; Delaney, K. T.; Fredrickson, G. H. Small Ion Effects on Self-Coacervation Phenomena in Block Polyampholytes. *J. Chem. Phys.* **2019**, *151*, 034904. https://doi.org/10.1063/1.5109045.

(96) Kudlay, A.; Ermoshkin, A. V.; De La Cruz, M. O. Complexation of Oppositely Charged Polyelectrolytes: Effect of Ion Pair Formation. *Macromolecules* **2004**, *37* (24), 9231–9241. https://doi.org/10.1021/ma048519t.

(97) Kudlay, A.; De la Cruz, M. O. Precipitation of Oppositely Charged Polyelectrolytes in Salt Solutions. *J. Chem. Phys.* **2004**, *120*, 404–412. https://doi.org/10.1063/1.1629271.

(98) Perry, S. L.; Sing, C. E. PRISM-Based Theory of Complex Coacervation: Excluded Volume versus Chain Correlation. *Macromolecules* **2015**, *48* (14), 5040–5053. https://doi.org/10.1021/acs.macromol.5b01027.

(99) Lytle, T. K.; Salazar, A. J.; Sing, C. E. Interfacial Properties of Polymeric Complex Coacervates from Simulation and Theory. *J. Chem. Phys.* **2018**, *149*, 163315. https://doi.org/10.1063/1.5029934.

(100) Adhikari, S.; Leaf, M. A.; Muthukumar, M. Polyelectrolyte Complex Coacervation by Electrostatic Dipolar Interactions. *J. Chem. Phys.* **2018**, *149*, 163308. https://doi.org/10.1063/1.5029268.

(101) Zhang, P.; Shen, K.; Alsaifi, N. M.; Wang, Z. G. Salt Partitioning in Complex Coacervation of Symmetric Polyelectrolytes. *Macromolecules* **2018**, *51* (15), 5586–5593. https://doi.org/10.1021/acs.macromol.8b00726.

(102) Radhakrishna, M.; Basu, K.; Liu, Y.; Shamsi, R.; Perry, S. L.; Sing, C. E. Molecular Connectivity and Correlation Effects on Polymer Coacervation. *Macromolecules* **2017**, *50* (7), 3030–3037. https://doi.org/10.1021/acs.macromol.6b02582.

(103) Wang, Q.; Schlenoff, J. B. The Polyelectrolyte Complex/Coacervate Continuum. *Macromolecules* **2014**, *47*, 3108–3116. https://doi.org/10.1021/ma500500q.

(104) Lytle, T. K.; Radhakrishna, M.; Sing, C. E. High Charge Density Coacervate Assembly via Hybrid Monte Carlo Single Chain in Mean Field Theory. *Macromolecules* **2016**, *49* (24), 9693–9705. https://doi.org/10.1021/acs.macromol.6b02159.

(105) Sing, C. E.; Perry, S. L. Recent Progress in the Science of Complex Coacervation. *Soft Matter* **2020**, *16* (12), 2885–2914. https://doi.org/10.1039/d0sm00001a.

(106) Perry, S. L. Phase Separation: Bridging Polymer Physics and Biology. *Curr. Opin. Colloid Interface Sci.* **2019**, *39*, 86–97. https://doi.org/10.1016/j.cocis.2019.01.007.

(107) Vieregg, J. R.; Lueckheide, M.; Marciel, A. B.; Leon, L.; Bologna, A. J.; Rivera, J. R.; Tirrell, M. V. Oligonucleotide-Peptide Complexes: Phase Control by Hybridization. *J. Am. Chem. Soc.* **2018**, *140*, 1632–1638. https://doi.org/10.1021/jacs.7b03567.

(108) Chambon, F.; Petrovic, Z. S.; MacKnight, W. J.; Winter, H. H. Rheology of Model Polyurethanes at the Gel Point. *Macromolecules* **1986**, *19* (8), 2146–2149. https://doi.org/10.1021/ma00162a007.

(109) Chang, L. W.; Lytle, T. K.; Radhakrishna, M.; Madinya, J. J.; Vélez, J.; Sing, C. E.; Perry, S. L. Sequence and Entropy-Based Control of Complex Coacervates. *Nat. Commun.* **2017**, *8*, 1273. https://doi.org/10.1038/s41467-017-01249-1.

(110) Sun, J.; Perry, S. L.; Schiffman, J. D. Electrospinning Nanofibers from Chitosan/Hyaluronic Acid Complex Coacervates. *Biomacromolecules* **2019**, *20* (11), 4191–4198. https://doi.org/10.1021/acs.biomac.9b01072.

(111) Gu, Y.; Huang, X.; Wiener, C. G.; Vogt, B. D.; Zacharia, N. S. Large-Scale Solvent Driven Actuation of Polyelectrolyte Multilayers Based on Modulation of Dynamic Secondary Interactions. *ACS Appl. Mater. Interfaces* **2015**, *7* (3), 1848–1858. https://doi.org/10.1021/am507573m.

(112) Dubas, S. T.; Schlenoff, J. B. Factors Controlling the Growth of Polyelectrolyte Multilayers. *Macromolecules* **1999**, *32* (24), 8153–8160. https://doi.org/10.1021/ma981927a.

(113) Borges, J.; Mano, J. F. Molecular Interactions Driving the Layer-by-Layer Assembly of Multilayers. *Chem. Rev.* **2014**, *114* (18), 8883–8942. https://doi.org/10.1021/cr400531v.

(114) Kim, B. S.; Lebedeva, O. V.; Koynov, K.; Gong, H.; Glasser, G.; Lieberwith, I.; Vinogradova, O. I. Effect of Organic Solvent on the Permeability and Stiffness of Polyelectrolyte Multilayer Microcapsules. *Macromolecules* **2005**, *38* (12), 5214–5222. https://doi.org/10.1021/ma050493y.

(115) Gu, Y.; Zacharia, N. S. Self-Healing Actuating Adhesive Based on Polyelectrolyte Multilayers. *Adv. Funct. Mater.* **2015**, *25* (24), 3785–3792. https://doi.org/10.1002/adfm.201501055.

(116) Gu, Y.; Ma, Y.; Vogt, B. D.; Zacharia, N. S. Contraction of Weak Polyelectrolyte Multilayers in Response to Organic Solvents. *Soft Matter* **2016**, *12* (6), 1859–1867. https://doi.org/10.1039/c5sm02313k.

Chapter 2. Mechanism of Solid-Liquid Transition in Polyelectrolyte Complexes

2.1 Introduction

Since the very early study on the complexation behavior of polyelectrolytes by Bungenberg de Jong in 1929,[1] polyelectrolyte complexes have received continued scientific interest due to its increasingly recognized occurrence in biological and natural systems,[2–7] as well in a variety of emerging applications in biopharmaceuticals, underwater adhesives, and consumer products.[8–15] One intriguing attribute of PECs is that their physical states can span from glassy solids to low-viscosity liquids (coacervates). However, upon the selection of a polycation and a polyanion, this outcome remains unpredictable, and a molecular level understanding of how polyelectrolytes govern self-assembly, hierarchical structures, and material properties remains somewhat elusive.[16,17] PEC studies on experiments, simulations, and theory have found that these oppositely charged polymeric assemblies are dependent not only on the features of the polymer chains, for instance, the chemical structure of the monomers,[18] chain length,[19] ion-pairing strength,[20] charge density[21] and monomer sequence,[22–26] but also on the resulting non-covalent interactions, such as chirality,[27–29] hydrophobicity,[21,30] hydrogen bonding,[31–33] cation-π interactions,[34] and π-π stacking.[35,36] The intricate balance of these underlying chemical contributions underpins the rich diversity observed in PEC materials that ultimately motivates interdisciplinary research efforts across polymer physics, interface and colloid science, cell biology, and supramolecular assembly. In addition to the starting polymeric materials and the resultant noncovalent driving forces, another factor that complicates the attributes of the complexes is the external environment. As a class of

"smart" materials, PECs can respond to various stimuli in water, with salt as one of the most frequently employed agents. In a PEC, polycations and polyanions are believed to interact through forming *intrinsic* ion pairs. With the addition of salt, these pairings between polyelectrolyte segments are broken and compensated by the salt counterions, which transform them into *extrinsic* pairs. Over the decades, numerous efforts were dedicated to exploring how the physical properties of PECs (e.g., structure, dynamics, phase behavior, and thermal transition) can be tuned by adjusting salt content.[37,38] A recent report by Wang *et al.* demonstrated that salt, as a plasticizing agent, can continuously drive the phase transformation of a strongly interacting PEC system, from solid precipitates to liquid coacervates, and eventually, to homogenous solutions.[39] This key finding has enabled new research directions in better characterizing universal PEC properties over the entire complex/coacervate continuum,[40] exploring the mechanism of the phase transition between these two physical states,[41] modulating the phase change process through manipulating other environmental factors[42] and pinpointing the role of the water molecule arrangement around ion pairs in facilitating thermal transitions for pH-sensitive and pH-independent PECs alike.[43]

Despite these recent advances in PECs, our understanding of this class of materials is still incomplete in many aspects. Although bio-inspired liquid coacervates are highly investigated, solid-state PECs have received much less attention. Secondly, typical experimental works on PECs have only characterized one or two aspects in detail. Few of them have employed multiple tools in an integrated way to elucidate the connections among structures and properties of PECs. Furthermore, because many foundational models and theories were established from a limited selection of commercially available polyelectrolytes, secondary interactions that control self-assembly are seldomly inspected. As an example, we have recently made a rigorous comparison of the classic Voorn-Overbeek model with data on the phase behavior and salt partitioning of a

model PEC comprising a pair of charged hydrophilic peptides, in order to mitigate potential hydrophobic effects in influencing phase behavior.[44] Thus, to obtain more general and comprehensive results toward the goal of fine-tuning PEC materials to meet technological application needs, systematic repertoires of synthetic charged systems with controllable molecular structures are required.

Here, we address the above-mentioned gaps by extensively characterizing the physical assembly of a synthetic model PEC system throughout its complex/coacervate continuum, combining controlled polymer synthesis, optical imaging, rheology, thermal analysis, synchrotron scattering, and cryogenic imaging. This PEC system was designed to deliberately comprise two strong (pH-invariant) styrenic polyelectrolytes, poly[(vinylbenzyl) trimethylammonium chloride] (PVBTMA) and poly[sodium 4-styrenesulfonate] (PSS), at similar overall chain lengths and low dispersity in the chain length distributions. To our surprise, we found that the physical behavior of this PEC material was remarkably different from other reported systems in terms of physical appearance, mechanical properties, phase behavior, and structure. We first employed small amplitude oscillatory shear (SAOS) linear viscoelastic measurements to evaluate mechanical response and physical states (i.e., whether the sample was a solid or liquid) at various added salt and thermal conditions. Counterintuitively, in the solid phase, the PECs became stiffer as salt concentration and/or temperature increased; at a certain salt or temperature threshold, these PECs transitioned into a viscoelastic liquid before eventually becoming a one-phase solution. Complementary small-angle X-ray scattering (SAXS), cryogenic transmission electron microscopy (cryo-TEM), and thermogravimetric analysis (TGA) were then employed to probe the polyelectrolyte structure, as well as water and salt content in both complex and supernatant phases comprising this PVBTMA/PSS system. Together, the conformation, rheological response, and

composition profile demonstrated excellent agreement and elucidated an integrated mechanism that captures the unusual stimuli-responsive behavior of this PEC system.

2.2 Experimental Details

2.2.1 Materials

The following chemicals were reagent grade and used as received unless otherwise specified: 4-cyano-4-(phenylcarbonothioylthio) pentanoic acid (CPhPA, Sigma), (vinylbenzyl)trimethylammonium chloride (VBTMA, Sigma, 99%), 2,2'-azobis[2-(2-imidazolin-2-yl)propane]dihydrochloride (VA-044, Wako Chemicals, USA), acetic acid (glacial, Sigma, ≥99.85%), sodium acetate trihydrate (Sigma, ≥99%), SnakeSkin dialysis tubing (MWCO 3.5K, 22 mm, Thermo Scientific), poly(styrene sulfonate, sodium salt) (PSS, 20,700 g/mol, Polymer Standards Service), and sodium bromide (Fisher Scientific, >99%). The acetate buffer solution was prepared with 0.1 M acetic acid and 0.1 M sodium acetate trihydrate (0.1 M) (42/158, *v/v*) at pH 5.2. All water used during the experiment was filtered from a Milli-Q water purification system at a resistivity of 18.2 MΩ-cm at 25 °C.

2.2.2 Polymer Synthesis

The chemical structures of PVBTMA and PSS are shown in Figure 2.1. PSS_{100} was used as received. $PVBTMA_{100}$ (where the subscript denotes the degree of polymerization) was synthesized with aqueous reversible addition-fragmentation chain transfer (RAFT) polymerization to be approximately symmetric to PSS, based on previous work in our group.[45] Desired amount of VA-044 initiator (0.015 mmol, 0.00485 g), VBTMA monomer (15 mmol, 3.18 g), and CPhPA

chain transfer agent (0.15 mmol, 0.0419 g) were added to 15 mL acetate buffer solution in a dried 25 mL round bottom flask, maintaining molar equivalence of 1:1000:10 of initiator to monomer to chain transfer agent, respectively. The flask was then sealed, degassed with dried nitrogen, and heated at 50 °C and constant stirring for at least 21 h. The reaction was then cooled to room temperature and opened to air to obtain the crude pink polymer. Afterward, the crude polymer was dialyzed against Milli-Q water for 4 cycles of 8 h each. In the end, the samples were lyophilized and we achieved ca. 2.5 g polymer.

Figure 2. 1: Chemical structures of (a) PVBTMA and (b) PSS.

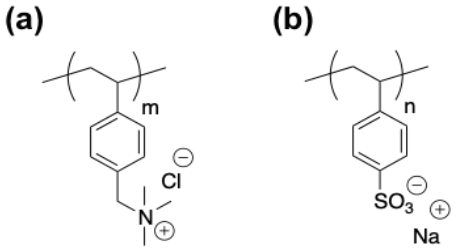

2.2.3 PEC Sample Preparation

PECs were prepared under 1:1 stoichiometric charge-matched conditions between polycation and polyanion. The “as prepared” polymer concentration was fixed at 1 wt%. Stock solutions of polycations and polyanions were added sequentially to a solution with desired amount of NaBr stock solution (5 M) and Milli-Q water in Eppendorf Tubes. Samples were then immediately vortexed for at least 30 s.

2.2.4 Optical Light Microscopy Imaging

Optical phase contrast microscopy (Leica DMI 6000B using Leica Application Suite (LAS) image acquisition software, Wetzlar, Germany) was used to directly visualize PEC samples at

microscale. PEC samples were first prepared in 1.5 mL microcentrifuge tubes and immediately 100 μL of the samples were transferred into ultra-low attachment 96-well plates (Costar, Corning Inc.). To prevent water evaporation, the plates were carefully sealed. Imaging was performed one day after the sample preparation in order to make sure that phase separation was largely completed. The contrast of the acquired images was then enhanced with ImageJ software for visual clarity.

2.2.5 Rheology

Rheology experiments were performed on a strain-controlled ARES-G2 rheometer (TA Instruments). An 8 mm parallel plate was used as top geometry. For room-temperature measurements, a Peltier plate was coupled as bottom geometry. A solvent trap attachment, together with Kimwipe straps soaked with water, were used to keep the environment moisturized and to ensure minimal water evaporation during the measurement. For measurements with changing temperature, an 8 mm parallel plate was used as bottom geometry, and oil was used to seal the sample and prevent drying. After the samples were prepared following the *PEC Sample Preparation* protocols, they were centrifuged for 15 mins at 4000 × *g* and aged for one day in a sealed sample container. Afterward, the complex phase was carefully extracted and then loaded onto the bottom geometry. The applied strain amplitude in the frequency sweep measurements was between 0.1% to 1%, which was confirmed by strain sweep experiments to be within the linear viscoelastic regime.

2.2.6 Small-Angle X-ray Scattering

Small-angle X-ray scattering measurements were carried out at beamline 12-ID-B in Advanced Photon Source (APS) at Argonne National Laboratory (ANL). The beamline has 13

keV X-rays with a q-range of 0.002-0.5 $Å^{-1}$, and the distance between sample and detector was set to 4 m. Exposure times were maintained at 0.1 s, and experiments were conducted at 25 °C. The complexes were prepared in the Eppendorf Tubes following the *PEC Sample Preparation* protocol. After that, these complexes were centrifuged for 15 mins at 4000 × g and aged for one day in a sealed sample container. Afterward, the complex phase materials were scooped out and carefully loaded to the small holes on a metal strip. The holes were then sealed by Kapton tape (Fisher Scientific Company) on both sides to ensure minimal water loss. With the SAXSLee package at beamline 12-ID-B, 2D images generated experimentally were converted into the $q = \frac{4\pi}{\lambda} \sin(\frac{\theta}{2})$ scattering vector, where λ and θ are the X-ray incident wavelength and scattering angle, respectively. SAXS data were processed and analyzed using the Irena package.[46]

2.2.7 Cryogenic Transmission Electron Microscopy

Cryogenic transmission electron microscopy (cryo-TEM) was utilized to directly visualize solvated PEC samples. FEI (Thermal Fisher Scientific) with 16k CETA CCD Camera was used to image samples. A droplet of 3.5 μL samples were deposited on lacey carbon film grids (LC200-CU, Electron Microscopy Sciences, Hatfield, PA) that were plasma cleaned beforehand using Gatan Solarus for 30 s. The grids were then blotted for 1 s on the Vitrobot and then plunged and frozen in liquid ethane. Images were taken at magnifications of 120,000x and -3.0 μm defocus. ImageJ software was later used to enhance the contrast of the acquired images and to count the particles on images.

2.2.8 Thermogravimetric Analysis

After PEC samples were prepared with the *PEC Sample Preparation* method, they were centrifuged in the 1.5 mL Eppendorf tubes at 4000 × *g* for 15 min and aged for one day in a sealed sample container. Next, 20-30 μL of the supernatant and around 5-15 mg complex materials were extracted and transferred onto aluminum pans whose weights were recorded beforehand. After the samples were loaded, the weights of samples together with pans were measured again so that the mass of samples on the pans were determined. Then the pans with samples in them were carefully transferred into a Barnstead Thermolyne Furnace 1400. The furnace temperature was first set to 110 °C and held for 2.5 hr to evaporate all the water in the samples. The weights were measured again afterwards to estimate water mass. Next, the pans were placed back into the furnace once again and heated at 600 °C for 12 hr to burn away all the polymer contents. The weights were recorded the last time, from which we can calculate the burnt polymer mass as well as the remaining salt mass left on the aluminum pans. For each salt condition, at least three different repeating samples were measured. Dixon's Q test was performed later to identify and remove outliers.

2.3 Results and Discussions

2.3.1 Morphology of Polyelectrolyte Complexes

The PEC samples were prepared by mixing together water and stock solutions of NaBr, PVBTMA, and PSS sequentially, following the protocol of the *direct dissolution* method.[47] It is worth mentioning here that the salt we initially tried was NaCl because Na^+ and Cl^- ions matched

the counterions of PSS and PVBTMA, respectively. However, we found that adding up to 4.0 M NaCl did not visually affect the morphology of the PVBTMA/PSS solids (Figure 2.3). We then switched to NaBr since salts containing Br^- have previously shown stronger doping capabilities relative to salts containing Cl^-.[38] Although the counterion of the synthesized PVBTMA used in the subsequent studies was Cl^-, the effective number of added bromide anions ranged from 100 to 1000 times the chloride counterions on the polymer chains. Furthermore, we conducted counterion exchange of a small batch of PVBTMA-Cl to PVBTMA-Br and found that upon complexation with PSS, representative material compositions remained the same (Figure 2.4, Table 2.1). Thus, we believe that the resultant PEC properties were not influenced by this difference.

After all the solution components were mixed together and centrifuged, the complex phase was separated from the supernatant phase (Figure 2.2a). Interestingly, instead of being tough and dense glassy solids as seen in other PEC systems,[39] the undoped PVBTMA/PSS PECs formed soft, white, solid particulates that can flow along a spatula smoothly (Figure 2.2b). With increasing NaBr, we observed neither any significant increase in the complex phase volume, nor a sudden change into clear and fluid material, as reported in previous studies on other PEC systems.[39,40] This low-salt state persisted until 2.0 M NaBr. In the narrow 2.0 to 2.5 M window, we observed a change in the physical appearance in this PEC: there appeared to be an abrupt drop in the amount of complex formed. Also, at this higher salt regime, the texture of the complexes transformed from particulate-like into gel-like materials that can retain free-standing structures on a flat surface (Figure 2.2c). Optical microscopy enabled us to visualize the PEC morphologies at microscale with increasing NaBr content (Figure 2.2d). Images revealed opaque and cloudy aggregates in the low salt regime (0-1.5 M), characteristic features of solid precipitates. At the high salt regime (2.0-5.0 M), these complexes became transparent and amorphous structures, which coincided with what

we observed macroscopically. Above 5.5 M, these broke up into spherical liquid droplets and were completely dissolved into solution at 7.0 M NaBr. These optical images provide a qualitative way to show the distinct states that PVBTMA/PSS complexes can take on with added NaBr salt.

Figure 2. 2: Macroscopic and microscopic morphologies of PVBTMA/PSS doped with NaBr.

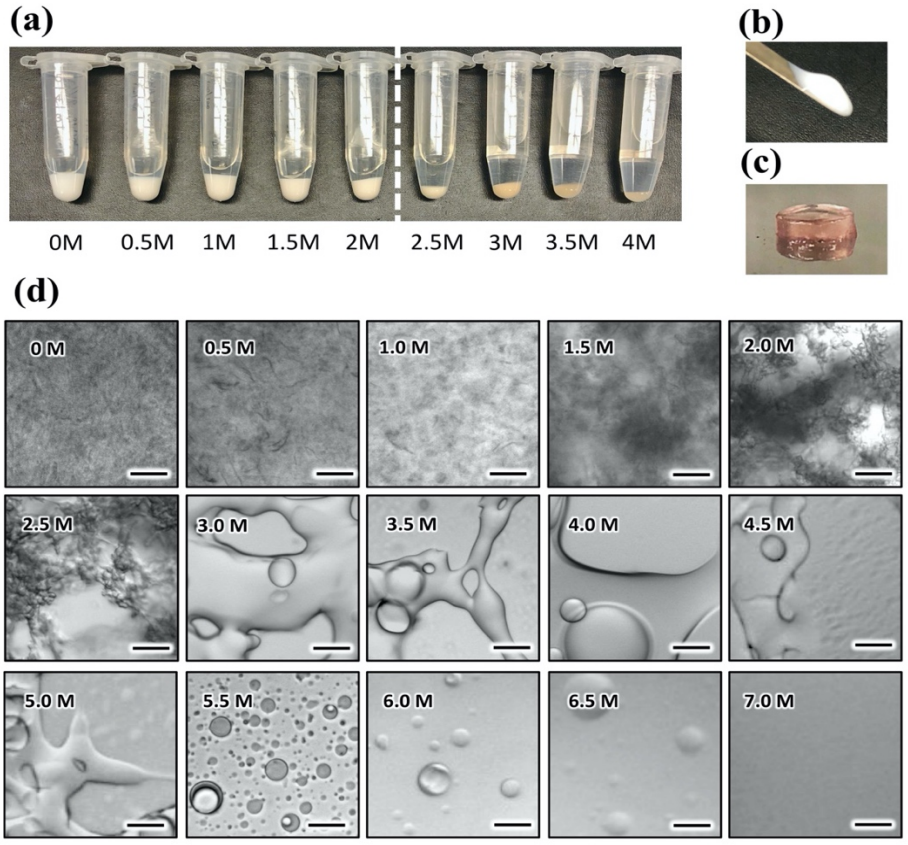

(a) Photographs of PVBTMA/PSS complexes after centrifugation under 0-4.0 M NaBr salt conditions. The dashed white line separates the low salt (≤ 2.0 M NaBr) and high salt (> 2.5 M NaBr) regimes, based on the macroscopic appearance of this PEC. (b) A picture of PVBTMA/PSS complex under 0 M NaBr. (c) A picture of PVBTMA/PSS under 3.0 M NaBr. (d) Optical micrographs of the complexes at 0-7.0 M. All scale bars denote 100 μm.

Figure 2. 3: Microscopical images of the PVBTMA/PSS complexes doped with NaCl.

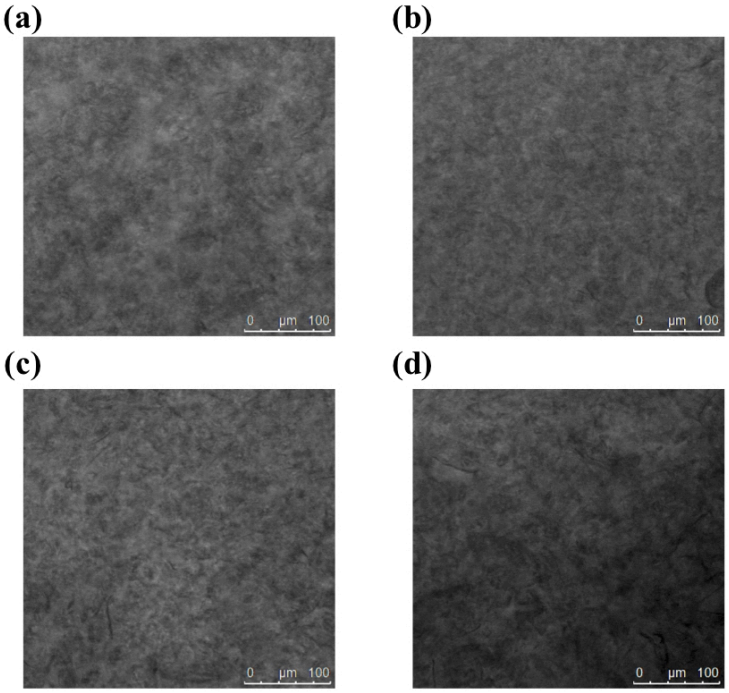

The salt concentrations are under (a) 1.0 M (b) 2.0 M (c) 3.0 M and (d) 4.0 M. All scale bars denote 100 µm

Figure 2. 4: Phase diagram for PVBTMA-Cl/PSS and PVBTMA-Br/PSS complex under 0, 0.5 and 1 M NaBr

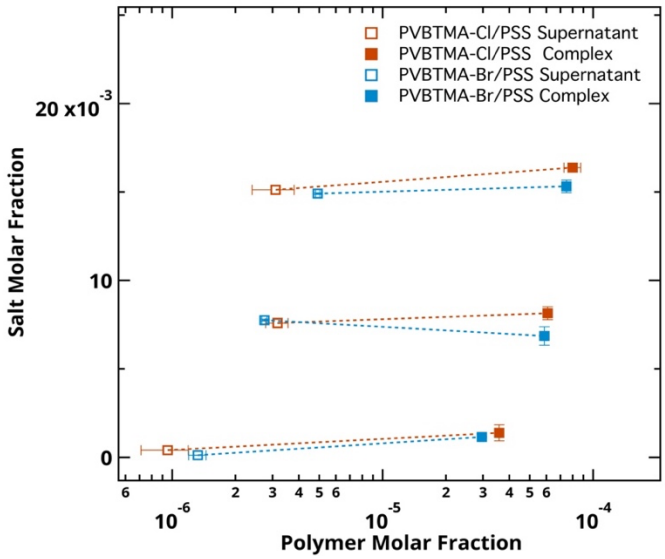

Table 2. 1: Molar percentage of water, polymer and salt component in the supernatant and complex of PVBTMA-Cl/PSS and PVBTMA-Br/PSS complex.

(PVBTMA-Cl/PSS and PVBTMA-Br/PSS complex are abbreviated as PVB-Cl and PVB-Br in the table.)

		Water		Polymer		Salt	
		PVB-Cl	PVB-Br	PVB-Cl	PVB-Br	PVB-Cl	PVB-Br
0M NaBr	Supernatant	99.96	99.99	9.51E-05	1.32E-04	0.04	0.01
	Complex	99.86	99.88	3.58E-03	2.96E-03	0.14	0.12
0.5M NaBr	Supernatant	99.24	99.22	3.16E-04	2.74E-04	0.76	0.78
	Complex	99.18	99.31	6.08E-03	5.87E-03	0.82	0.69
1M NaBr	Supernatant	98.49	98.51	3.10E-04	4.92E-04	1.51	1.49
	Complex	98.35	98.46	7.99E-03	7.47E-03	1.64	1.53

2.3.2 Salt and Temperature Effects on the Rheological Responses

Small amplitude oscillatory shear (SAOS) measurements enabled us to quantitatively determine further the physical states (i.e., solid precipitate or liquid coacervate), mechanical properties, and viscoelastic responses of the PECs under varying salt concentrations. As shown in Figure 2.5, from 0 M to 1.5 M NaBr, the complex displayed gel-like responses, with storage moduli (G') dominating over loss moduli (G'') throughout the entire measured frequency range and both moduli were independent of frequency (ω). At 2.0 M NaBr, G' and G'' curves varied slightly with frequency and demonstrated a trend to cross over at low frequency domain that is inaccessible to the rheometer, implying that this PEC started to transform into viscoelastic liquid state.

Figure 2. 5: Frequency sweep results for PECs under 0-2.0 M NaBr.

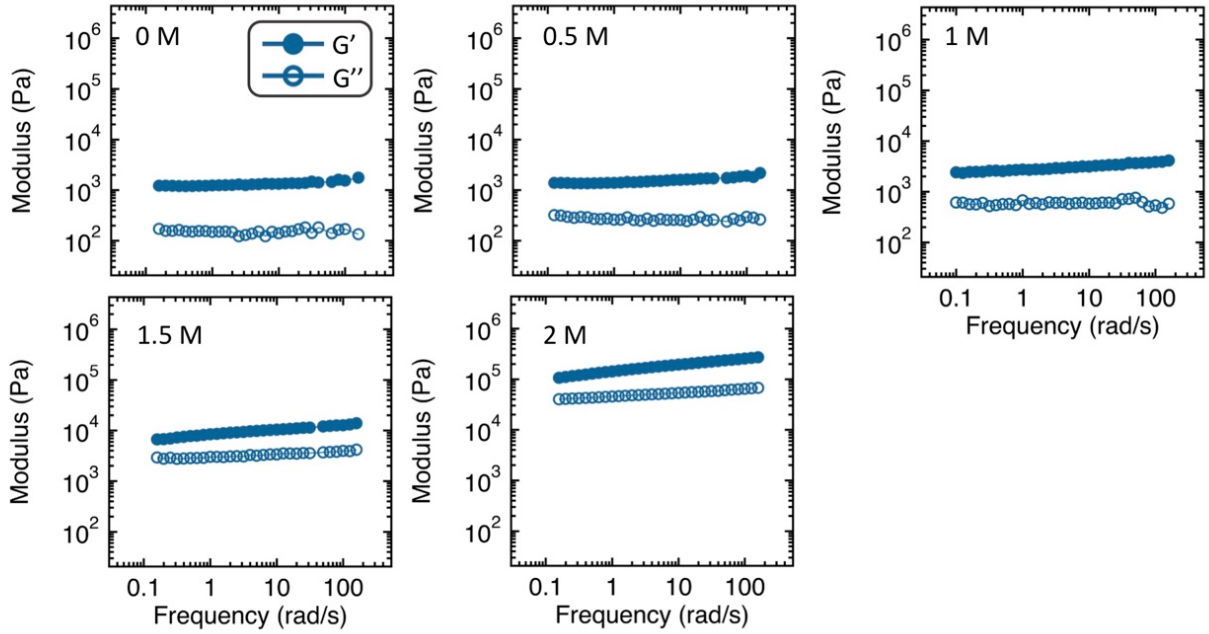

Numbers on each figure denoted the NaBr concentration under which the samples were prepared.

As seen in Figure 2.6 (a), we were intrigued that the frequency sweep data showed an increase in the magnitude of G' from ~10^3 to 10^5 Pa in modulus, with increasing NaBr concentration from 0 to 2.0 M. In other words, adding salt stiffened the complex by approximately two orders of magnitude. Such an observation is quite atypical for ionic assemblies and is contrary to recent experimental results in other PEC systems.[30,39,41] We believe that this distinct salt-stiffening trend originates from dehydration in the complex phase, which will be demonstrated in the following section. It is important to note here that in the undoped (0 M NaBr) state, the PVBTMA/PSS complex also stiffened at elevated temperature (20-50 °C), as shown in Figure 2.6 (b), completely analogous with the salt-stiffening tendency in SAOS.

Figure 2. 6: Storage modulus (G') versus frequency profiles for solid PVBTMA/PSS.

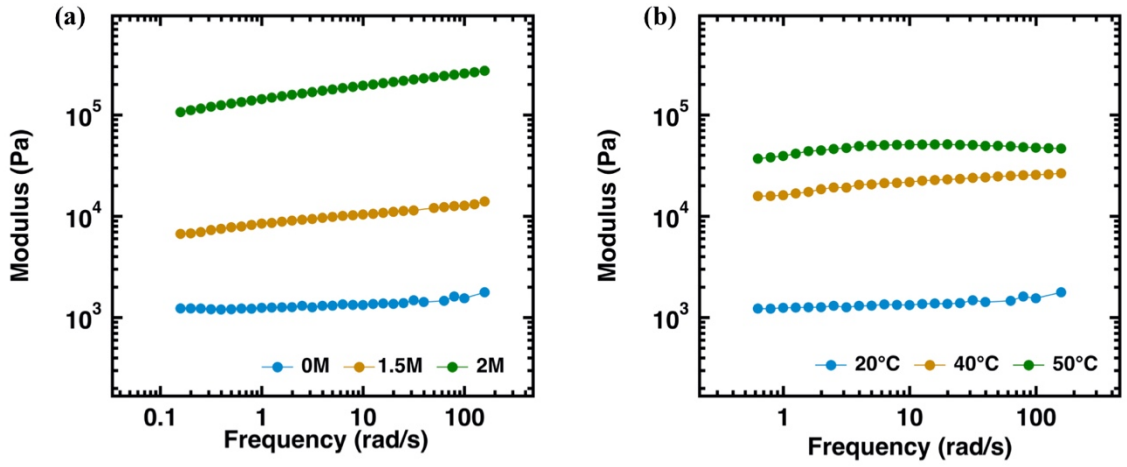

(a) Samples were prepared at 0 M (blue), 1.5 M (orange), and 2.0 M (green) NaBr under room temperature (set at 20 °C). (b) 0 M NaBr sample measured at 20 °C (blue), 40 °C (orange), and 50 °C (green). All experiments were conducted in the linear regime.

To explore further temperature effects on the mechanical properties of these complexes, we also conducted frequency sweep measurements under increasing temperatures for PECs self-assembled in 1.5 M and 2.0 M NaBr. We found that coupling temperature and salt alters the materials differently, as seen in Figure 2.7. Again, as in Figure 2.6b, in the undoped state, increasing temperature continuously drove the material to become stiffer. However, at 1.5 M, the PEC material demonstrated gel-like responses at the beginning (10 °C), with both G' and G'' being invariant with frequency. From 10 to 30 °C, they exhibited thermal-stiffening trend at first, but as temperature increased from 30 to 40 °C, it softened and started to show the tendency of shifting into viscoelastic liquid state (Figure 2.7a). In Figure 2.7b, at 2.0 M NaBr, the PEC first showed more solid-like response (G' > G'') in the probed frequency range at lower temperature (5 to 15 °C). From 15 to 55 °C, it softened and gradually appeared liquid-like behaviors as crossover points

between G' and G'' were observed. The crossover points gradually migrated to higher frequency domain, suggesting faster relaxation in chains with higher temperature.

Figure 2. 7: Frequency sweep measurements for PVBTMA/PSS under different temperatures.

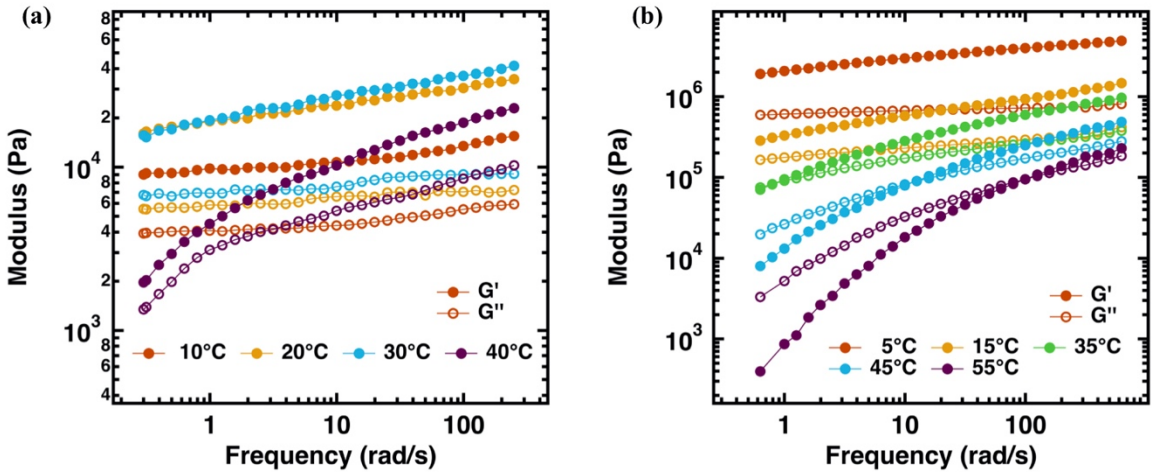

(a) Under 1.5 M NaBr at increasing temperatures from 10-40 °C and (b) 2.0 M NaBr at increasing temperatures from 5-55 °C. All experiments were conducted in the linear regime. Closed and open circles denote the storage (G') and loss (G") modulus, respectively.

At 2.5 M NaBr, the appearance of crossover point between G' and G'' indicated that the PEC displayed viscoelastic liquid characteristic at the measured frequency range (Figure 2.9a, Figure 2.8). This viscoelastic liquid response persisted until 4.0 M NaBr, the highest salt concentration we probed rheologically. From Figure 2.9a, we found that from 2.5 to 4.0 M NaBr, the crossover points shifted to higher frequency regime with increasing salt, meaning that chains were relaxing faster at higher salt concentrations. Following previous works that have shown analogies between salt and temperature in extending the range of probed timescales in chain dynamics,[19,48] we conducted time-salt superposition on these liquid samples to produce a master curve for the dynamic responses of this system in the liquid coacervate regime from 2.0 to 4.0 M

NaBr (Figure 2.9b). All frequency sweep curves for the liquid samples were shifted horizontally and vertically relative to the 2.0 M NaBr sample. This superposition performance extended the accessible frequency range by around four orders of magnitude. One feature we noticed here is that at low frequency, the data showed strong resemblance to the terminal region, with G' and G'' scaling as $\omega^2$and ω^1, respectively. Horizontal shift factors (a_S) obtained from the superposition have been utilized to quantity further the dynamics of polyelectrolyte coacervates.[19,48–53] We found that our data conformed reasonably well to the correlation $a_S \sim \exp\left(-\sqrt{c_{salt}}\right)$ anticipated by the sticky Rouse model (Figure 2.10a). Vertical shift factors (b_S) that dictated relative stiffness of the material under certain salt condition were gradually increasing as NaBr concentration went higher, except from 2.0 to 2.5 M NaBr (Figure 2.10b). This indicated that salt doping generally softened the PECs within the liquid coacervates regime, which displayed opposite trend to what we saw in the solid phase.

Figure 2. 8: Frequency sweep results for PECs under 2.5-4.0 M NaBr.

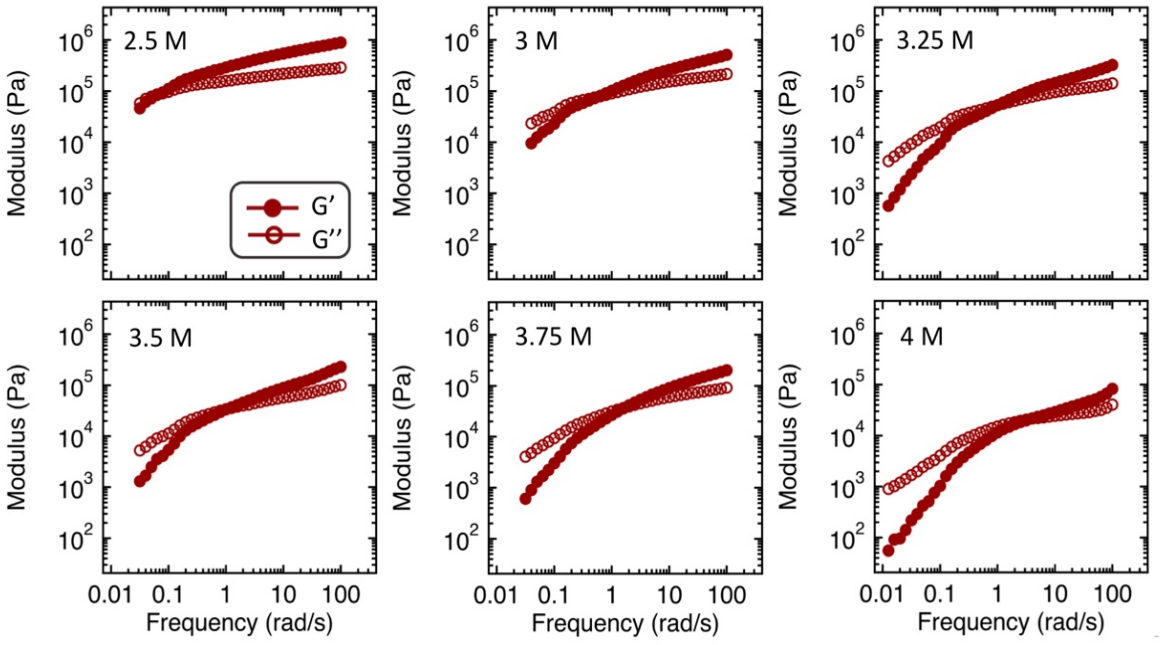

Numbers on each figure denoted the NaBr concentration under which the samples were prepared.

Figure 2. 9: Frequency sweep measurements for PVBTMA/PSS in liquid regime.

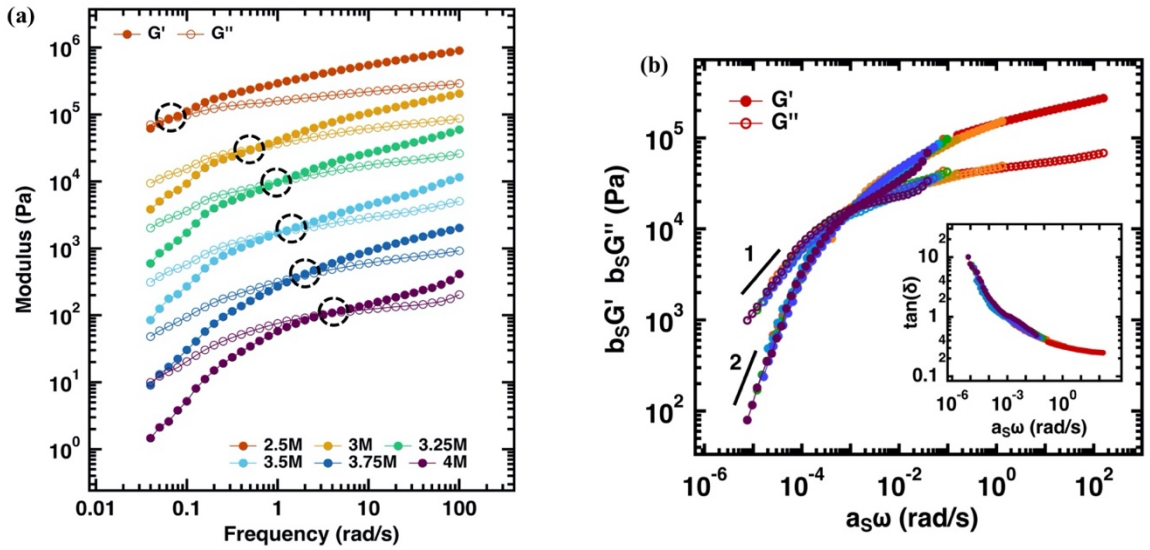

(a) Linear viscoelasticity of PVBTMA/PSS under 2.5-4.0 M NaBr. G' and G" crossover points are emphasized with dashed black circles. All experiments were conducted in the linear regime. For visual purposes, data under 3.0 M, 3.25 M, 3.5 M, 3.75 M and 4.0 M NaBr were shifted vertically by a factor of 0.3, 0.18, 0.05, 0.01, and 0.005, respectively. (b) Time-salt superposition of the frequency sweep data for the complexes in viscoelastic liquid regime (2.0-4.0 M NaBr). Data were shifted horizontally and vertically with respect to the curve of sample under 2.0 M. The slopes denoting a 2 and 1 scaling for G' and G", respectively, are shown as reference for terminal behavior associated with polymers.

Figure 2. 10: Horizontal and vertical shift factors for the time-salt superposition.

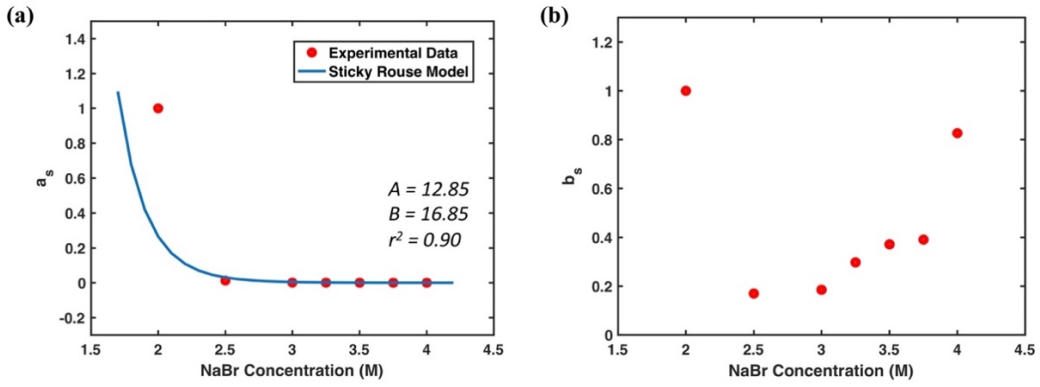

(a) Horizontal shift factors for the time-salt superposition as a function of salt concentration. The solid blue line represents fitting to the Sticky Rouse model. (b) Vertical shift factors for the time-salt superposition as a function of salt concentraton.

2.3.3 Water Composition and Binodal Phase Diagram

To investigate how the actual compositions of the complex correlate with their mechanical properties, we conducted thermogravimetric analysis (TGA) to quantify the exact distribution of water, polymer, and salt components in the complex and supernatant phases. As depicted in Figure 2.11(a), without any added salt, around 92 wt % of the complex was water. Compared with previous studies on other PEC systems,[16] this PVBTMA/PSS PEC system is highly solvated. Within the low-salt regime, the measured water content dropped drastically from 92 into 73 wt % as added NaBr increased from 0 to 2.0 M. This expulsion of water aligns with our previous observations in rheology: as the concentration of added salt increases, the complex assemblies become dehydrated and simultaneously stiffen. At the high-salt liquid coacervate regime, the water component becomes more stable and drops at a much slower rate from 73 to 56 wt% as NaBr increased to 5.5 M.

In terms of distinguishing salt and polymer content, the phase behaviors were very different between the solid and liquid states (Figure 2.11b). In the solid regime, polymer content increased with increasing salt. In addition, we note that the tie-lines are essentially flat, implying no selective partitioning of salt at this stage. In the liquid phase, polymer content continued to increase with increasing salt at first from 2.0 to 2.5 M NaBr. However, it started to decrease with salt starting from 2.5 M NaBr. The tie-lines are negatively sloped, demonstrating the preferential partitioning of salt into the supernatant phase. This trend is in sharp contrast to the Voorn-Overbeek model predictions of positively sloped tie-lines,[54] but matches with more recent studies on PECs comprising weakly charged polypeptides[23,25,44] and strongly charged polyelectrolytes.[41,55]

We emphasize here that the water displacement effect with added salt seems to deviate from classical PEC mechanisms, where salt doping induces the breaking of intrinsic ion pairs formed by oppositely charged polyelectrolytes and brings water molecules into the complex domain.[16] It is worth pointing out that salt-induced dehydration has also been reported in two previous studies on PECs comprising poly(diallyldimethylammonium) (PDADMA) and PSS at low salt concentrations, doped with NaCl[56] and KBr,[39] respectively. In the former study, the researchers attributed this dehydration to external osmotic pressure from additional NaCl. We believe that this explanation can also reasonably apply to the PVBTMA/PSS system. To be more specific, this unique salt responsivity is a result of the distinct physical nature of the PECs. In the previous rheological analysis, this PEC was shown to self-assemble into polyelectrolyte gel. As described by the Donnan theory used in numerous experimental and simulation studies,[57–60] polyelectrolyte gels generally demonstrate osmotic shrinking behaviors as the concentration of salt increases.

Figure 2. 11: Water content and phase behavior of PVBTMA/PSS doped with NaBr.

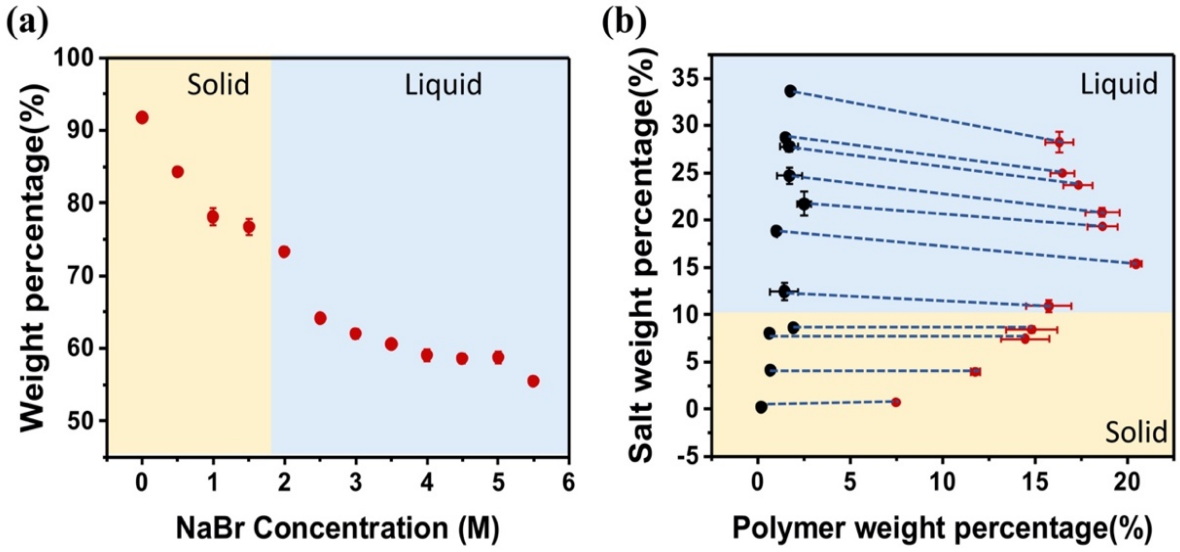

Figure 2.11 (continued)
(a) Weight percentage of water in the complex phase as a function of NaBr concentration. Red circles and error bars denote the mean and standard deviation of measurements, respectively. (b) Binodal curve for PVBTMA/PSS polyelectrolyte complex as a function of polymer and salt weight percentage. Black circles represent the supernatant phase, and red circles represent the complex phase. Error bars denote the standard deviation of multiple measurement results. Light yellow and light blue shaded backgrounds represent the solid phase and liquid phase samples, respectively, as determined by microscopy and rheology.

2.3.4 Structural Evolution Study by SAXS and Cryo-TEM

In this section, we aimed to unveil the structural evolution of the PVBTMA/PSS PEC system with salt doping using SAXS of the isolated complex phase. Figure 2.12(a) shows an overlay of vertically shifted scattering patterns for this system in the low-salt states. The intensity versus scattering vector (q) curves have three main regimes for the 0-1.5 M NaBr solid samples and two main regimes of interest for the 2 M NaBr sample. For the former, at intermediate q-range (the regime between dashed black lines in Figure 2.12a), a $I \sim q^{-4}$ dependency was observed, indicating that the polyelectrolyte chains aggregated into clusters with near-spherical conformation. As salt concentration increased, this intermediate q regime shifted to lower q range. We rationalize that this is due to salt ions loosening the intrinsic associations within the localized clusters and causing them to expand in size. The diameters of the clusters were estimated by $D_{Cluster} \approx 1/q^*$, where q^* was taken as the lower bound of the intermediate q regime for each salt concentration. The change in the diameter size from 5.9 to 14.3 nm as NaBr concentration increased from 0 to 2 M is shown in the inset of Figure 2.12a. At 2.0 M NaBr, the cluster size information exceeded the low q range of the SAXS instrument setup here.

Figure 2. 12: Background subtracted and vertically shifted SAXS profiles for PVBTMA/PSS complexes.

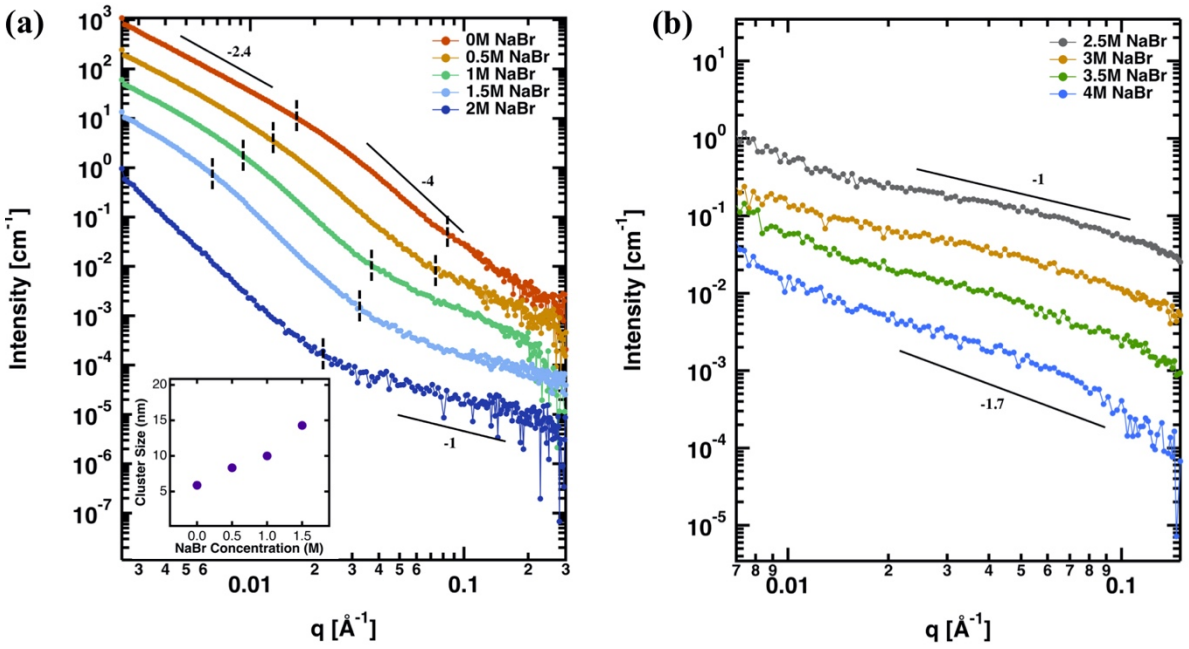

(a) under 0-2.0 M NaBr (the vertical black dashed lines denote the regimes for low, intermediate, and high q and the inset figure represents the cluster size corresponding to the intermediate regime on the plot as a function of salt concentration) and (b) under 2.5-4.0 M. NaBr.

In the low q regime of the PECs in Figure 2.12a, upturns were detected for all 0-1.5 M NaBr samples, indicating that the polyelectrolyte clusters further percolated into larger aggregates, and consequently, density fluctuations arising from hierarchical aggregation exist in these PECs. This idea of micron-sized particles scattering light is consistent with the white opaque physical appearance of the PEC samples. Finally, the high q regime exhibits a $I \sim q^{-1}$ correlation. This feature is ascribed to the association of a few individual polyelectrolyte chains into rigid rod structures.[61]

As shown in Figure 2.12b, at 2.5 – 4.0 M, the PECs displayed strikingly different SAXS profiles from the patterns in Figure 2.12a. In the intermediate and low q regime from about 0.01 to 0.1 Å^{-1} that matches with a length-scale of a few nanometers to tens of nanometers, the SAXS

curves display an $I \sim q^{-1}$ scaling that gradually shifts to $I \sim q^{-1.7}$ as salt increases from 2.5 to 4.0 M. We postulate that in this salt range, the polyelectrolyte chains no longer assemble into near spherical aggregates, but pair up into stiffer ladder-like arrangements at nanoscale.[62] Eventually, at 4.0 M NaBr, the polyelectrolyte chains behave as random-walk Gaussian coils. Additionally, the low q regime is not shown because the scattering signal from the sample overlaps with the background in this range (Figure 2.13 shows a representative pattern). This tells us that starting from 2.5 M NaBr, the coacervate became amorphous at micro- or even larger scale and no longer forms the spherical-like aggregates identified in the low-salt regime, which is consistent with their transparent appearance under optical microscope or by eye. It is important to emphasize the difference between this styrenic system and previously studied pairings. For instance, Marciel et al. reported on solid complexes comprising poly(lysine) and poly(glutamic acid) adopting a ladder-like conformation, induced by hydrogen-bonded β-sheets; in the SAXS patterns, low q upturns indicated the formation of large aggregates, which remained unchanged upon further salt addition.[61] By comparison, because PVBTMA and PSS do not have specific hydrogen bonding capability, potential hydrophobic effects and pi-pi stacking may instead drive the formation of the ladder-like structures in the viscoelastic liquid-like state. Further addition of salt resulted in a gradual transition to Gaussian chains, showing another key molecular difference between the peptide-based and synthetic systems.

Figure 2. 13: SAXS profiles for PVBTMA/PSS complexes under 2.5M NaBr.

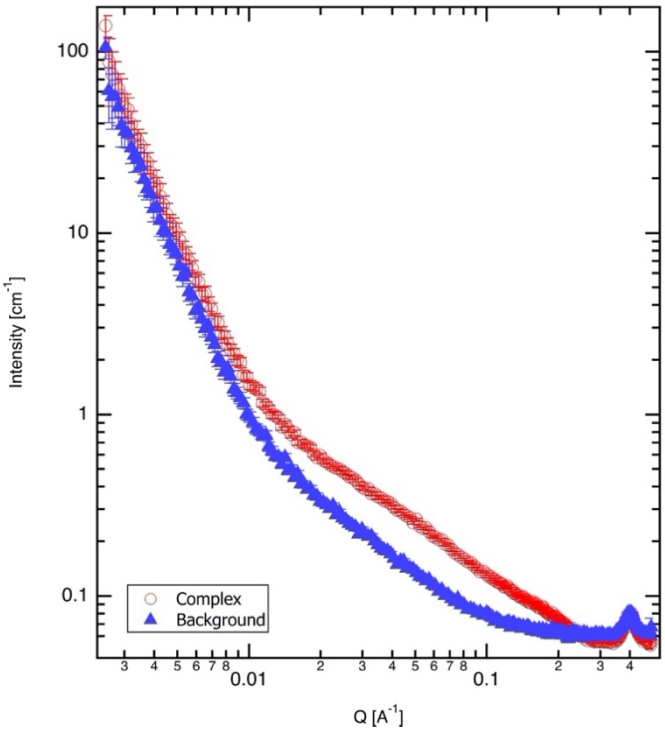

Red circles show the signals from the complex sample before background subtraction, including scattering from Kapton tape. Blue triangles are from the background (2.5 M NaBr solution with Kapton tape).

To confirm our interpretation of the SAXS results, we attempted to directly visualize the nanoscale PEC structures with cryo-TEM. It is important to note here that in order to guarantee the clear visualization under the microscope, the "as prepared" polymer concentration for the cryo-TEM samples was 1 mg/mL, which was 10 times more dilute than the SAXS samples. From the yellow circles on Figure 2.14a, the cryo-TEM image for the PVBTMA/PSS sample at 0 M NaBr were consisted of 1-3 nm structures resembling "cobble stones", which suggests the formation of local aggregations of polyelectrolyte chains and is consistent with the high *q* profile from SAXS. With the particle analysis function in ImageJ,[63] we were able to obtain the average dimensions of the smaller aggregate structures. Of the 2948 particles analyzed, the average maximum and

minimum distances between two points on individual particle boundaries are 2.6 nm and 1.6 nm, respectively. On a larger scale, we observe from the blue circles on Figure 2.14a that these tiny structures aggregate into larger near spherical clusters, consistent with the intermediate q profile from SAXS. The larger spherical clusters link with each other and formed interconnected branched structures (white outline on Figure 2.14a), corresponding to what we see in the low q regime on SAXS plot. Figure 2.14b shows a representative cryo-TEM image of the 3.0 M NaBr coacervate sample. No large aggregates were detected in this coacervate sample, which is in stark contrast to the solid complex shown in Figure 2.14a. We believe this cryo imaging over the entire coacervate sample revealed mostly solution background, although it is not possible to unambiguously conclude whether the texture is free polymer chains or not due to the low polymer concentration required for cryo imaging.

Figure 2. 14: Cryo-TEM images of PVBTMA/PSS complex.

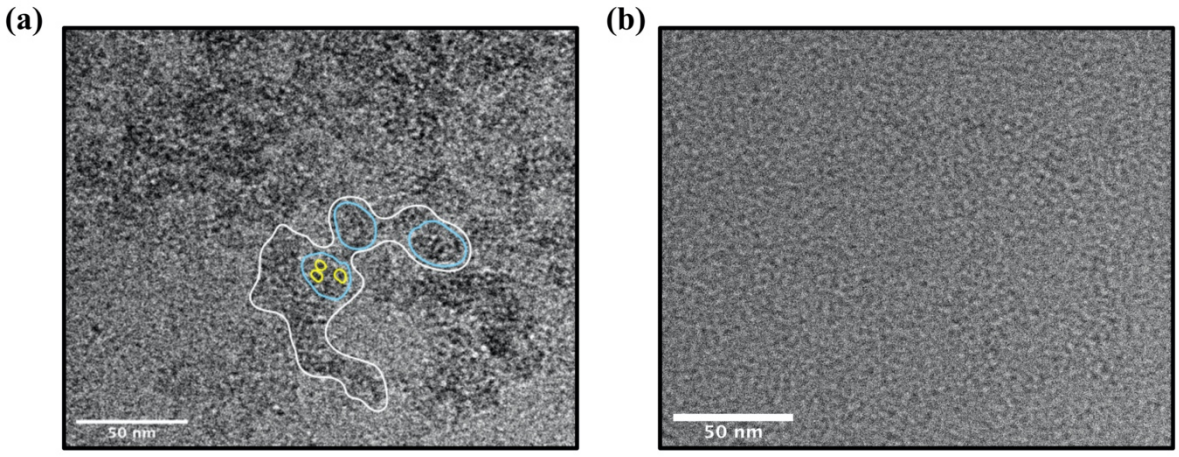

(a) under 0 M NaBr and (b) 3.0 M NaBr conditions (not adjusted in contrast). In (a), yellow circles show representative small "cobble stone" structures, blue circle show the larger near-spherical clusters, and white outline demonstrates large interconne
cted branched structures.

2.3.5 Proposed Mechanism for Solid-to-Liquid Phase Transition

Altogether, the combination of rheological responses, water composition, phase behavior, and structural analysis suggests a new mechanism of a salt-driven solid-to-liquid phase transition in PVBTMA/PSS complexes. As stated previously, we have identified a salt-stiffening phenomenon that can be explained by the decrease in water content and the reconfiguration of polyelectrolyte chain conformation within the complex phase. Figure 2.15 illustrates this idea. In the undoped state, the PEC is a soft solid gel composed of tightly coiled and physically crosslinked aggregates. At this stage, around 90 wt. % of the complex phase is water, and thus, it appears to be very soft initially. As salt is added to the system, within individual clusters, the associations are loosened. However, globally, osmotic deswelling induces dehydration and generates a denser material. Therefore, upon shearing, the frictional interactions between chains increase, resulting in stiffening of the complex phase. Above certain salt threshold, these relaxed clusters are completely disentangled and the polyelectrolyte chains rearranged themselves into paired ladder-like configuration, leading to phase transition from solid into viscoelastic liquid. Within this liquid domain, further salt doping continues to disrupt intrinsic ion pairs and eventually dissociate the coacervate into a homogenous solution.

Figure 2. 15: Scheme showing the proposed structural evolution of polyelectrolyte chains in the complex phase during the salt-driven phase transition.

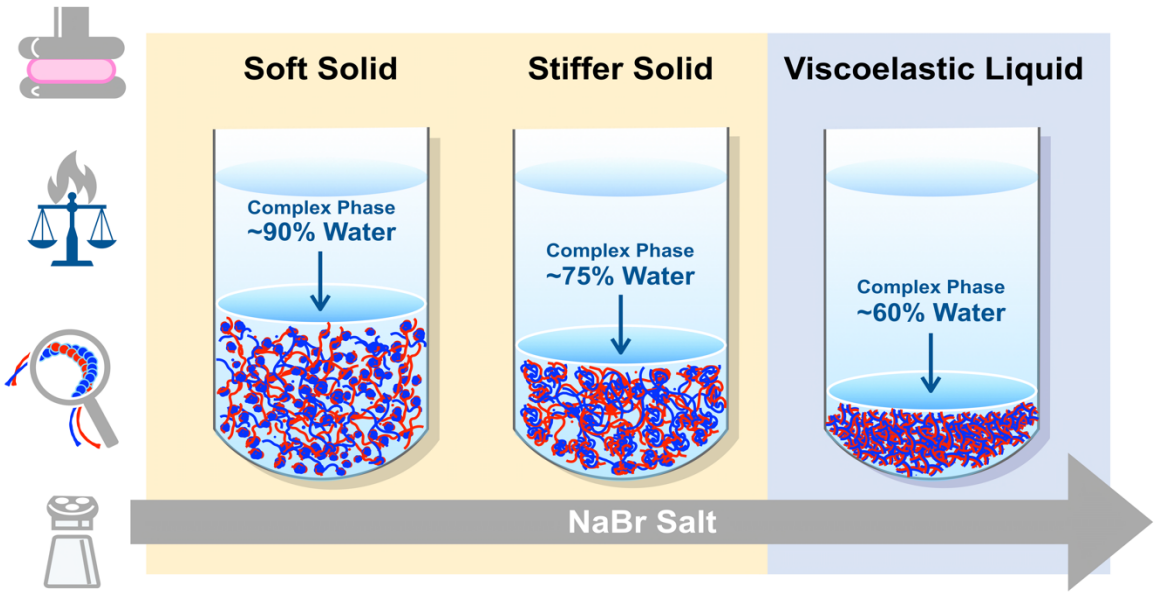

2.4 Conclusion

In summary, we have comprehensively investigated the unique properties of a PEC system comprising two oppositely charged, strong styrenic polyelectrolytes during salt-driven solid-to-liquid phase transition using a combination of multiple experimental methodologies. Given the similarity in chemical structure, well-defined PVBTMA and PSS were rationally selected to incorporate the effects of discrete non-covalent interactions in bulk complexes from 0 to 7.0 M NaBr conditions. This custom-built material platform enabled us to precisely probe and identify new structure and functional features of PECs from this system.

In the solid regime under low-salt conditions, these PECs exhibited unexpected salt-stiffening behavior that was attributed to water loss and rearrangement of the polyelectrolyte chain conformation. Initially, polyelectrolyte chains assembled into tightly coiled, crosslinked

aggregates that unraveled and expanded upon salt addition. At the same time, due to osmotic deswelling, salt addition expelled water molecules into supernatant phase and densified the packing of polymer chains, which translated to a higher modulus from dehydration and increasing collisions and friction between chains. In the liquid regime above a certain salt threshold, the PECs evolved into a viscoelastic liquid phase, and the chains equilibrated to paired ladder-like structures. In this liquid phase domain, as more salt is added, we have shown that polyelectrolyte chains can further relax and water content continued to decrease. Furthermore, the differences between solid and liquid phases were also corroborated by the phase diagram that illustrated the partitioning of polymer and salt.

To our knowledge, this is one of the first experimental reports to capture and highlight salt-stiffening behavior, water loss, phase behavior, nanoscale cluster formation, and a structural evolution spanning high salt content during solid-to-liquid phase transition in bulk PEC assemblies. The styrenic polyelectrolytes represent only one set of possible monomer families that can be constructed to further explore this wide parameter space. These findings advance our fundamental understanding on the physical behavior of polyelectrolyte complexes, specifically those formed by strongly interacting polyelectrolytes, and thus will bring new insights into the design and applicability of complex-based materials. This work will also contribute toward expanding the platforms of polymeric materials with tunable and controllable structures on the molecular level, which ultimately enhances the prediction of material properties and functionality based on their chemical structures.

2.5 Reference

(1) Bungenberg de Jong, H. G.; Kruyt, H. R. Coacervation. (Partial Miscibility in Colloid Systems). (Preliminary Communication). *Proc. K. Ned. Akad. Wet.* **1929**, *131*, 849–856.

(2) Zhao, H.; Sun, C.; Stewart, R. J.; Waite, J. H. Cement Proteins of the Tube-Building Polychaete Phragmatopoma Californica. *J. Biol. Chem.* **2005**, *280*, 42938–42944. https://doi.org/10.1074/jbc.M508457200.

(3) Widom, J. Structure, Dynamics, and Function of Chromatin in Vitro. *Annu. Rev. Biophys. Biomol. Struct.* **1998**, *27*, 285–327. https://doi.org/10.1146/annurev.biophys.27.1.285.

(4) Brangwynne, C. P.; Tompa, P.; Pappu, R. V. Polymer Physics of Intracellular Phase Transitions. *Nat. Phys.* **2015**, *11*, 899–904. https://doi.org/10.1038/nphys3532.

(5) Vieregg, J. R.; Lueckheide, M.; Marciel, A. B.; Leon, L.; Bologna, A. J.; Rivera, J. R.; Tirrell, M. V. Oligonucleotide-Peptide Complexes: Phase Control by Hybridization. *J. Am. Chem. Soc.* **2018**, *140*, 1632–1638. https://doi.org/10.1021/jacs.7b03567.

(6) Smith, J.; Calidas, D.; Schmidt, H.; Lu, T.; Rasoloson, D.; Seydoux, G. Spatial Patterning of P Granules by RNA-Induced Phase Separation of the Intrinsically-Disordered Protein MEG-3. *Elife* **2016**, *5*, 1–18. https://doi.org/10.7554/eLife.21337.

(7) Brangwynne, C.; Hyman, T. In Retrospect: The Origin of Life. *Nature* **2012**, *491*, 524–525. https://doi.org/10.1038/491524a.

(8) Kuo, C. H.; Leon, L.; Chung, E. J.; Huang, R. T.; Sontag, T. J.; Reardon, C. A.; Getz, G. S.; Tirrell, M.; Fang, Y. Inhibition of Atherosclerosis-Promoting MicroRNAs via Targeted Polyelectrolyte Complex Micelles. *J. Mater. Chem. B* **2014**, *2*, 8142–8153. https://doi.org/10.1039/c4tb00977k.

(9) Zhao, Q.; Lee, D. W.; Ahn, B. K.; Seo, S.; Kaufman, Y.; Israelachvili, J. N.; Waite, J. H. Underwater Contact Adhesion and Microarchitecture in Polyelectrolyte Complexes Actuated by Solvent Exchange. *Nat. Mater.* **2016**, *15*, 407–412. https://doi.org/10.1111/mec.13536.Application.

(10) Marras, A. E.; Vieregg, J. R.; Ting, J. M.; Rubien, J. D.; Tirrell, M. V. Polyelectrolyte Complexation of Oligonucleotides by Charged Hydrophobic-Neutral Hydrophilic Block Copolymers. *Polymers (Basel).* **2019**, *11*, 83. https://doi.org/10.3390/polym11010083.

(11) Lueckheide, M.; Vieregg, J. R.; Bologna, A. J.; Leon, L.; Tirrell, M. V. Structure-Property Relationships of Oligonucleotide Polyelectrolyte Complex Micelles. *Nano Lett.* **2018**, *18*, 7111–7117. https://doi.org/10.1021/acs.nanolett.8b03132.

(12) Anraku, Y.; Kishimura, A.; Kamiya, M.; Tanaka, S.; Nomoto, T.; Toh, K.; Matsumoto, Y.; Fukushima, S.; Sueyoshi, D.; Kano, M. R.; et al. Systemically Injectable Enzyme-Loaded Polyion Complex Vesicles as in Vivo Nanoreactors Functioning in Tumors. *Angew. Chemie - Int. Ed.* **2016**, *55*, 560–565. https://doi.org/10.1002/anie.201508339.

(13) Black, K. A.; Priftis, D.; Perry, S. L.; Yip, J.; Byun, W. Y.; Tirrell, M. Protein Encapsulation via Polypeptide Complex Coacervation. *ACS Macro Lett.* **2014**, *3*, 1088–1091. https://doi.org/10.1021/mz500529v.

(14) Gouin, S. Microencapsulation: Industrial Appraisal of Existing Technologies and Trends. *Trends Food Sci. Technol.* **2004**, *15*, 330–347. https://doi.org/10.1016/j.tifs.2003.10.005.

(15) De Kruif, C. G.; Weinbreck, F.; De Vries, R. Complex Coacervation of Proteins and Anionic Polysaccharides. *Curr. Opin. Colloid Interface Sci.* **2004**, *9*, 340–349. https://doi.org/10.1016/j.cocis.2004.09.006.

(16) Zhang, Y.; Batys, P.; O'Neal, J. T.; Li, F.; Sammalkorpi, M.; Lutkenhaus, J. L. Molecular Origin of the Glass Transition in Polyelectrolyte Assemblies. *ACS Cent. Sci.* **2018**, *4*, 638–644. https://doi.org/10.1021/acscentsci.8b00137.
(17) Tirrell, M. Polyelectrolyte Complexes: Fluid or Solid? *ACS Cent. Sci.* **2018**, *4*, 532–533. https://doi.org/10.1021/acscentsci.8b00284.
(18) Lou, J.; Friedowitz, S.; Qin, J.; Xia, Y. Tunable Coacervation of Well-Defined Homologous Polyanions and Polycations by Local Polarity. *ACS Cent. Sci.* **2019**, *5*, 549–557. https://doi.org/10.1021/acscentsci.8b00964.
(19) Spruijt, E.; Cohen Stuart, M. A.; Van Der Gucht, J. Linear Viscoelasticity of Polyelectrolyte Complex Coacervates. *Macromolecules* **2013**, *46*, 1633–1641. https://doi.org/10.1021/ma301730n.
(20) Fu, J.; Fares, H. M.; Schlenoff, J. B. Ion-Pairing Strength in Polyelectrolyte Complexes. *Macromolecules* **2017**, *50*, 1066–1074. https://doi.org/10.1021/acs.macromol.6b02445.
(21) Huang, J.; Morin, F. J.; Laaser, J. E. Charge-Density-Dominated Phase Behavior and Viscoelasticity of Polyelectrolyte Complex Coacervates. *Macromolecules* **2019**, *52*, 4957–4967. https://doi.org/10.1021/acs.macromol.9b00036.
(22) Herzog-Arbeitman, A.; Ting, J. M.; Meng, S.; Wu, H.; Tirrell, M. V. Patterning Polyelectrolyte Complexes with Alternating Monomer Sequence Distributions. *ChemRxiv* **2019**. https://doi.org/10.26434/chemrxiv.11320439.v1.
(23) Lytle, T. K.; Chang, L. W.; Markiewicz, N.; Perry, S. L.; Sing, C. E. Designing Electrostatic Interactions via Polyelectrolyte Monomer Sequence. *ACS Cent. Sci.* **2019**, *5*, 709–718. https://doi.org/10.1021/acscentsci.9b00087.
(24) Rumyantsev, A. M.; Jackson, N. E.; Yu, B.; Ting, M.; Chen, W.; Tirrell, M. V; Pablo, J. J. De. Controlling Complex Coacervation via Random Polyelectrolyte Sequences. *ACS Macro Lett.* **2019**, *9*, 1296–1302. https://doi.org/10.1021/acsmacrolett.9b00494.
(25) Madinya, J. J.; Chang, L.-W.; Perry, S. L.; Sing, C. E. Sequence-Dependent Self-Coacervation in High Charge-Density Polyampholytes. *Mol. Syst. Des. Eng.* **2020**, *5*, 632–644. https://doi.org/10.1039/c9me00074g.
(26) McCarty, J.; Delaney, K. T.; Danielsen, S. P. O.; Fredrickson, G. H.; Shea, J. E. Complete Phase Diagram for Liquid-Liquid Phase Separation of Intrinsically Disordered Proteins. *J. Phys. Chem. Lett.* **2019**, *10*, 1644–1652. https://doi.org/10.1021/acs.jpclett.9b00099.
(27) Perry, S. L.; Leon, L.; Hoffmann, K. Q.; Kade, M. J.; Priftis, D.; Black, K. A.; Wong, D.; Klein, R. A.; Pierce, C. F.; Margossian, K. O.; et al. Chirality-Selected Phase Behaviour in Ionic Polypeptide Complexes. *Nat. Commun.* **2015**, *6*, 6052. https://doi.org/10.1038/ncomms7052.
(28) Pacalin, N. M.; Leon, L.; Tirrell, M. Directing the Phase Behavior of Polyelectrolyte Complexes Using Chiral Patterned Peptides. *Eur. Phys. J. Spec. Top.* **2016**, *225*, 1805–1815. https://doi.org/10.1140/epjst/e2016-60149-6.
(29) Hoffmann, K. Q.; Perry, S. L.; Leon, L.; Priftis, D.; Tirrell, M.; De Pablo, J. J. A Molecular View of the Role of Chirality in Charge-Driven Polypeptide Complexation. *Soft Matter* **2015**, *11*, 1525–1538. https://doi.org/10.1039/c4sm02336f.
(30) Sadman, K.; Wang, Q.; Chen, Y.; Keshavarz, B.; Jiang, Z.; Shull, K. R. Influence of Hydrophobicity on Polyelectrolyte Complexation. *Macromolecules* **2017**, *50*, 9417–9426. https://doi.org/10.1021/acs.macromol.7b02031.
(31) Batys, P.; Kivistö, S.; Lalwani, S. M.; Lutkenhaus, J. L.; Sammalkorpi, M. Comparing

Water-Mediated Hydrogen-Bonding in Different Polyelectrolyte Complexes. *Soft Matter* **2019**, *15*, 7823–7831. https://doi.org/10.1039/c9sm01193e.
(32) Tabandeh, S.; Leon, L. Engineering Peptide-Based Polyelectrolyte Complexes with Increased Hydrophobicity. *Molecules* **2019**, *24*, 868. https://doi.org/10.3390/molecules24050868.
(33) Suarez-Martinez, P. C.; Batys, P.; Sammalkorpi, M.; Lutkenhaus, J. L. Time-Temperature and Time-Water Superposition Principles Applied to Poly(Allylamine)/Poly(Acrylic Acid) Complexes. *Macromolecules* **2019**, *52*, 3066–3074. https://doi.org/10.1021/acs.macromol.8b02512.
(34) Kim, S.; Huang, J.; Lee, Y.; Dutta, S.; Young Yoo, H.; Mee Jung, Y.; Jho, Y.; Zeng, H.; Hwang, D. S. Complexation and Coacervation of Like-Charged Polyelectrolytes Inspired by Mussels. *Proc. Natl. Acad. Sci. U. S. A.* **2016**, *113*, E847–E853. https://doi.org/10.1073/pnas.1521521113.
(35) Zhou, K.; Zang, J.; Chen, H.; Wang, W.; Wang, H.; Zhao, G. On-Axis Alignment of Protein Nanocage Assemblies from 2D to 3D through the Aromatic Stacking Interactions of Amino Acid Residues. *ACS Nano* **2018**, *12*, 11323–11332. https://doi.org/10.1021/acsnano.8b06091.
(36) Zhao, M.; Zacharia, N. S. Sequestration of Methylene Blue into Polyelectrolyte Complex Coacervates. *Macromol. Rapid Commun.* **2016**, *37*, 1249–1255. https://doi.org/10.1002/marc.201600244.
(37) Sadman, K.; Wang, Q.; Shull, K. R. Guanidinium Can Break and Form Strongly Associating Ion Complexes. *ACS Macro Lett.* **2019**, *8*, 117–122. https://doi.org/10.1021/acsmacrolett.8b00824.
(38) Ghostine, R. A.; Shamoun, R. F.; Schlenoff, J. B. Doping and Diffusion in an Extruded Saloplastic Polyelectrolyte Complex. *Macromolecules* **2013**, *46*, 4089–4094. https://doi.org/10.1021/ma4004083.
(39) Wang, Q.; Schlenoff, J. B. The Polyelectrolyte Complex/Coacervate Continuum. *Macromolecules* **2014**, *47*, 3108–3116. https://doi.org/10.1021/ma500500q.
(40) Fares, H. M.; Ghoussoub, Y. E.; Delgado, J. D.; Fu, J.; Urban, V. S.; Schlenoff, J. B. Scattering Neutrons along the Polyelectrolyte Complex/Coacervate Continuum. *Macromolecules* **2018**, *51*, 4945–4955. https://doi.org/10.1021/acs.macromol.8b00699.
(41) Liu, Y.; Momani, B.; Winter, H. H.; Perry, S. L. Rheological Characterization of Liquid-to-Solid Transitions in Bulk Polyelectrolyte Complexes. *Soft Matter* **2017**, *13*, 7332–7340. https://doi.org/10.1039/c7sm01285c.
(42) Meng, S.; Liu, Y.; Yeo, J.; Ting, J. M.; Tirrell, M. V; Tirrell, M. V. Effect of Mixed Solvents on Polyelectrolyte Complexes with Salt. *Colloid Polym Sci* **2020**, *298*, 887–894. https://doi.org/10.1007/s00396-020-04637-0.
(43) Zhang, Y.; Li, F.; Valenzuela, L. D.; Sammalkorpi, M.; Lutkenhaus, J. L. Effect of Water on the Thermal Transition Observed in Poly(Allylamine Hydrochloride)-Poly(Acrylic Acid) Complexes. *Macromolecules* **2016**, *49*, 7563–7570. https://doi.org/10.1021/acs.macromol.6b00742.
(44) Li, L.; Srivastava, S.; Andreev, M.; Marciel, A. B.; De Pablo, J. J.; Tirrell, M. V. Phase Behavior and Salt Partitioning in Polyelectrolyte Complex Coacervates. *Macromolecules* **2018**, *51*, 2988–2995. https://doi.org/10.1021/acs.macromol.8b00238.
(45) Ting, J. M.; Wu, H.; Herzog-Arbeitman, A.; Srivastava, S.; Tirrell, M. V. Synthesis and

Assembly of Designer Styrenic Diblock Polyelectrolytes. *ACS Macro Lett.* **2018**, *7*, 726–733. https://doi.org/10.1021/acsmacrolett.8b00346.
(46) Ilavsky, J.; Jemian, P. R. Irena: Tool Suite for Modeling and Analysis of Small-Angle Scattering. *J. Appl. Crystallogr.* **2009**, *42*, 347–353. https://doi.org/10.1107/S0021889809002222.
(47) Wu, H.; Ting, J. M.; Werba, O.; Meng, S.; Tirrell, M. V. Non-Equilibrium Phenomena and Kinetic Pathways in Self-Assembled Polyelectrolyte Complexes. *J. Chem. Phys.* **2018**, *149*, 163330. https://doi.org/10.1063/1.5039621.
(48) Spruijt, E.; Sprakel, J.; Lemmers, M.; Stuart, M. A. C.; Van Der Gucht, J. Relaxation Dynamics at Different Time Scales in Electrostatic Complexes: Time-Salt Superposition. *Phys. Rev. Lett.* **2010**, *105*, 208301. https://doi.org/10.1103/PhysRevLett.105.208301.
(49) Rubinstein, M.; Semenov, A. N. Dynamics of Entangled Solutions of Associating Polymers. *Macromolecules* **2001**, *34*, 1058–1068. https://doi.org/10.1021/ma0013049.
(50) Hamad, F. G.; Chen, Q.; Colby, R. H. Linear Viscoelasticity and Swelling of Polyelectrolyte Complex Coacervates. *Macromolecules* **2018**, *51*, 5547–5555. https://doi.org/10.1021/acs.macromol.8b00401.
(51) Ali, S.; Prabhu, V. M. Relaxation Behavior by Time-Salt and Time-Temperature Superpositions of Polyelectrolyte Complexes from Coacervate to Precipitate. *Gels* **2018**, *4*, 11. https://doi.org/10.3390/gels4010011.
(52) Yang, M.; Shi, J.; Schlenoff, J. B. Control of Dynamics in Polyelectrolyte Complexes by Temperature and Salt. *Macromolecules* **2019**, *52*, 1930–1941. https://doi.org/10.1021/acs.macromol.8b02577.
(53) Shamoun, R. F.; Hariri, H. H.; Ghostine, R. A. Thermal Transformations in Extruded Saloplastic Polyelectrolyte Complexes. **2012**. https://doi.org/10.1021/ma302075p.
(54) Overbeek, J. T. G.; Voorn, M. J. Phase Separation In Polyelectrolyte Solutions. Theory Of Complex Coacervation. *J. Cell. Comp. Physiol.* **1957**, *49*, 7–26. https://doi.org/10.1002/jcp.1030490404.
(55) Radhakrishna, M.; Basu, K.; Liu, Y.; Shamsi, R.; Perry, S. L.; Sing, C. E. Molecular Connectivity and Correlation E Ff Ects on Polymer Coacervation. **2017**, No. 1. https://doi.org/10.1021/acs.macromol.6b02582.
(56) Shamoun, R. F.; Reisch, A.; Schlenoff, J. B. Extruded Saloplastic Polyelectrolyte Complexes. *Adv. Funct. Mater.* **2012**, *22* (9), 1923–1931. https://doi.org/10.1002/adfm.201102787.
(57) Jeon, C. H.; Makhaeva, E. E.; Khokhlov, A. R. Swelling Behavior of Polyelectrolyte Gels in the Presence of Salts. *Macromol. Chem. and Phys.* **1998**, *199* (12), 2665–2670. https://doi.org/10.1002/(SICI)1521-3935(19981201)199:12<2665::AID-MACP2665>3.0.CO;2-6.
(58) Horkay, F.; Tasaki, I.; Basser, P. J. Osmotic Swelling of Polyacrylate Hydrogels in Physiological Salt Solutions. *Biomacromolecules* **2000**, *1* (1), 84–90. https://doi.org/10.1021/bm9905031.
(59) Mussel, M.; Basser, P. J.; Horkay, F. Effects of Mono- and Divalent Cations on the Structure and Thermodynamic Properties of Polyelectrolyte Gels. *Soft Matter* **2019**, *15*, 4153–4161. https://doi.org/10.1039/c9sm00464e.
(60) Košovan, P.; Richter, T.; Holm, C. Modeling of Polyelectrolyte Gels in Equilibrium with Salt Solutions. *Macromolecules* **2015**, *48* (20), 7698–7708.

https://doi.org/10.1021/acs.macromol.5b01428.
(61) Marciel, A. B.; Srivastava, S.; Tirrell, M. V. Structure and Rheology of Polyelectrolyte Complex Coacervates. *Soft Matter* **2018**, *14*, 2454–2464. https://doi.org/10.1039/C7SM02041D.
(62) Jaber, J. A.; Schlenoff, J. B. Mechanical Properties of Reversibly Cross-Linked Ultrathin Polyelectrolyte Complexes. *J. Am. Chem. Soc.* **2006**, *128*, 2940–2947. https://doi.org/10.1021/ja055892n.
(63) Schneider, C. A.; Rasband, W. S.; Eliceiri, K. W. NIH Image to ImageJ: 25 Years of Image Analysis. *Nat. Methods* **2012**, *9*, 671–675. https://doi.org/10.1038/nmeth.2089.

Chapter 3. Effect of Mixed Solvents on Polyelectrolyte Complexes

This chapter has been published in Meng, S., Liu, Y., Yeo, J. *et al.* Effect of mixed solvents on polyelectrolyte complexes with salt. *Colloid Polym Sci* **298,** 887–894 (2020).

3.1 Introduction

Polyelectrolyte complexes (PECs, the polymer-dense phase formed when two oppositely charged polyelectrolyte solutions are mixed together[1–6]) are very common in biological and natural systems.[7–12] In addition, they have utility in a wide range of practical applications that are broadly pertinent to overlapping areas in materials science, colloidal science, and engineering, including consumer products, underwater adhesives, and biopharmaceuticals.[13–18] The complexation process is generally driven by a favorable gain in entropy upon releasing counterions, forming intrinsic ion pairs and restructuring water molecules around the complex assemblies.

In this mechanism, depending on the chemical and ionic nature of the pair of polyelectrolytes, the physical state of PEC materials can span from glassy solids to low viscosity liquids.[19–23] The phase of the final material has been conventionally hypothesized to be undoubtedly dominated by the nature of polyelectrolyte chain components.[18,24–26] For instance, Li et al. has shown that the self-assembly of two charged hydrophilic polypeptides (poly(lysine) and poly(glutamic acid)) resulted in a low viscosity liquid in water.[27] The polypeptides have carbonyl and amino groups along the chain backbone that facilitate hydrogen bonding, and the charged moieties can deprotonate depending on pH conditions. In contrast, the PEC system studied in this present work, composed of poly[(vinylbenzyl) trimethylammonium chloride] (PVBTMA) and poly[sodium 4-styrenesulfonate] (PSS), formed solid precipitates in water (Figure 3.1). Here, the aliphatic backbone and aromatic side groups increase the hydrophobicity of the polyelectrolytes, and the trimethylammonium and sulfonate groups are pH-independent. Marras et al. previously

compared how the phase behavior of oligonucleotide-containing complexes depends on the selection of PVBTMA versus poly(lysine) at various degrees of polymerization,[14] illustrating the importance of molecular level details that are responsible for solid or liquid PEC formation.

Figure 3. 1: Chemical Structure and picture of PVBTMA/PSS.

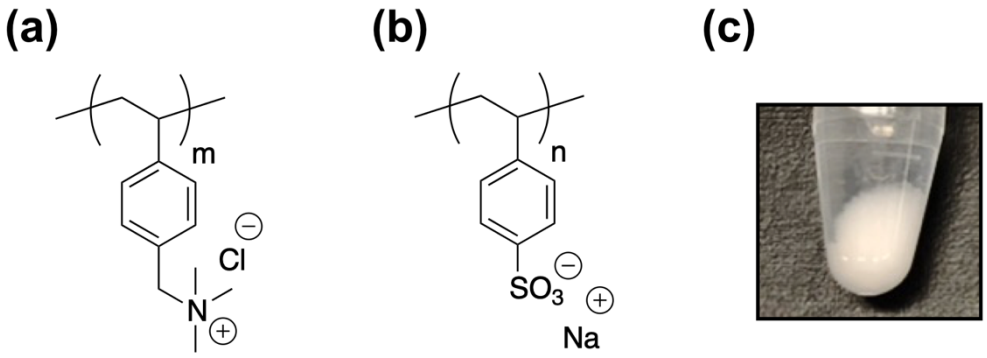

(a) Poly[(vinylbenzyl) trimethylammonium chloride] (PVBTMA) chemical structure, (b) poly(sodium 4-styrenesulfonate) (PSS) chemical structure, and (c) a representative photograph of the solid PVBTMA/PSS polyelectrolyte complex.

In addition to the selection of starting materials, the condition of the external environment also plays a critical role in controlling the physical state of the resultant PECs. For instance, salt is commonly used as a stimulus to break and compensate the ion pairs between oppositely charged chains, and consequently, dissociate the PECs. For strongly interacting PECs that are initially solid precipitates, the addition of salt can transition solids into liquid coacervates and, ultimately, to homogenous solutions.[20] Following this established phenomenon, we employed sodium bromide (NaBr) salt to examine the phase transition of PVBTMA/PSS complexes through its complex/coacervate continuum. A full study of the rheological properties, phase behavior, and structure of this system is underway and remains outside the scope of this current work.

Although salt has been highly investigated as an additive over recent decades, the interplay between salt and solvent in PEC materials has received far less attention. In this study, we attempt

to fill this gap by exploring how co-solvents (that introduce a hydrophobic constituent) and salinity together can tune the properties of the PVBTMA/PSS system. Selective binary mixtures of water and organic solvents enables a facile way to progressively modulate PEC behavior. Ethylene glycol and ethanol were deliberately selected as organic solvents due to their miscibility with water (Table 3.1). We first studied how solvent hydrophobicity alone influenced PEC properties by assembling the complex in salt-free ethylene glycol/water co-solvent conditions. Then we incorporated another dimension and added salt into the system to investigate the mutual effect of solvent and salinity. Optical microscopy was mainly used as the experimental approach to qualitatively map out the phase behaviors of these complexes. This study demonstrates how PECs, as a class of "smart" stimuli-responsive materials, can change their properties and respond to the external environment. We believe the results we present in this study will provide useful new insights into enriching and controlling the properties and functionalities of PECs through controlling the solvent environment in complex materials.

Table 3. 1: Physical Properties of Investigated Solvents.

Solvent	Dielectric Constant (at 0 °C)[28]	Surface Tension (dyn/cm, at 25 °C)[28]	Viscosity (mPa-s, at 25 °C)[28]	Relative Polarity[28]
Water	78.5	71.97	0.8937	1.000
Ethylene Glycol	37.7	47.99	16.1	0.790
Ethanol	24.6	22.39	1.04	0.654

3.2 Experimental Details

3.2.1 Materials

The following chemicals were reagent grade and used as received unless otherwise specified: ethanol (HPLC Grade, Millipore Sigma), ethylene glycol (Reagent Plus, ≥99%, Millipore Sigma), (vinylbenzyl)trimethylammonium chloride (VBTMA, Sigma, 99%), poly(styrene sulfonate, sodium salt) (PSS, 201,700 g/mol, Polymer Standards Service), sodium bromide (Fisher Scientific, >99%), 4-cyano-4-(phenylcarbonothioylthio) pentanoic acid (CPhPA, Sigma), 2,2'-azobis[2-(2-imidazolin-2-yl)propane]dihydrochloride (VA-044, Wako Chemicals, USA), acetic acid (glacial, Sigma, ≥99.85%), sodium acetate trihydrate (Sigma, ≥99%), and SnakeSkin dialysis tubing (MWCO 3.5K, 22 mm, Thermo Scientific). All water used during the experiment was filtered from a Milli-Q water purification system at a resistivity of 18.2 MΩ-cm at 25 °C. The acetate buffer solution was prepared with 0.1 M acetic acid and 0.1 M sodium acetate trihydrate (0.1 M) (42/158, *v/v*) at pH 5.2.

3.2.2 Polymer Synthesis

The complex system studied here is formed by $PVBTMA_{100}$ and PSS_{100} (Chemical structures are shown in Scheme 1 and the subscripts denote the degree of polymerization). PSS_{100} was used as received (purchased from Polymer Standards Service). $PVBTMA_{100}$ was synthesized with aqueous reversible addition-fragmentation chain transfer (RAFT) polymerization to be approximately symmetric to PSS, based on previous work in our group.[29] Desired amount of VA-044 initiator, VBTMA monomer, and CPhPA chain transfer agent (molar equivalence of 1 to 1000 to 10, respectively) were added to the acetate buffer solution in a dried 25 mL round bottom flask.

The flask was then sealed, degassed with dried nitrogen, and heated at 50 °C and constant stirring for at least 21 h. The reaction was then cooled to room temperature and opened to air and we obtained the crude pink polymer. The crude polymer was then dialyzed against Milli-Q water for 4 cycles of 8 h each. Lastly, the samples were lyophilized and we achieved ca. 2 g polymer in the end.

3.2.3 PEC Sample Preparation

PECs were prepared under 1:1 stoichiometric charge-matched conditions between polycation and polyanion. The "as prepared" polymer concentration was fixed at ~1 wt% (10 mg/ml). Following the protocol of the *direct dissolution method*,[30] we added stock solutions of polycations and polyanions sequentially to a solution with desired amount of NaBr stock solution (5 M) and co-solvent of Milli-Q water and ethylene glycol or ethanol. After the all the solutions were added, samples were immediately vortexed for at least 30 s.

3.2.4 Optical Light Microscopy Imaging

To visualize PECs directly at the microscale and determine the phases of these samples, we used optical phase contrast microscopy (Leica DMI 6000B with Leica Application Suite (LAS) image acquisition software, Wetzlar, Germany). PEC samples were first prepared in 1.5 mL microcentrifuge tubes and immediately 100 μL of the well-mixed samples were transferred into ultra-low attachment 96-well plates (Costar, Corning Inc.). The plates were carefully sealed to prevent water evaporation. Imaging was performed one day after sample preparation to guarantee complete phase separation. Using ImageJ software, we later adjusted and enhanced the contrast of the acquired images.

3.2.5 Thermogravimetric Analysis

After PEC samples were prepared in the 1.5 mL Eppendorf tubes, they were centrifuged at 4000 × g for 15 min. Then 30 μL of the supernatant and around 5 mg complex materials were loaded onto aluminum pans whose weights were measured beforehand. After the samples were transferred, the weights of samples together with pans were recorded again. In this way, the mass of samples on the pans can be calculated. Next, the pans loaded with samples were carefully transferred into a Barnstead Thermolyne Furnace 1400.

The furnace temperature was first set to 200 °C and held for 2.5 h to evaporate all the water within the samples. The weights of pans with samples were measured again afterwards so that we were able to achieve the weight of water. After that, pans loaded with dried samples were put back into the furnace once again and heated at 600 °C for 12 h. During this process, all the polymer contents were burned and removed. The weights were recorded for the last time, from which we can calculate the removed polymer mass and the mass of salt remains. For each condition, at least three different repeating samples were measured. Dixon's Q test was performed later to identify and discard outliers.

3.3 Results and Discussion

3.3.1 Salt-Free PECs in ethylene glycol/water solvent mixtures

We first prepared PVBTMA/PSS complexes under salt-free conditions and characterized the resultant assembly morphologies with microscopy. Figure 3.2 shows a gallery of optical images of PECs assembled in increasing co-solvent ratios of ethylene glycol to water. As the ethylene

glycol content increases, there was no evident change in the samples, which remained dense, amorphous, and opaque solid aggregates. This suggests that any potential co-solvent effect on the PEC material was not visually detectable on the micron scale. To support this observation, we then conducted thermogravimetric analysis (TGA) to quantify the exact distribution of the total solvent (water and ethylene glycol), polymer, and counterion components within the complex. This thermal technique provides a straightforward way to quantitatively measure the relative weights of the liquid, polymer, and salt in the PEC phase.[27] As shown in Figure 3.3, the weight percentage of these three components were invariant to the addition of ethylene glycol in the binary solvent mixture, thus confirming the previous conclusions from the microscopy images, that addition of co-solvent does not itself disrupt the complex.

Figure 3. 2: Optical micrographs of PVBTMA/PSS complexes in ethylene glycol/water mixed solvents under salt free conditions.

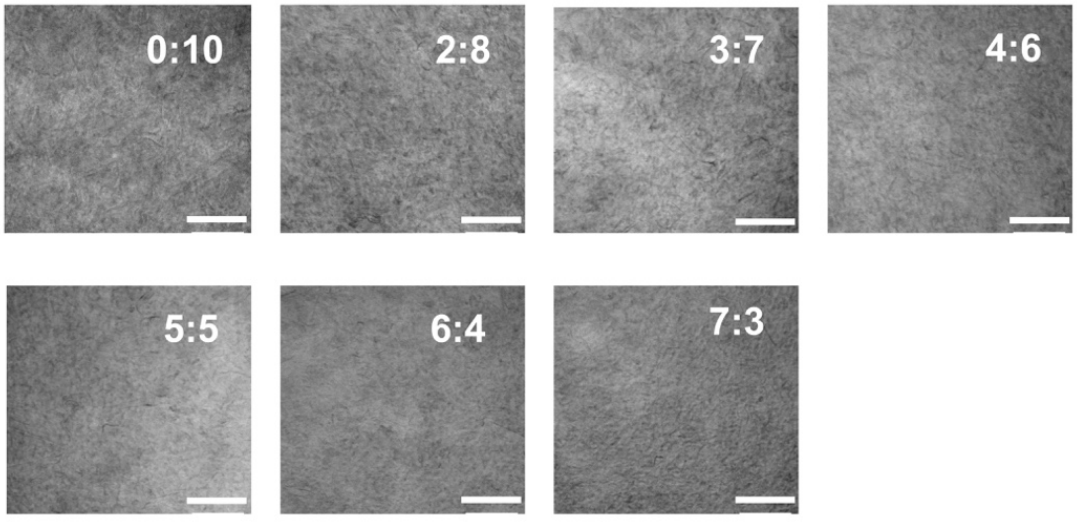

The white numbers on the top right of each image denotes the volumetric ratio of ethylene glycol to water. All scale bars denote 100 μm.

Figure 3. 3: Weight percentage of the total (a) solvent, (b) polymer, and (c) counterions in salt-free PVBTMA/PSS.

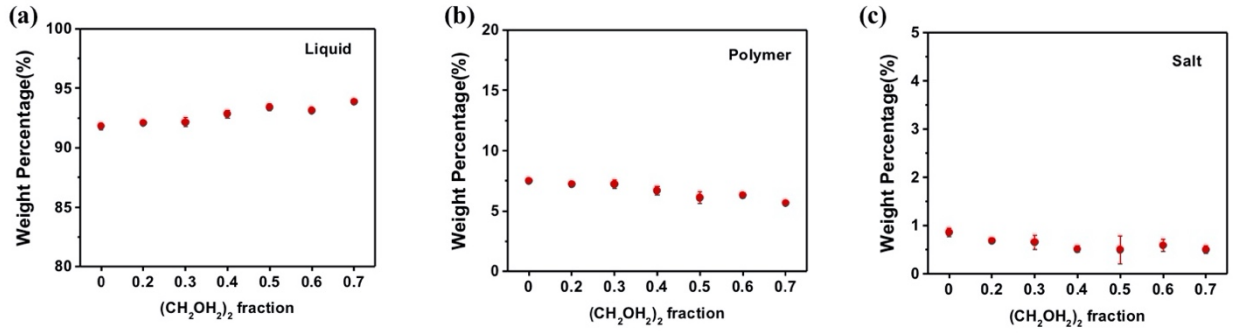

Weight percentages were plotted as a function of the ethylene glycol fraction within the co-solvent. Circles and vertical error bars represent the mean and standard deviation of at least 3 measurements, respectively.

3.3.2 NaBr doped PECs in ethylene glycol/water solvent mixtures

Next, we incorporated externally added salt into the PEC assemblies and observed the resultant behavior by microscopy. In the series of PECs in pure water only (i.e, without an ethylene glycol as a co-solvent), a phase transition of this system from solid to liquid was qualitatively determined by a visual change in their physical appearance in between 2.0 M and 2.5 M NaBr, from cloudy and dense aggregates into a fluid-like transparent network (Figure 3.4). In other words, the advent of a liquid state can be judged through the emergence of clear structures on microscopy images. This method of determining physical states of this PEC has been confirmed by rheology measurements, which we will discuss in a forthcoming paper.

Although there were no noticeable differences in the PEC as co-solvent effects were introduced in the previous salt-free case, we notice an interesting trend as salt was brought into the PEC system containing ethylene glycol. In the gallery of optical images arranged in Figure 3.4, if we navigate vertically from top to bottom, the fraction of ethylene glycol in the co-solvent

gradually increases from 0 to 0.7, and accordingly, the solvent environment becomes more hydrophobic for the PEC phase. As marked by the solid red line, the solid-to-liquid phase transition occurred at lower salt conditions with increasing ethylene glycol content. Additionally, the critical point in salt resistance, where the two-phase PEC system turns into a one-phase, homogenous polyelectrolyte solution across the binodal phase boundary, was also lowered as ethylene glycol content increased. This is marked by the solid blue line in Figure 3.4. Overall, this set of experiments demonstrates how two orthogonal parameters can be used to transverse the complex-coacervate continuum state space.

Figure 3. 4: Optical micrographs of PVBTMA/PSS complexes in ethylene glycol/water with added NaBr.

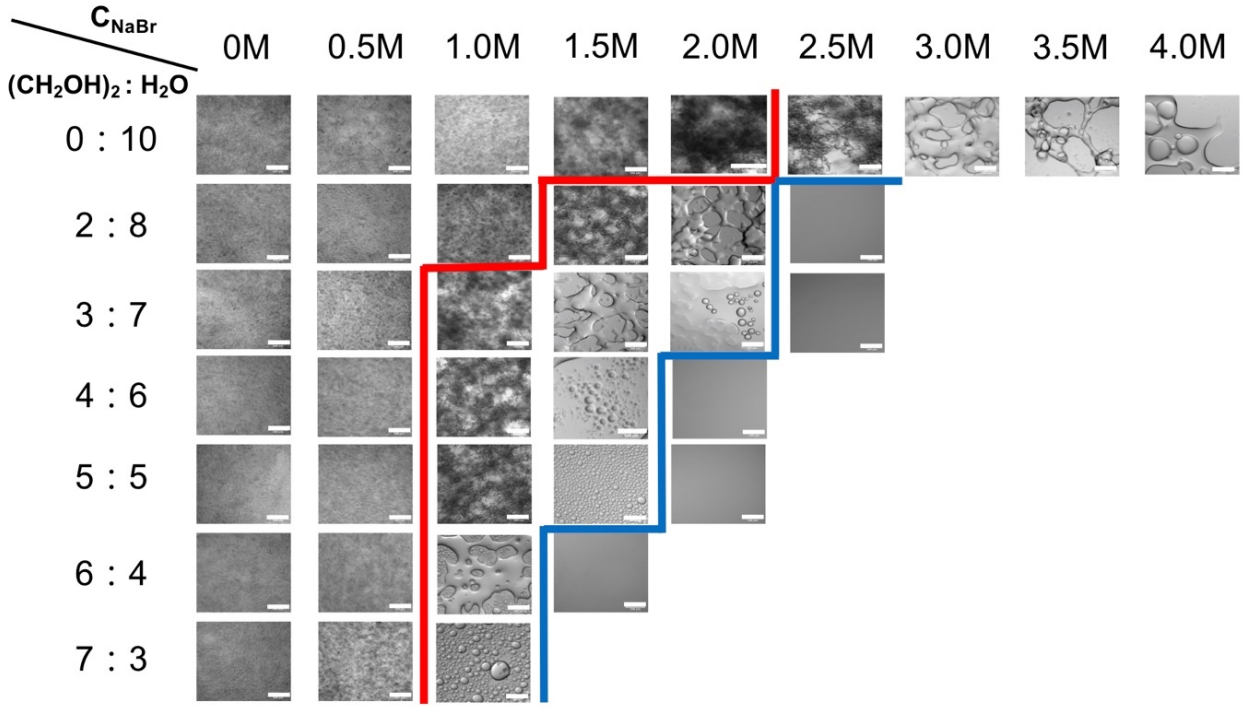

The complexes were prepared at 0 to 4.0 M NaBr (left to right) and in 0:10 to 7:3 volumetric ratios of ethylene glycol/water mixtures (top to bottom). To guide the eye, the solid red line represents the point where the complexes phase transitions from solid to liquid, and the solid blue line denotes the phase transition from liquid to solution. All scale bars denote 100 μm.

3.3.3 NaBr doped PECs in ethanol/water co-solvent mixtures

To further expand on the intriguing findings shown in Figure 3.4, we prepared otherwise identical PEC samples using ethanol as a co-solvent with water instead of ethylene glycol. As shown in Figure 3.5, the same overall pattern was identified by microscopy. Both phase transitions can be carefully tuned as a function of ethanol fraction and NaBr salt concentration. Furthermore, when directly comparing these two solvent choices, we noticed that at equivalent ratios of organic solvent to water, both phase transitions with ethylene glycol occurred at higher NaBr salt concentration levels than with ethanol. For example, at 4:6 organic solvent to water mixtures, for ethylene glycol solid precipitates converted into liquid coacervates at 0.5-1.0 M NaBr and into solution at 1.5-2.0 M NaBr. For ethanol, these transition points were measured to be 0-0.5 M NaBr and 1.0-1.5 M NaBr, respectively.

We hypothesize that this difference is due to the physical properties of ethanol and ethylene glycol that influence the associative driving force and salt resistance of this PEC system in water. For instance, the relative polarities of ethanol and ethylene glycol are 0.654 and 0.79, respectively.[28] Therefore, under the same ratio of organic solvent and water, ethanol/water co-solvent creates a more "hydrophobic" environment for the complex phase, causing the bulk complex to be less salt resistant. It is worth pointing out here that our observation is the opposite of what has been mentioned in previous publications. Chang et al.[31] has reported an increase in salt resistance for polypeptide-based coacervates when solvent was switched from water to a more hydrophobic mixture of isopropanol and water. Similarly, Sun et al.[32] has discovered that as the co-solvent became more hydrophobic, there was an increase in the salt concentrations needed to drive solid-to-liquid phase transition and complete dissociation of polysaccharide-based PECs. We

think this striking difference between our work and previous studies came from the difference in the nature of polymer materials: PVBTMA and PSS are very hydrophobic, while both polypeptides polysaccharides are quite hydrophilic. Nevertheless, there are clearly other subtle factors that govern the effects of solvent on PECs. More rigorous investigations to test the universality of what we have observed in these two limiting cases are underway.

Figure 3. 5: Optical micrographs of PVBTMA/PSS complexes in NaBr and ethanol/water.

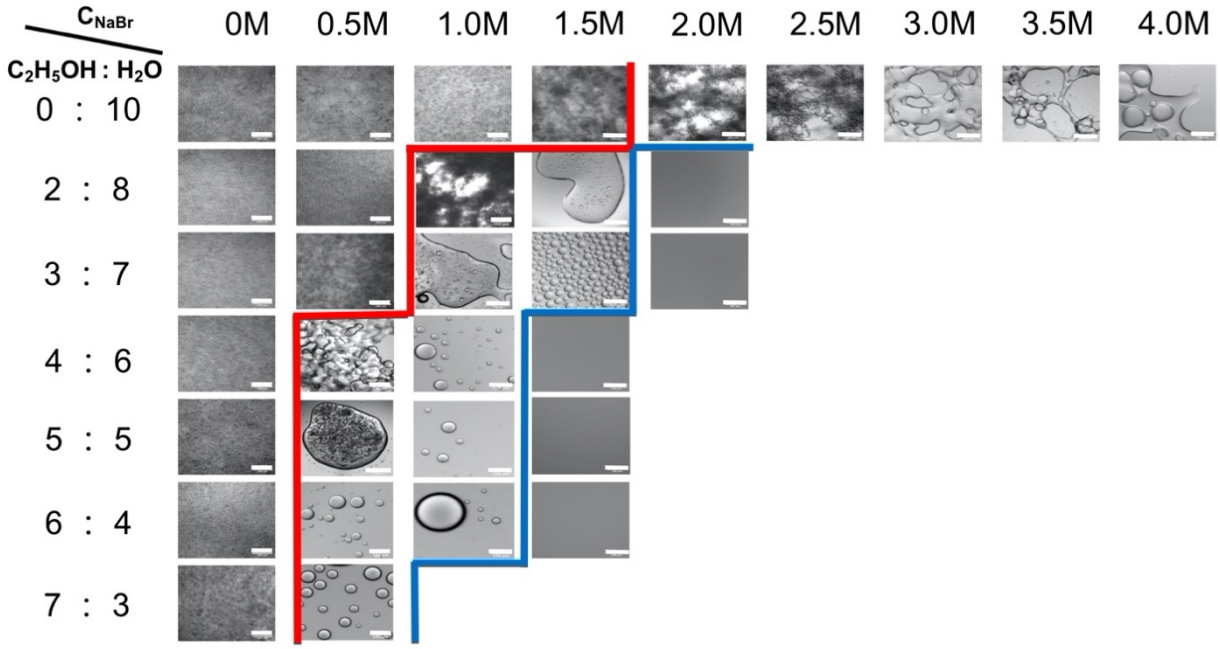

The complexes were prepared at 0 to 4.0 M NaBr (left to right) and in 0:10 to 7:3 volumetric ratios of ethanol/water mixtures (top to bottom). To guide the eye, the solid red lines represents the point where the complexes phase transitions from solid to liquid, and the solid blue line denotes the phase transition from liquid to solution. All scale bars denote 100 μm.

3.4 Conclusion

In summary, by studying comprehensively the assembly of a model PEC system under various co-solvent and salinity conditions in its solution, we report a straightforward method of

modulating the complex stability and responsivity. To this end, PVBTMA and PSS were ideal since this strong polycation-polyanion pairing resulted in solid precipitates that exhibited high salt resistance in water for systematic co-solvent and salt studies.

When we introduced co-solvents of ethylene glycol and ethanol, both solid-to-liquid and liquid-to-solution phase transitions were tunable and occurred at much lower salt concentrations. This finding suggests that co-solvents can be exploited as a powerful agent to modulate the behavior of strongly interacting PECs upon the addition of salt. Furthermore, by progressively adjusting the co-solvent ratios, we were able to demonstrate a clear correlation between salt resistance and solvent quality: aqueous solvent mixtures can weaken the salt resistance of PEC systems in a systematic manner.

Altogether, this work provides practical insights into enriching our understanding of the phase behavior along the coacervate/complex continuum. Future work in our group will expand on the fundamental mechanisms and molecular details behind this physical behavior for charge-driven assemblies. For amphiphilic surfactants and polymers, solvent quality is a known important factor for both the thermodynamics and kinetics of these self-assembled systems. The extension of this general idea for charged polymers has not yet been fully realized, but careful examination of controlled systems can elucidate important structure-property relationships for the continued integration of PECs into advanced applications.

3.5 Reference

(1) Michaels, A. S. Polyelectrolyte Complexes. *Ind. Eng. Chem.* **1965**, *57*, 32–40. https://doi.org/10.1021/ie50670a007.

(2) Philipp, B.; Dautzenberg, H.; Linow, K. J.; Kötz, J.; Dawydoff, W. Polyelectrolyte Complexes - Recent Developments and Open Problems. *Prog. Polym. Sci.* **1989**, *14*, 91–172. https://doi.org/10.1016/0079-6700(89)90018-X.

(3) Srivastava, S.; Tirrell, M. V. Polyelectrolyte Complexation. *Adv. Chem. Phys.* **2016**, *161*, 499–544. https://doi.org/10.1002/9781119324560.

(4) Veis, A. A Review of the Early Development of the Thermodynamics of the Complex Coacervation Phase Separation. *Adv. Colloid Interface Sci.* **2011**, *167*, 2–11. https://doi.org/10.1016/j.cis.2011.01.007.

(5) Voorn, M. J. Complex Coacervation, 1956. https://doi.org/10.1002/jcp.1030490404.

(6) Priftis, D.; Xia, X.; Margossian, K. O.; Perry, S. L.; Leon, L.; Qin, J.; De Pablo, J. J.; Tirrell, M. Ternary, Tunable Polyelectrolyte Complex Fluids Driven by Complex Coacervation. *Macromolecules* **2014**, *47*, 3076–3085. https://doi.org/10.1021/ma500245j.

(7) Zhao, H.; Sun, C.; Stewart, R. J.; Waite, J. H. Cement Proteins of the Tube-Building Polychaete Phragmatopoma Californica. *J. Biol. Chem.* **2005**, *280*, 42938–42944. https://doi.org/10.1074/jbc.M508457200.

(8) Widom, J. Structure, Dynamics, and Function of Chromatin in Vitro. *Annu. Rev. Biophys. Biomol. Struct.* **1998**, *27*, 285–327. https://doi.org/10.1146/annurev.biophys.27.1.285.

(9) Brangwynne, C. P.; Tompa, P.; Pappu, R. V. Polymer Physics of Intracellular Phase Transitions. **2015**, *11*, 899–904. https://doi.org/10.1038/NPHYS3532.

(10) Vieregg, J. R.; Lueckheide, M.; Marciel, A. B.; Leon, L.; Bologna, A. J.; Rivera, J. R.; Tirrell, M. V. Oligonucleotide-Peptide Complexes: Phase Control by Hybridization. *J. Am. Chem. Soc.* **2018**, *140*, 1632–1638. https://doi.org/10.1021/jacs.7b03567.

(11) Smith, J.; Calidas, D.; Schmidt, H.; Lu, T.; Rasoloson, D.; Seydoux, G. Spatial Patterning of P Granules by RNA-Induced Phase Separation of the Intrinsically-Disordered Protein MEG-3. *Elife* **2016**, *5*, 1–18. https://doi.org/10.7554/eLife.21337.

(12) Brangwynne, C.; Hyman, T. In Retrospect: The Origin of Life. *Nature* **2012**, *491*, 524–525. https://doi.org/10.1038/491524a.

(13) Kuo, C. H.; Leon, L.; Chung, E. J.; Huang, R. T.; Sontag, T. J.; Reardon, C. A.; Getz, G. S.; Tirrell, M.; Fang, Y. Inhibition of Atherosclerosis-Promoting MicroRNAs via Targeted Polyelectrolyte Complex Micelles. *J. Mater. Chem. B* **2014**, *2*, 8142–8153. https://doi.org/10.1039/c4tb00977k.

(14) Marras, A. E.; Vieregg, J. R.; Ting, J. M.; Rubien, J. D.; Tirrell, M. V. Polyelectrolyte Complexation of Oligonucleotides by Charged Hydrophobic-Neutral Hydrophilic Block Copolymers. *Polymers (Basel).* **2019**, *11*, 83. https://doi.org/10.3390/polym11010083.

(15) Lueckheide, M.; Vieregg, J. R.; Bologna, A. J.; Leon, L.; Tirrell, M. V. Structure-Property Relationships of Oligonucleotide Polyelectrolyte Complex Micelles. *Nano Lett.* **2018**, *18*,

7111–7117. https://doi.org/10.1021/acs.nanolett.8b03132.

(16) De Kruif, C. G.; Weinbreck, F.; De Vries, R. Complex Coacervation of Proteins and Anionic Polysaccharides. *Curr. Opin. Colloid Interface Sci.* **2004**, *9*, 340–349. https://doi.org/10.1016/j.cocis.2004.09.006.

(17) Gouin, S. Microencapsulation: Industrial Appraisal of Existing Technologies and Trends. *Trends Food Sci. Technol.* **2004**, *15*, 330–347. https://doi.org/10.1016/j.tifs.2003.10.005.

(18) Perry, S. L.; Leon, L.; Hoffmann, K. Q.; Kade, M. J.; Priftis, D.; Black, K. A.; Wong, D.; Klein, R. A.; Pierce, C. F.; Margossian, K. O.; et al. Chirality-Selected Phase Behaviour in Ionic Polypeptide Complexes. *Nat. Commun.* **2015**, *6*, 6052. https://doi.org/10.1038/ncomms7052.

(19) Sadman, K.; Wang, Q.; Chen, Y.; Keshavarz, B.; Jiang, Z.; Shull, K. R. Influence of Hydrophobicity on Polyelectrolyte Complexation. *Macromolecules* **2017**, *50*, 9417–9426. https://doi.org/10.1021/acs.macromol.7b02031.

(20) Wang, Q.; Schlenoff, J. B. The Polyelectrolyte Complex/Coacervate Continuum. *Macromolecules* **2014**, *47*, 3108–3116. https://doi.org/10.1021/ma500500q.

(21) Liu, Y.; Momani, B.; Winter, H. H.; Perry, S. L. Rheological Characterization of Liquid-to-Solid Transitions in Bulk Polyelectrolyte Complexes. *Soft Matter* **2017**, *13*, 7332–7340. https://doi.org/10.1039/c7sm01285c.

(22) Tirrell, M. Polyelectrolyte Complexes: Fluid or Solid? *ACS Cent. Sci.* **2018**, *4*, 532–533. https://doi.org/10.1021/acscentsci.8b00284.

(23) Zhang, Y.; Batys, P.; O'Neal, J. T.; Li, F.; Sammalkorpi, M.; Lutkenhaus, J. L. Molecular Origin of the Glass Transition in Polyelectrolyte Assemblies. *ACS Cent. Sci.* **2018**, *4*, 638–644. https://doi.org/10.1021/acscentsci.8b00137.

(24) Sadman, K.; Wang, Q.; Shull, K. R. Guanidinium Can Break and Form Strongly Associating Ion Complexes. *ACS Macro Lett.* **2019**, *8*, 117–122. https://doi.org/10.1021/acsmacrolett.8b00824.

(25) Herzog-Arbeitman, A.; Ting, J. M.; Meng, S.; Wu, H.; Tirrell, M. V. Patterning Polyelectrolyte Complexes with Alternating Monomer Sequence Distributions. *ChemRxiv* **2019**. https://doi.org/10.26434/chemrxiv.11320439.v1.

(26) Marciel, A. B.; Srivastava, S.; Tirrell, M. V. Structure and Rheology of Polyelectrolyte Complex Coacervates. *Soft Matter* **2018**, *14*, 2454–2464. https://doi.org/10.1039/C7SM02041D.

(27) Li, L.; Srivastava, S.; Andreev, M.; Marciel, A. B.; De Pablo, J. J.; Tirrell, M. V. Phase Behavior and Salt Partitioning in Polyelectrolyte Complex Coacervates. *Macromolecules* **2018**, *51*, 2988–2995. https://doi.org/10.1021/acs.macromol.8b00238.

(28) Lemmon, E. W.; McLinden, M. O.; Friend, and D. G. *NIST Chemistry WebBook, NIST Standard Reference Database*; 2017. https://doi.org/10.18434/T4D303.

(29) Ting, J. M.; Wu, H.; Herzog-Arbeitman, A.; Srivastava, S.; Tirrell, M. V. Synthesis and Assembly of Designer Styrenic Diblock Polyelectrolytes. *ACS Macro Lett.* **2018**, *7*, 726–733. https://doi.org/10.1021/acsmacrolett.8b00346.

(30) Wu, H.; Ting, J. M.; Werba, O.; Meng, S.; Tirrell, M. V. Non-Equilibrium Phenomena and Kinetic Pathways in Self-Assembled Polyelectrolyte Complexes. *J. Chem. Phys.* **2018**, *149*, 163330. https://doi.org/10.1063/1.5039621.

(31) Chang, L. W.; Lytle, T. K.; Radhakrishna, M.; Madinya, J. J.; Vélez, J.; Sing, C. E.; Perry, S. L. Sequence and Entropy-Based Control of Complex Coacervates. *Nat. Commun.* **2017**, *8*, 1273. https://doi.org/10.1038/s41467-017-01249-1.

(32) Sun, J.; Perry, S. L.; Schiffman, J. D. Electrospinning Nanofibers from Chitosan/Hyaluronic Acid Complex Coacervates. *Biomacromolecules* **2019**, *20* (11), 4191–4198. https://doi.org/10.1021/acs.biomac.9b01072.

Chapter 4. Accelerating and Reversing Solid-Liquid Transition of Polyelectrolyte Complexes by Tuning Salt and Solvent

This chapter will be published in the future as a journal article.

4.1 Introduction

The physical states of bulk polyelectrolyte complexes[1–6] can range from glassy solids to low viscosity liquids, governed by the chemical and physical nature of their polyelectrolyte components. Over the past decades, most academic efforts have been dedicated to investigating PECs in the liquid form (often termed as liquid coacervates)[7–11] because of their resemblance to membrane-less organelles in partitioning macromolecules and processes, as well as their longstanding uses for highly efficient encapsulation and release in materials science and engineering. More recently however, an increasing number of studies have reported probing the structures, properties, and applications of solid PECs,[12–17] as well as the mechanisms behind solid-liquid transitions.[18–23] By outlining well-defined routes to produce designer PECs that are moldable, injectable, and dynamic/responsive to external stimuli, these emerging efforts hold immense potential for accessing supersoft matter that can also transform into reinforced gels, tough elastomers, and extensible materials.[24,25]

No matter what end-use applications PECs are prepared for, they need to be engineered into an appropriate form for basic unit operations. The most broadly exploited means of processing large quantities of PECs is by adding salt, disrupting the internal associations of PECs. The dynamics,[26–29] phase behavior,[7] structural evolution,[8] and thermal responses[30] of PECs during salt-driven dissociation have all been extensively studied, with the cited works representing only a small fraction of the polyelectrolyte community's reports. We focus on one specific general

paradigm: salt can break boundaries between solid and liquid PECs,[31] opening plentiful application routes in tuning PEC properties along the complex-coacervate continuum by modulating environmental factors to modulate the effective number of intrinsic ion pairs in the complex phase. In comparison to the progress in understanding salt effects on PECs, far fewer PEC studies systematically describe the influence of factors other than ionic strength. For example, solvent quality can strongly affect the properties of PECs.[32–35] Incorporating cosolvents as another dimension may accelerate or slow down the salt-driven PEC dissociation process. For instance, strongly interacting PEC systems that start as solid precipitates need exceptionally high salt to dissociate, rendering them recalcitrant to plasticization. Increasing the solvent hydrophobicity can decrease the amount of salt required to disrupt the electrostatic associations.[20] Furthermore, water molecules play significant roles as plasticizers for self-assembled PECs.[21] Modulating solvent quality can accordingly enrich our knowledge of how water molecules interact with and respond to complexes comprising charged polymers.[36–38] Finally, certain industrially relevant PEC applications require solvent removal in the post-processing stage, such as biomedical nanofiber fabrication,[39,40] and can benefit from a less polar solvent mixture to speed up evaporation.

In this work, we explore the interplay between salt and cosolvent in the context of the solid-liquid transition process of a model PEC system, composed of two oppositely charged styrenic polyelectrolytes poly[(vinylbenzyl) trimethylammonium chloride] (PVBTMA) and poly[sodium 4-styrenesulfonate] (PSS) (Figure 4.1). In pure (salt-free) water, complexation forms solid precipitates with exceptionally high salt resistance to common monovalent salts.[18,20] As we added NaBr to 2.0 M, this system was found to phase change from solid to liquid, visually from cloudy aggregates to transparent network structures as captured by optical microscopy. The PEC continued to dissociate from liquid coacervates into homogenous solution at 7.0 M NaBr. In our

previous study, the physical states of this PEC under different salt concentrations were further verified by rheology with comprehensive examination of the underlying mechanism for the solid-to-liquid transition from the perspectives of viscoelasticity, phase behavior, and structural evolution.[18] This was one of the first experimental reports to capture a highly unusual salt-stiffening behavior in PEC phase behavior driven by water loss from self-assembled nanoscale clusters. To tune the solvent quality, we prepared PVBTMA/PSS complexes in binary mixtures of water and organic solvent; ethanol, methanol, 1,3 propanediol, and ethylene glycol were chosen because of their miscibility with water.

4.2 Experimental Details

4.2.1 Materials

The following chemicals were reagent grade and used as received unless otherwise specified: ethylene glycol (anhydrous, Sigma, 99.8%), ethanol (anhydrous, Sigma, ≥99.5%), methanol (anhydrous, Sigma, 99.8%), 1,3 propanediol (Sigma, 98%), poly(styrene sulfonate, sodium salt) (PSS, 20,700 g/mol, Polymer Standards Service), poly(acrylic acid sodium salt) (PAANa, 14,800 g/mol, Polymer Source), sodium bromide (Fisher Scientific, >99%), and 1-butyl-3-methylimidazolium bromide (BMI-Br, Sigma, >97%). All water used during the experiment was filtered from a Milli-Q water purification system at a resistivity of 18.2 MΩ-cm at 25 °C.

4.2.2 Polymer Synthesis

The chemical structures of PVBTMA and PSS are shown in Figure 4.1. PSS_{100} was used as received. (The subscript indicates the degree of polymerization). $PVBTMA_{100}$ with symmetric

length as PSS was synthesized with aqueous reversible addition-fragmentation chain transfer (RAFT) polymerization, followed the previous work in our group.[41]

Figure 4. 1: Chemical structures of (a) PVBTMA and (b) PSS.

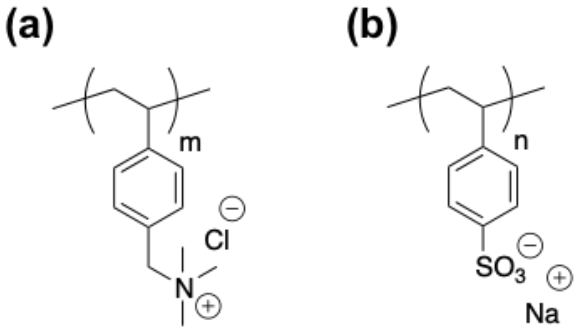

4.2.3 PEC Sample Preparation

PECs were prepared under 1:1 stoichiometric charge-matched conditions between polycation and polyanion and the "as prepared" polymer concentration was maintained at 1 wt%. Stock solutions of polycations and polyanions were added sequentially to a solution with desired amount of NaBr stock solution (5 M), organic solvent component and Milli-Q water in Eppendorf Tubes. Afterward, samples were immediately vortexed for at least 30 s.

4.2.4 Optical Light Microscopy Imaging

Optical phase contrast microscopy (Leica DMI 6000B using Leica Application Suite (LAS) image acquisition software, Wetzlar, Germany) was used to obtain optical micrographs of the PEC samples. After 100 μL of the PEC samples were prepared in 1.5 mL microcentrifuge tubes, they were immediately transferred into ultra-low attachment 96-well plates (Costar, Corning Inc.). The plates were then carefully sealed to prevent solvent evaporation. Imaging was performed one day

after the sample preparation so that phase separation was largely completed. The acquired images were then processed with ImageJ software to add on scale bars and enhance contrast for visual clarity.

4.2.5 Thermalgravimetric Analysis

The TGA measurements were conducted on TA Instrument SDT 600 TGA with aluminum pans in air environment. The temperature was ramped from 25-650 °C at 2 °C/min.

4.3 Results and Discussion

4.3.1 Effect of Cosolvent on the Salt Resistance of PECs

To figure out the effect of various miscible cosolvents on the behaviors of PVTBMA/PSS complexes, we first prepared samples in mixed solvents of ethylene glycol/water and dissociated it with added NaBr.[20] Optical light microscopy was employed to qualitatively determine the physical states of the PECs, and the same criterion of determining the advent of the liquid state from the emergence of clear, solid structures was followed. In the map of optical images in Figure 4.2, from the top to bottom of the gallery, as the volume fraction of ethylene glycol (ϕ_{EG}) was tuned from ϕ_{EG} = 0.2 to 0.7, the solvent environment present in both the complex and supernatant phases became more hydrophobic. The red and blue solid lines indicate the apparent solid-liquid and liquid-solution transitions of this PEC system, respectively. The solid-liquid transition is evaluated by the change in morphology from dense, cloudy aggregates to fluid-like transparent networks or droplets; the liquid-solution transition is defined as the critical point in salt resistance, or the binodal phase boundary that separates the two-phase complex system from the one-phase

homogeneous polyelectrolyte solution. From the outline of the red and blue boundaries, we observe a shift to lower NaBr concentrations with increasing ϕ_{EG}. For instance, an increase of ϕ_{EG} from 0.3 to 0.6 results in a huge reduction in salt resistance from 2.5 to 1.5 M NaBr. The same general trends were also seen when repeated with ethanol as the organic solvent component of the cosolvent instead of ethylene glycol. (Figure 4.3). These findings led to a clear correlation between solvent quality and NaBr salt for PVBTMA/PSS complexes: the salt resistance of PECs can be systematically weakened by increasing the relative hydrophobicity of the solvent environment.

Figure 4. 2: Optical micrographs of PVBTMA/PSS complexes with NaBr and ethylene glycol/water.

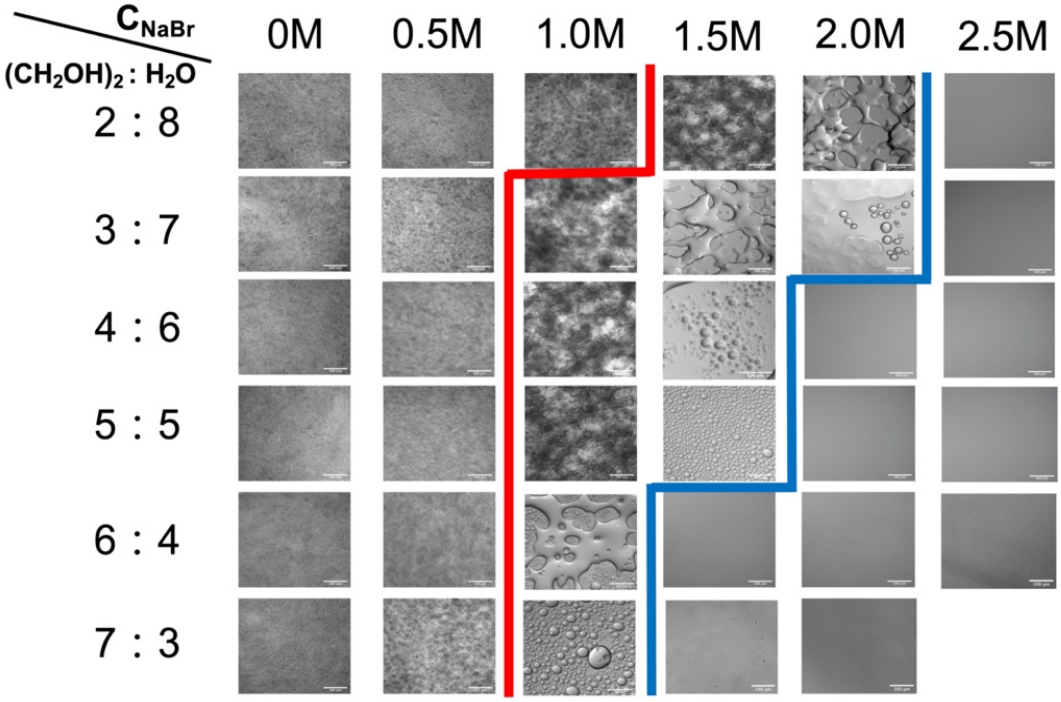

The PECs are prepared in 0 to 2.5 M NaBr (left to right) and in 2:8 to 7:3 volumetric ratios of ethylene glycol/ water mixtures (top to bottom). To guide the eye, the solid red line represents the point where the complexes phase transitions from solid to liquid, and the solid blue line denotes the phase transition from liquid to solution. All scale bars denote 100 μm. (adapted from Meng et al.[20])

Figure 4. 3: Optical micrographs of PVBTMA/PSS complexes with NaBr and ethanol/water (high salt, high organic solvent domain are excluded).

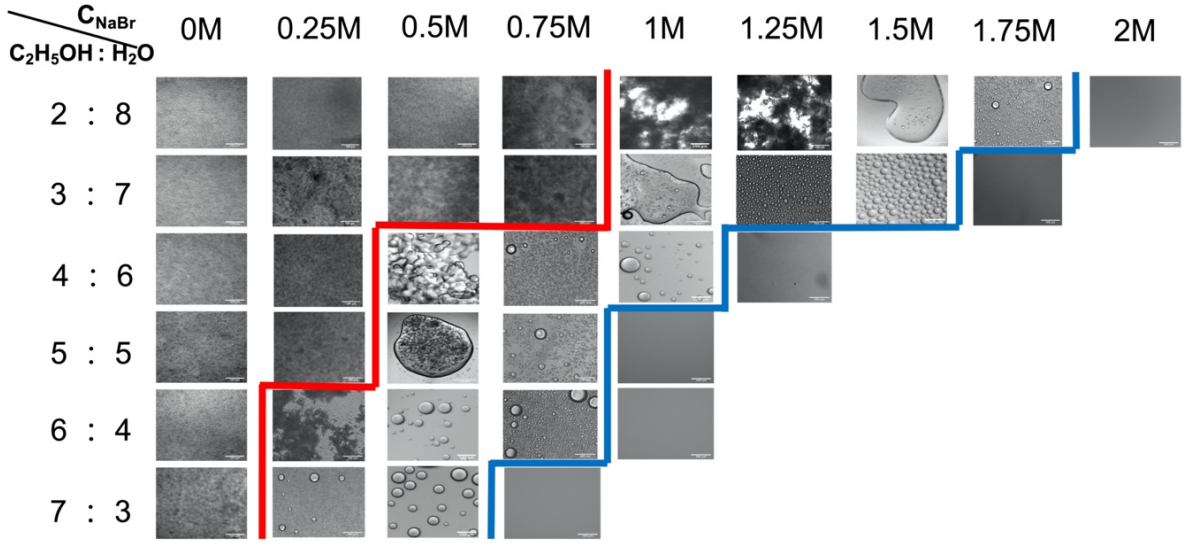

PECs are prepared in 0 to 2 M NaBr (left to right) and in 2:8 to 7:3 volumetric ratios of ethanol/water mixtures (top to bottom). To guide the eye, the solid red lines represent the point where the complexes phase transitions from solid to liquid, and the solid blue line denotes the phase transition from liquid to solution. All scale bars denote 100 μm. (adapted from Meng et al.[20])

4.3.2 Effect of the interplay between salt and solvent on the salt resistance of PEC

As we continued to explore how salt and solvent can be tuned together to modulate PEC states along the complex-coacervate continuum, we noticed that the role of salt in controlling PEC behavior is not necessarily general to all cosolvent-salt possibilities in the results above. Various inorganic salts have been well studied by the PEC community in the past decade,[42,43] often following a Hofmeister series rationale to group salts based on solvation by water. While poorly-solvated compounds like KBr interact strongly with common strongly interacting PECs, we were interested in utilizing a salt that can impart plasticizing properties in both aqueous and organic solvents. When we switched salt from NaBr into an ionic liquid salt, 1-butyl-3-methylimidazolium bromide (BMI-Br), we discovered a completely different trend. In pure water, BMI-Br worked

more effectively than NaBr in dissociating PEC. As displayed in Figure 4.4, lower concentrations of BMI-Br were needed than NaBr to drive PEC through the complete solid-liquid-coacervate spectrum. In ethylene glycol/water mixture, a very intriguing behavior was observed in this PEC with BMI-Br. At fixed salt levels by column in the optical image gallery of Figure 4.5, the phase transition driven by BMI-Br was not affected by changes in solvent quality.

Figure 4. 4: Optical micrographs of PVBTMA/PSS complexes doped with NaBr and BMI-Br in pure water.

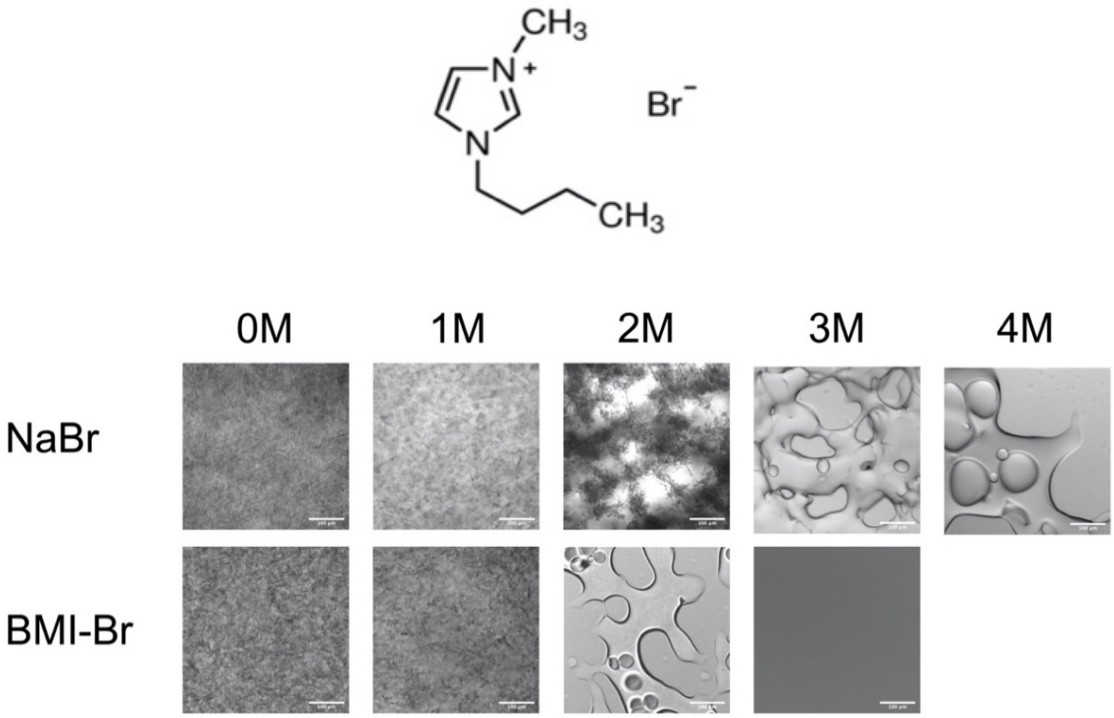

Figure 4. 5: Optical micrographs of PVBTMA/PSS complexes with BMI-Br and ethylene glycol/water.

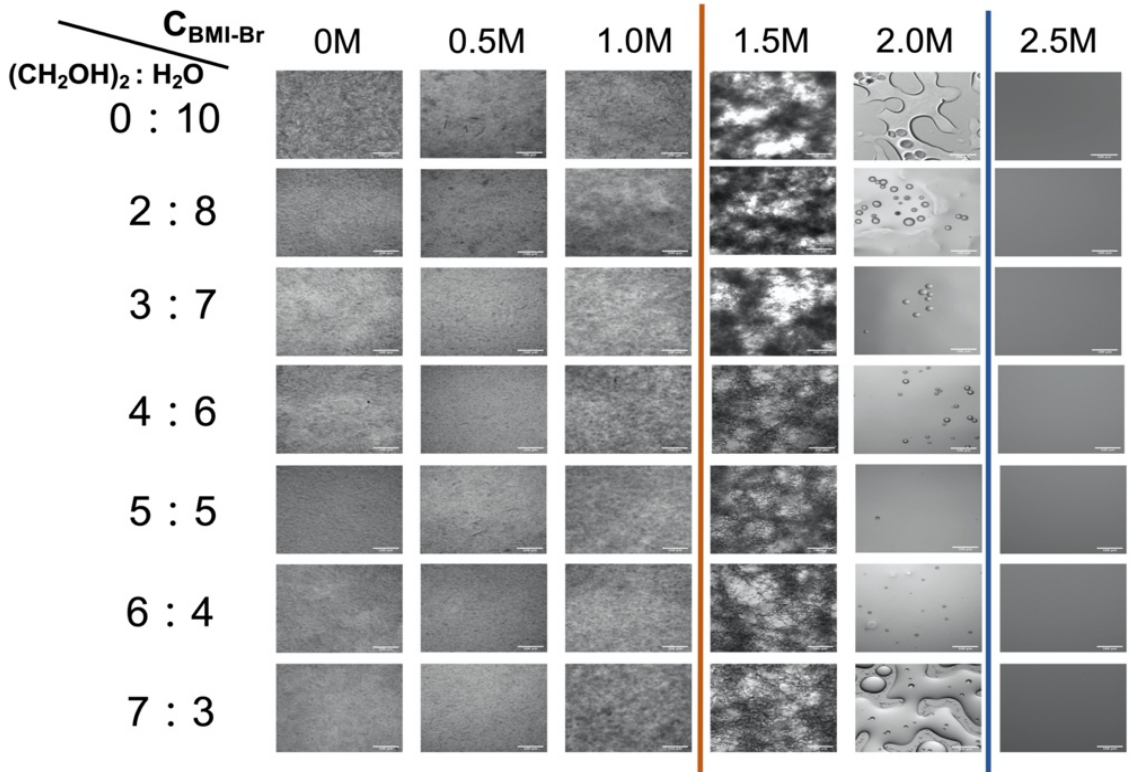

PECs are prepared in 0 to 2.5 M BMI-Br (left to right) and in 0:10 to 7:3 volumetric ratios of ethylene glycol/ water mixtures (top to bottom). To guide the eye, the solid red line represents the point where the complexes phase transitions from solid to liquid, and the solid blue line denotes the phase transition from liquid to solution. All scale bars denote 100 μm.

We highlight here that the behavior of PVBTMA/PSS self-assembled in ethylene glycol/water and dissociated by BMI-Br (Figure 4.5) is vastly distinct from the NaBr-doped PECs (Figure 4.2). We believe that such dissemblance can be attributed to solubility differences of NaBr and BMI-Br in the ethylene glycol/water co-solvent. To be more specific, the solubility of NaBr is much higher in water than in ethylene glycol.[44] Therefore, we hypothesize the following scheme to rationalize the phase transition behavior of PECs in mixed solvents and salts. As illustrated in Figure 4.6a, in pure water, well-dissolved Na^+ and Br^- ions are closely encompassed by shells of water molecules, whereas in mixed solvents of ethylene glycol and water, they are surrounded by

relatively looser solvent shells due to poorer solubility. Figure 4.6b depicts this using a polyanion chain cartoon as a representative example with NaBr – in a mixed solvent, the less soluble environment for added salt ions induces the formation of detached solvent shells and thereby enhances the propensity to strongly bind with the polyelectrolyte chains. As a result, when the same amount of salt is added, polyelectrolyte chains are more screened and coiled in mixed solvent than in water. Based on the same mechanism, a PEC system is more screened and dissociated in mixed solvents than in pure water (Figure 4.6c). In other words, PECs are less resistant to NaBr in a cosolvent mixture with higher ethylene glycol fraction. In comparison to NaBr, BMI-Br is well dissolved in both water and ethylene glycol.[45] Accordingly, adjusting the ratios between ethylene glycol and water does not significantly alter the solubility of BMI-Br, and thus, the resistance of PVBTMA/PSS PECs to BMI-Br is the same across all examined ratios of ethylene glycol to water. (Figure 4.5)

Figure 4. 6: Schematic illustrating the molecular details of salt, single chains and PECs in different solvents.

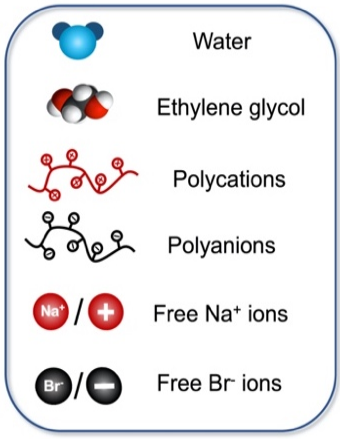

Figure 4.6 (Continued)

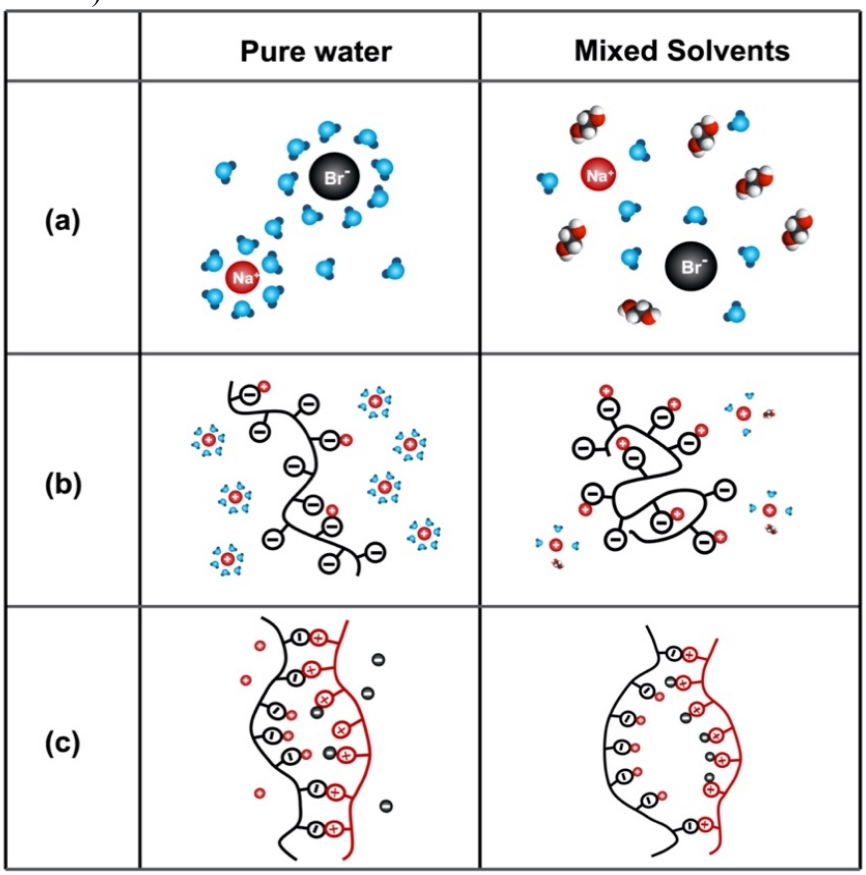

(a) Na^+ and Br^- ions, (b) single polyanion chain doped with Na^+ ions, and (c) PEC doped with NaBr in pure water and mixed solvents of water and ethylene glycol.

From the above-mentioned differences between NaBr and BMI-Br, we concluded that the resistance of PECs towards certain type of salt was not dominated by the solvent hydrophobicity alone, as we originally believed. Instead, it was governed by the solubility of the added salt in its solvent environment: The investigated PEC becomes more resistant to certain salt when the salt is in a more soluble environment. To further support this, we next explored the NaBr-driven phase transition of this PEC in two additional cosolvents: 1,3 propanediol/water (Figure 4.7) and methanol/water (Figure 4.8). These two organic solvents were deliberately selected due to their miscibility with water and also their resemblance to the two previously studied solvents, ethylene

glycol and ethanol. The resistance of PVBTMA/PSS to NaBr in these four solvents are summarized in Figure 4.9. The height of each bar indicates the salt concentration where the complexes transitioned from solid into liquid under certain cosolvent condition. Accordingly, taller bars in the phase diagram indicate higher concentrations of added salt are required to drive the complexes to transfer from solids into liquids. In ranking how cosolvents affect solid/liquid dissolution from Figure 4.9, we observe that at fixed organic solvent levels, the PEC generally has the highest NaBr salt resistance with ethylene glycol, followed by 1,3 propanediol, methanol, and ethanol as the organic solvent component with water. Comparing this solvent trend of salt resistance with the solubility of NaBr in these four solvents, we found that these two ordered sequences agree with each other. NaBr dissolves best in ethylene glycol (4.28 M), followed by 1,3 propanediol (2.46 M), methanol (1.29 M), and ethanol (0.18 M). This demonstrates that added cosolvents and salt can be rationally combined to tune the salt resistance in solid/liquid/solution transitions of PVBTMA/PSS in solutions.

Figure 4. 7: Optical micrographs of PVBTMA/PSS in NaBr and propanediol/water.

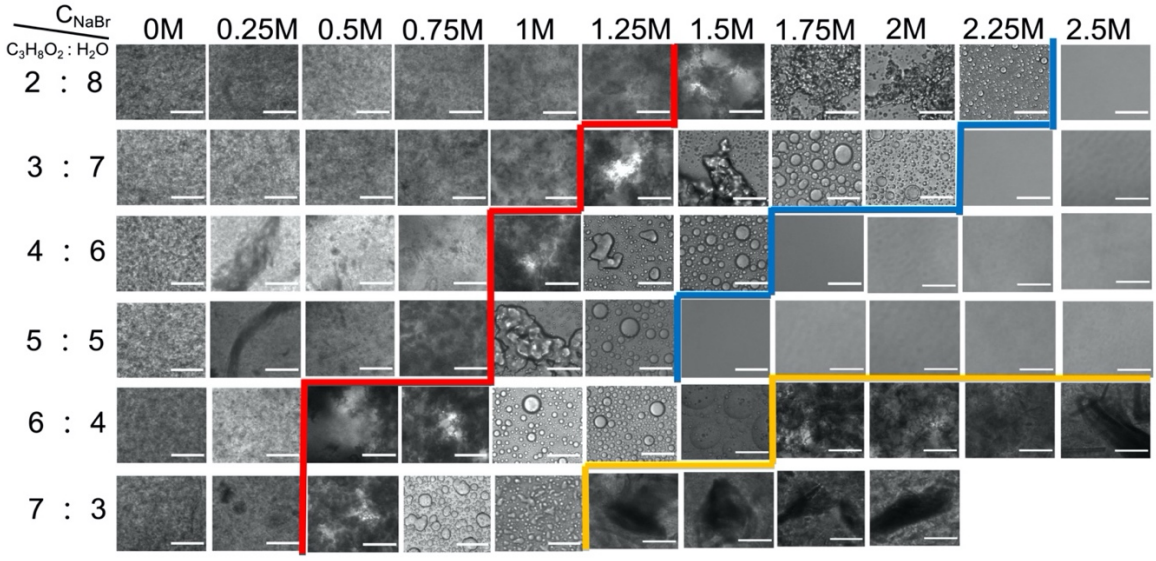

Figure 4.7 (Continued)
PECs are prepared in 0 to 2.5 M NaBr (left to right) and in 2:8 to 7:3 volumetric ratios of propanediol/water mixtures (top to bottom). To guide the eye, the solid red lines represent the point where the complexes phase transitions from solid to liquid, the solid blue line denotes the phase transition from liquid to solution, and the solid yellow line dictates where the complexes transitions back from liquid to solid. All scale bars denote 100 μm.

Figure 4. 8: Optical micrographs of PVBTMA/PSS complexes in NaBr and methanol/water.

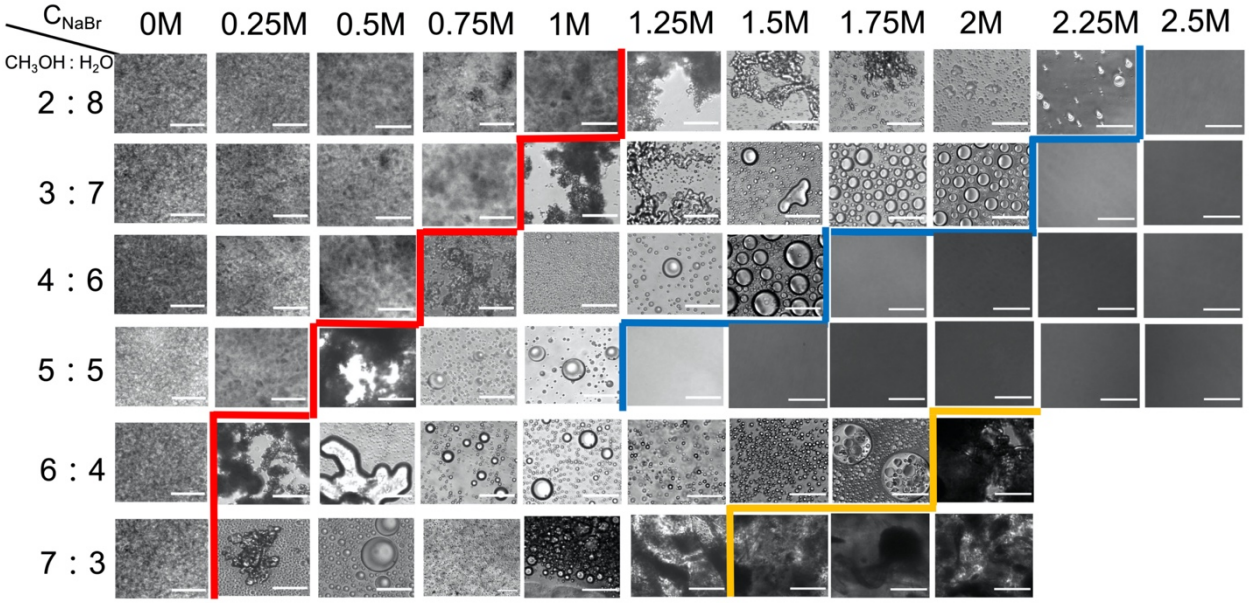

PECs are prepared in 0 to 2.5 M NaBr (left to right) and in 2:8 to 7:3 volumetric ratios of methanol/water mixtures (top to bottom). To guide the eye, the solid red lines represent the point where the complexes phase transitions from solid to liquid, the solid blue line denotes the phase transition from liquid to solution, and the solid yellow line dictates where the complexes transitions back from liquid to solid. All scale bars denote 100 μm.

Figure 4. 9: Summary of NaBr concentrations where the solid-liquid phase transition of PVBTMA/PSS complexes occurred in 4 co-solvent systems.

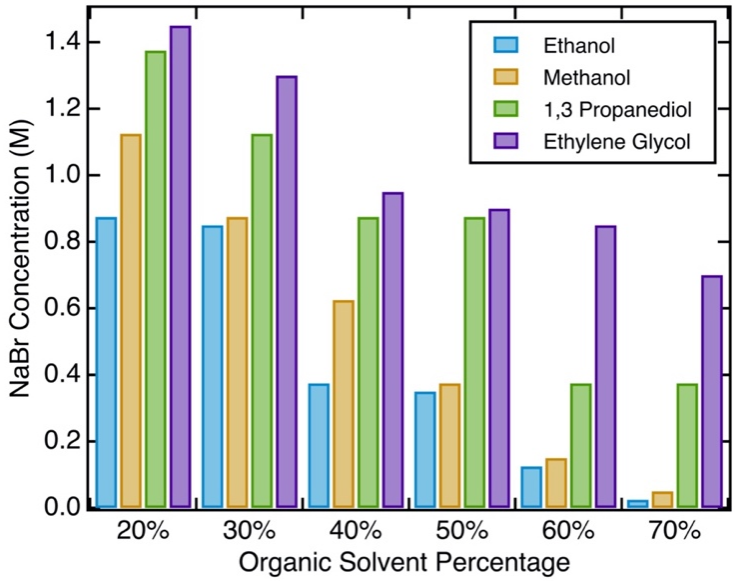

Ethanol (blue), methanol (orange), 1,3 propanediol (green), and ethylene glycol (purple) are the organic solvent component in the co-solvent. The x-axis and y-axis represent the percentages of organic solvents in the cosolvent mixtures and NaBr salt concentrations, respectively.

4.3.3 Gel Collapse

As we probed the regime beyond the one-phase solution stage in select cosolvent conditions across the complex-coacervate continuum, we were encountered unexpected behavior of PVBTMA/PSS complexes that involved the reformation of droplets or precipitates under high salt and high organic solvent conditions. This "reverse phase transition" was observed with ethanol, methanol, and propanediol, but not with ethylene glycol. In ethanol/water (Figure 4.10a and 4.10c), when the fraction of ethanol ϕ_{Ethanol} in the cosolvent reached 0.5, liquid droplet surprisingly reemerged from the homogenous solution at 2.0 M NaBr. At ϕ_{Ethanol} = 0.6 and 0.7, liquids further transformed into solid aggregates at high salt conditions. As marked by the purple and yellow lines in Figure 4.10a, ϕ_{Ethanol} of 0.5 to 0.7, both the solution-liquid and liquid-solid transitions occurred

at lower salt concentrations with increasing ethanol content. Similar behavior was also observed in methanol/water and propanediol/water mixtures as summarized in Figures 4.10d and 4.10e, respectively (full microscopy images are shown in respective Figures 4.7 and 4.8). Here, liquid droplets required >0.6 fraction of organic cosolvent to reform. Additionally, at 0.6 and 0.7 fraction of methanol or propanediol, the PEC never fully dissolved into homogenous solution, but instead, the liquid state persisted until it transferred into solid state.

Figure 4. 10: Optical micrographs of PVBTMA/PSS complexes with NaBr and ethanol/water and maps that summarize physical state of this PEC in different solvents.

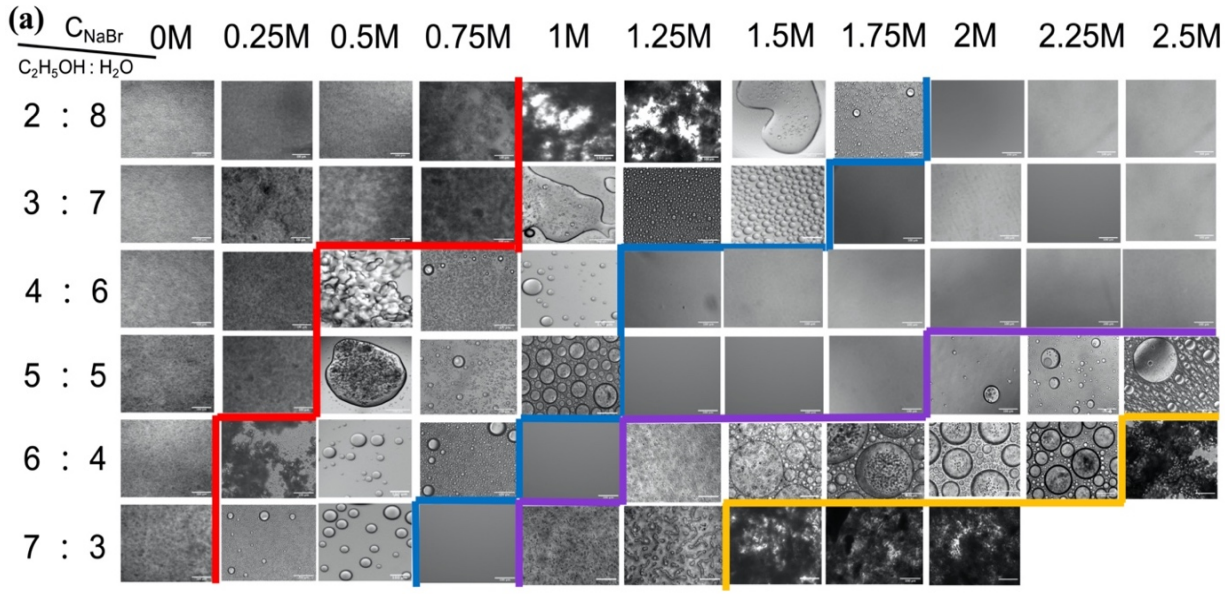

Figure 4.10 (Continued)

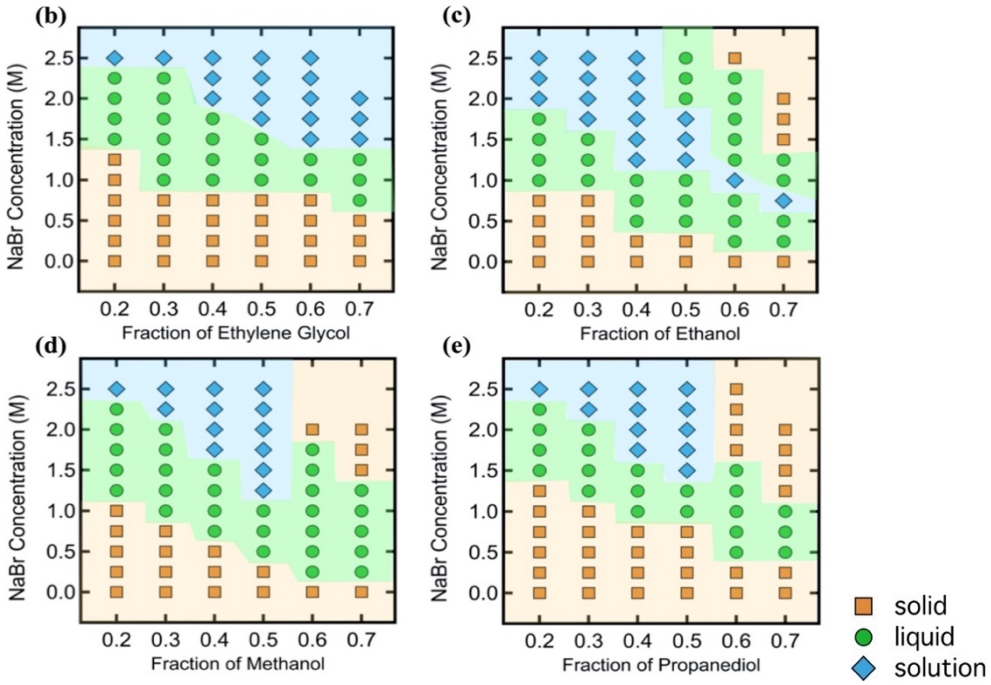

(a) PECs are prepared in 0 to 2.5 M NaBr (left to right) and in 2:8 to 7:3 volumetric ratios of ethanol/water mixtures (top to bottom). To guide the eye, the solid red lines represent the point where the complexes phase transitions from solid to liquid, the solid blue line denotes the phase transition from liquid to solution, the purple line tells the transition from solution to liquid, and the solid yellow line dictates where the complexes transitions back from liquid to solid. All scale bars denote 100 μm. (b)-(e) Maps depicting the physical states of the PECs as a function of NaBr concentration and fraction of ethylene glycol, ethanol, methanol and propanediol. The symbols correspondence is as follows—orange square: solid state, green circle: liquid state, and blue diamond: solution state. The background shading has been added to guide the eye.

To identify the reason behind this reverse phase transition behavior, we investigated the material compositions of the liquids and solids formed under high salt and high organic solvent conditions, corresponding the images at lower right corner of the optical micrograph map (Figure 4.10a, 4.7, and 4.8). When we dissolved PVBTMA and PSS single chains separately in 0.25 M NaBr salt and 0-0.7 cosolvent, under the microscope we found that PVBTMA remained dissolved at high salt and high organic solvent conditions across all the four types of cosolvent mixtures (Figure 4.11). For PSS chains, while no reverse phase transition occurred in ethylene glycol/water,

(Figure 4.12) liquids and solids at high salt and high organic solvent conditions emerged in the other three cosolvents (Figure 4.13, 4.14 and 4.15). The conditions where PSS chains precipitated out from the solution coincided with where the "reverse phase transition" was found in the PECs. This suggests that the droplets and precipitates were composed solely of PSS. By using thermogravimetric analysis (TGA), we took advantage of the difference in the decomposition temperature (T_d) of PVBTMA ($T_d \cong 250$ °C) and PSS ($T_d \cong 450$ °C) individually and demonstrated that the TGA profile of the separated complex phase at high salt and high organic solvent followed the degradation profile of PSS alone (Figure 4.16). Together, these findings demonstrate that the reformed solids and liquids at high salt and organic solvent conditions emerge from the precipitation of single polyelectrolyte chains and not by a re-complexation of oppositely charged chains.

Figure 4. 11: Optical micrographs of PVBTMA single chain in different mixed solvent conditions.

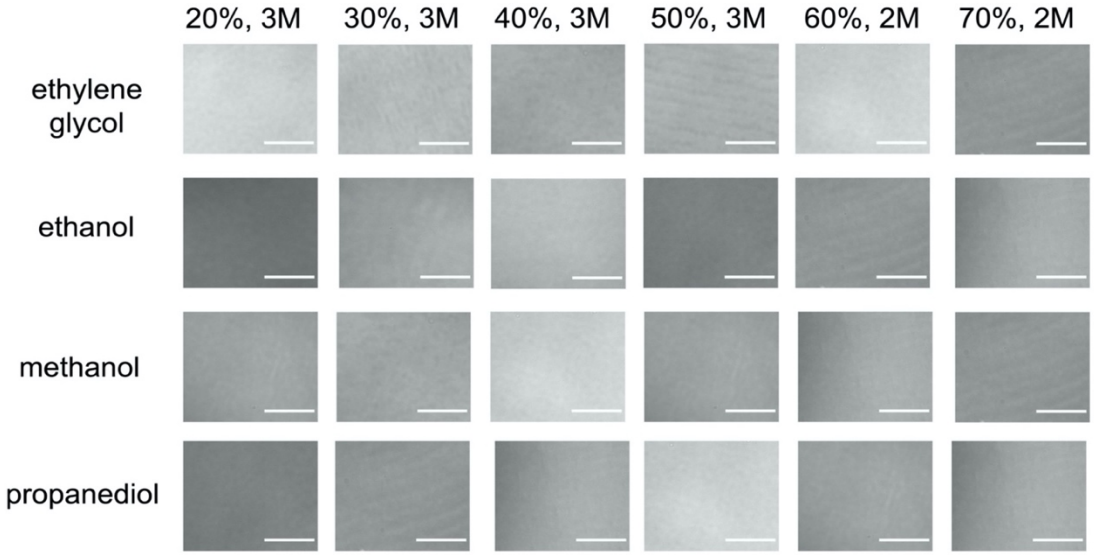

The types of organic solvent in the co-solvent were labeled on the left of the images. Numbers on the top of each column represent the percentage of organic solvent in the solvent mixture and the concentrations of added NaBr.

Figure 4. 12: Optical micrographs of PSS single chain in ethylene glycol/water co-solvents.

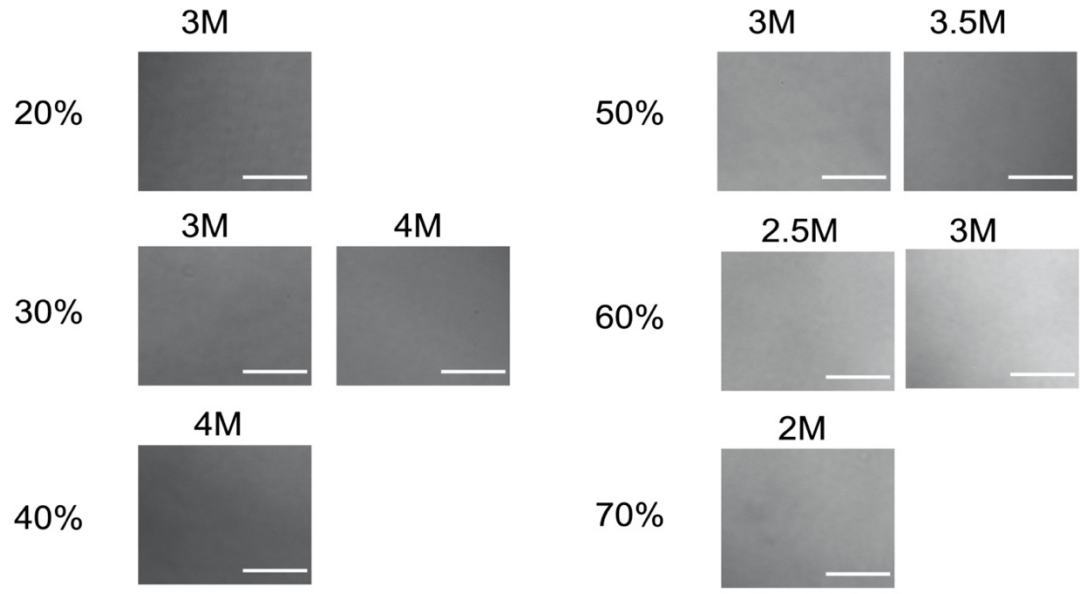

Numbers on the left of each image represent the percentages of organic solvent in the solvent mixture. Numbers on the top of the images are the concentrations of added NaBr.

Figure 4. 13: Optical micrographs of PSS single chain in ethanol/water co-solvents.

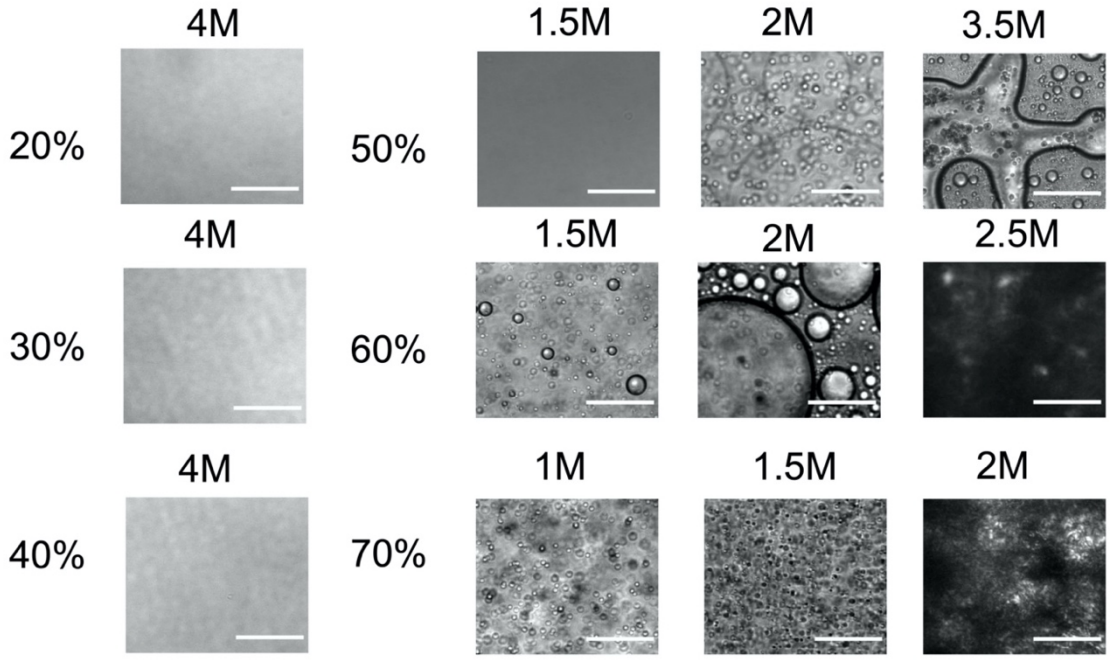

Numbers on the left of each image represent the percentages of organic solvent in the solvent mixture. Numbers on the top of the images are the concentrations of added NaBr.

Figure 4. 14: Optical micrographs of PSS single chain in methanol/water co-solvents.

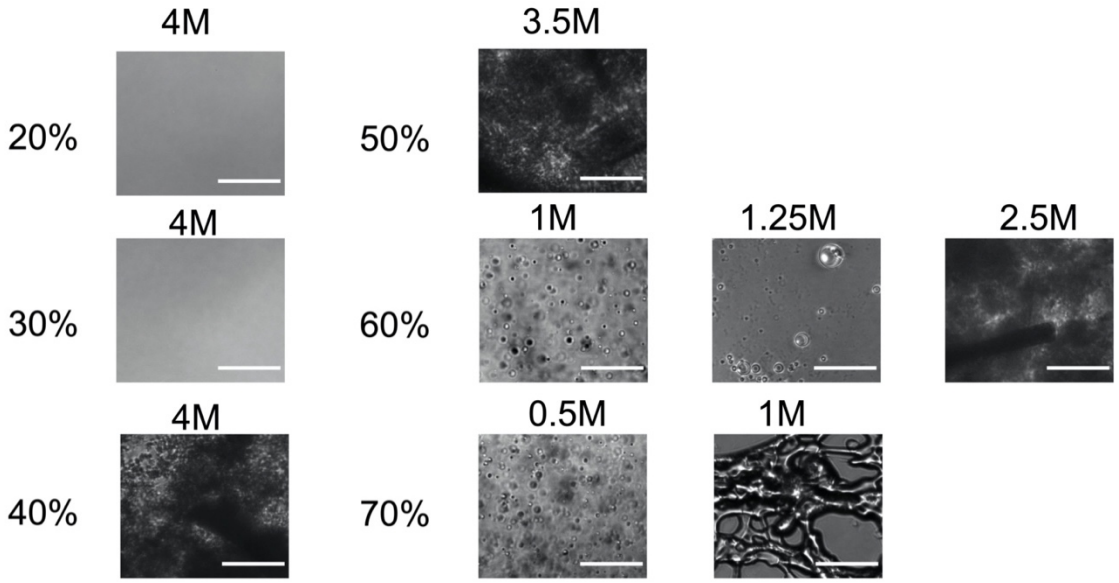

Numbers on the left of each image represent the percentages of organic solvent in the solvent mixture. Numbers on the top of the images are the concentrations of added NaBr.

Figure 4. 15: Optical micrographs of PSS single chain in 1,3 propanediol/water co-solvents.

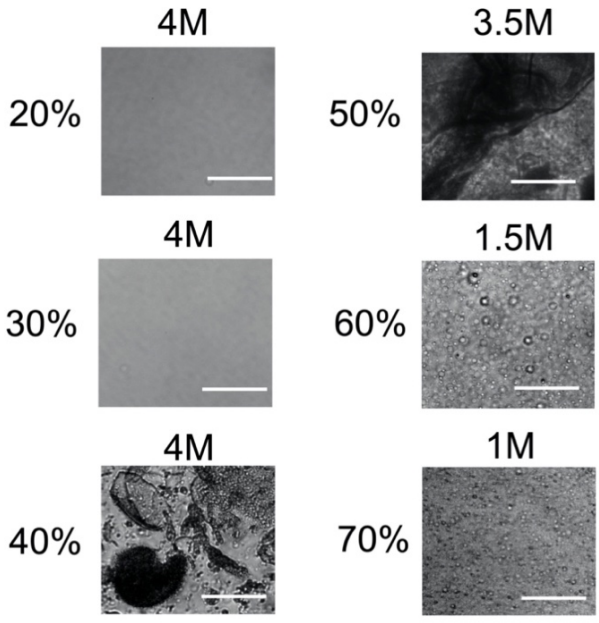

Numbers on the left of each image represent the percentages of organic solvent in the solvent mixture. Numbers on the top of the images are the concentrations of added NaBr.

Figure 4. 16: TGA measurements for PEC and single chains.

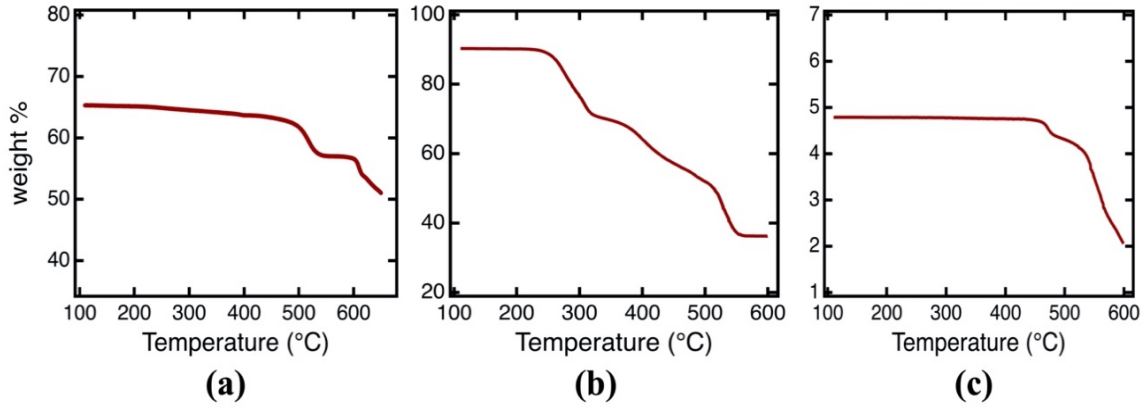

(a) PVBTMA/PSS complex in ethanol/water co-solvent with 70% ethanol and doped with 1.5 M NaBr, (b) PVBTMA single chain in the solid form, and (c) PSS single chain in water solution.

From a larger body of literature, we found that the mechanism of the single chain precipitation at high salt and high organic cosolvent conditions can be well explained by polyelectrolyte gel collapse, which occurs because of the formation of ion-pairs and subsequent aggregation into ion clusters.[46] To be more specific, PSS chains were highly screened at high salt concentration and transformed from a polyelectrolyte state into an ionomer state.[47] Driven by the attractive dipole interactions and hydrophilic/hydrophobic interactions, the ion pairs on ionomers have been shown known to aggregate and form multiplets or ionic clusters, which result in the collapse of the polyelectrolyte gel.[48,49] As shown in numerous previous experimental and theoretical works, the collapse transition in polyelectrolytes is largely dependent on the quality of the solvent and will become progressively significant when the solvent is poor for polyelectrolytes.[50] Therefore, PSS did not exhibit collapse transition in ethylene glycol/water, as ethylene glycol is a better solvent than ethanol, methanol, and propanediol due to its higher polarity and dielectric constant.

The reason that this collapse transition only occurred in PSS not PVBTMA can be found from the differences in their chemical structures. Even though PVBTMA and PSS are largely similar in chemical structures and both have styrenic groups on their backbones, their charge-carrying groups are hugely different. The charge-carrying group ammonium in PVBTMA are closely surrounded by three methyl groups. Therefore, ion pair formation between salt ions and polyelectrolytes is much more sterically hindered for PVBTMA than PSS. Under the same salt condition, PSS chains are more screened than PVBTMA. Accordingly, at high salt, PSS transformed into ionomer state and precipitated out the solution, but PVBTMA remained as dissolved polyelectrolytes.

4.4 Conclusion

In summary, we have systematically investigated the mutual effects of salt and cosolvent on the solid-liquid transition of a synthetic styrenic PEC system. When NaBr was used to dissociate PVBTMA/PSS formed in the binary solvent mixtures, its solid-to-liquid transitions greatly accelerated as the fraction of the organic solvent content in the solvent mixture increased. A careful comparison of the PEC with added NaBr and in ethanol, methanol, 1,3 propanediol, and ethylene glycol revealed that the differences in salt resistance was a consequence of salt solubility in different solvent conditions. As we probed the high NaBr concentration / high ethanol, methanol, and 1,3 propanediol organic solvent regime, we observed a surprising reverse phase transition, where PECs transferred from liquid droplets back to solid aggregates as NaBr concentration increased. Further analysis unveiled that the droplets and aggregates in this domain were composed

of PSS single chains alone, attributed to polyelectrolyte collapse of PSS as a result of the transition from polyelectrolyte states into ionomer states.

To the best of our knowledge, this is one of the first experimental reports to demonstrate the acceleration of solid-liquid phase transitions in PEC using both salt and solvent hydrophobicity, the correlation between salt solubility and PEC salt resistance, and the reverse phase transitions in PECs by the reemergence collapse of the polyelectrolyte gel. In unlocking this new dimension of properties, many questions still remain to be addressed. At the molecular level, PECs formed in both salt and cosolvent is complicated by interdependent environmental parameters, such as the dielectric constant, salt solubility, and solvent polarity, in addition to traditional considerations in PEC design, such as polymer swelling/dehydration, electrostatic strength/ionic character, and the chemical nature of polyelectrolyte chains. Many of these parameters can induce opposing effects that is challenging to predict a priori. For instance, in a PEC system with added salt, lower dielectric constant in solvent environment can weaken PEC stability by inhibiting complexation between oppositely charged chains, but at the same time, it can also strengthen its salt resistance through hindering interactions between salt and polymers. We hope that our findings can encourage more systematic and detailed future efforts in exploring the wide parameter space this system contains.

4.5 Reference

(1) Bungenberg de Jong, H. G.; Kruyt, H. R. Coacervation. (Partial Miscibility in Colloid Systems). (Preliminary Communication). *Proc. K. Ned. Akad. Wet.* **1929**, *131*, 849–856.

(2) Michaels, A. S. Polyelectrolyte Complexes. *Ind. Eng. Chem.* **1965**, *57*, 32–40. https://doi.org/10.1021/ie50670a007.

(3) Philipp, B.; Dautzenberg, H.; Linow, K. J.; Kötz, J.; Dawydoff, W. Polyelectrolyte Complexes - Recent Developments and Open Problems. *Prog. Polym. Sci.* **1989**, *14*, 91–172. https://doi.org/10.1016/0079-6700(89)90018-X.

(4) Overbeek, J. T. G.; Voorn, M. J. Phase Separation In Polyelectrolyte Solutions. Theory Of Complex Coacervation. *J. Cell. Comp. Physiol.* **1957**, *49*, 7–26. https://doi.org/10.1002/jcp.1030490404.

(5) Srivastava, S.; Tirrell, M. V. Polyelectrolyte Complexation. *Adv. Chem. Phys.* **2016**, *161*, 499–544. https://doi.org/10.1002/9781119324560.

(6) Veis, A. A Review of the Early Development of the Thermodynamics of the Complex Coacervation Phase Separation. *Adv. Colloid Interface Sci.* **2011**, *167*, 2–11. https://doi.org/10.1016/j.cis.2011.01.007.

(7) Li, L.; Srivastava, S.; Andreev, M.; Marciel, A. B.; De Pablo, J. J.; Tirrell, M. V. Phase Behavior and Salt Partitioning in Polyelectrolyte Complex Coacervates. *Macromolecules* **2018**, *51*, 2988–2995. https://doi.org/10.1021/acs.macromol.8b00238.

(8) Marciel, A. B.; Srivastava, S.; Tirrell, M. V. Structure and Rheology of Polyelectrolyte Complex Coacervates. *Soft Matter* **2018**, *14*, 2454–2464. https://doi.org/10.1039/C7SM02041D.

(9) Priftis, D.; Xia, X.; Margossian, K. O.; Perry, S. L.; Leon, L.; Qin, J.; Pablo, J. J. De; Tirrell, M. Ternary , Tunable Polyelectrolyte Complex Fluids Driven by Complex Coacervation. **2014**. https://doi.org/10.1021/ma500245j.

(10) Priftis, D.; Tirrell, M. Phase Behaviour and Complex Coacervation of Aqueous Polypeptide Solutions. *Soft Matter* **2012**, *8*, 9396–9405. https://doi.org/10.1039/c2sm25604e.

(11) Chang, L. W.; Lytle, T. K.; Radhakrishna, M.; Madinya, J. J.; Vélez, J.; Sing, C. E.; Perry, S. L. Sequence and Entropy-Based Control of Complex Coacervates. *Nat. Commun.* **2017**, *8*, 1273. https://doi.org/10.1038/s41467-017-01249-1.

(12) Li, L.; Srivastava, S.; Meng, S.; Ting, J. M.; Tirrell, M. V. Effects of Non-Electrostatic Intermolecular Interactions on the Phase Behavior of PH-Sensitive Polyelectrolyte Complexes. *Macromolecules* **2020**, *53* (18), 7835–7844. https://doi.org/10.1021/acs.macromol.0c00999.

(13) Sadman, K.; Wang, Q.; Chen, Y.; Keshavarz, B.; Jiang, Z.; Shull, K. R. Influence of Hydrophobicity on Polyelectrolyte Complexation. *Macromolecules* **2017**, *50*, 9417–9426. https://doi.org/10.1021/acs.macromol.7b02031.

(14) Shamoun, R. F.; Reisch, A.; Schlenoff, J. B. Extruded Saloplastic Polyelectrolyte Complexes. *Adv. Funct. Mater.* **2012**, *22* (9), 1923–1931. https://doi.org/10.1002/adfm.201102787.

(15) Herzog-Arbeitman, A.; Ting, J. M.; Meng, S.; Wu, H.; Tirrell, M. V. Patterning Polyelectrolyte Complexes with Alternating Monomer Sequence Distributions. *ChemRxiv* **2019**. https://doi.org/10.26434/chemrxiv.11320439.v1.

(16) Ali, S.; Prabhu, V. M. Relaxation Behavior by Time-Salt and Time-Temperature Superpositions of Polyelectrolyte Complexes from Coacervate to Precipitate. *Gels* **2018**, *4*, 11. https://doi.org/10.3390/gels4010011.
(17) Yang, M.; Digby, Z. A.; Schlenoff, J. B. Precision Doping of Polyelectrolyte Complexes: Insight on the Role of Ions. *Macromolecules* **2020**, *53* (13), 5465–5474. https://doi.org/10.1021/acs.macromol.0c00965.
(18) Meng, S.; Ting, J. M.; Wu, H.; Tirrell, M. V. Solid-to-Liquid Phase Transition in Polyelectrolyte Complexes. *Macromolecules* **2020**, *53* (18), 7944–7953. https://doi.org/10.1021/acs.macromol.0c00930.
(19) Liu, Y.; Momani, B.; Winter, H. H.; Perry, S. L. Rheological Characterization of Liquid-to-Solid Transitions in Bulk Polyelectrolyte Complexes. *Soft Matter* **2017**, *13*, 7332–7340. https://doi.org/10.1039/c7sm01285c.
(20) Meng, S.; Liu, Y.; Yeo, J.; Ting, J. M.; Tirrell, M. V; Tirrell, M. V. Effect of Mixed Solvents on Polyelectrolyte Complexes with Salt. *Colloid Polym Sci* **2020**, *298*, 887–894. https://doi.org/10.1007/s00396-020-04637-0.
(21) Zhang, Y.; Batys, P.; O'Neal, J. T.; Li, F.; Sammalkorpi, M.; Lutkenhaus, J. L. Molecular Origin of the Glass Transition in Polyelectrolyte Assemblies. *ACS Cent. Sci.* **2018**, *4*, 638–644. https://doi.org/10.1021/acscentsci.8b00137.
(22) Tirrell, M. Polyelectrolyte Complexes: Fluid or Solid? *ACS Cent. Sci.* **2018**, *4*, 532–533. https://doi.org/10.1021/acscentsci.8b00284.
(23) Fares, H. M.; Ghoussoub, Y. E.; Delgado, J. D.; Fu, J.; Urban, V. S.; Schlenoff, J. B. Scattering Neutrons along the Polyelectrolyte Complex/Coacervate Continuum. *Macromolecules* **2018**, *51* (13), 4945–4955. https://doi.org/10.1021/acs.macromol.8b00699.
(24) Sheiko, S. S.; Dobrynin, A. V. Architectural Code for Rubber Elasticity: From Supersoft to Superfirm Materials. *Macromolecules* **2019**, *52* (20), 7531–7546. https://doi.org/10.1021/acs.macromol.9b01127.
(25) Zhalmuratova, D.; Chung, H.-J. Reinforced Gels and Elastomers for Biomedical and Soft Robotics Applications. *ACS Appl. Polym. Mater.* **2020**, *2* (3), 1073–1091. https://doi.org/10.1021/acsapm.9b01078.
(26) Spruijt, E.; Sprakel, J.; Lemmers, M.; Stuart, M. A. C.; Van Der Gucht, J. Relaxation Dynamics at Different Time Scales in Electrostatic Complexes: Time-Salt Superposition. *Phys. Rev. Lett.* **2010**, *105*, 208301. https://doi.org/10.1103/PhysRevLett.105.208301.
(27) Yang, M.; Shi, J.; Schlenoff, J. B. Control of Dynamics in Polyelectrolyte Complexes by Temperature and Salt. *Macromolecules* **2019**, *52*, 1930–1941. https://doi.org/10.1021/acs.macromol.8b02577.
(28) Hamad, F. G.; Chen, Q.; Colby, R. H. Linear Viscoelasticity and Swelling of Polyelectrolyte Complex Coacervates. *Macromolecules* **2018**, *51*, acs.macromol.8b00401. https://doi.org/10.1021/acs.macromol.8b00401.
(29) Spruijt, E.; Cohen Stuart, M. A.; Van Der Gucht, J. Linear Viscoelasticity of Polyelectrolyte Complex Coacervates. *Macromolecules* **2013**, *46*, 1633–1641. https://doi.org/10.1021/ma301730n.
(30) Shamoun, R. F.; Hariri, H. H.; Ghostine, R. A.; Schlenoff, J. B. Thermal Transformations in Extruded Saloplastic Polyelectrolyte Complexes. *Macromolecules* **2012**, *45* (24), 9759–9767. https://doi.org/10.1021/ma302075p.

(31) Wang, Q.; Schlenoff, J. B. The Polyelectrolyte Complex/Coacervate Continuum. *Macromolecules* **2014**, *47*, 3108–3116. https://doi.org/10.1021/ma500500q.
(32) Zhang, H. Effects of Solution Composition (Salts, PH, Dielectric Constant) on Polyelectrolyte Complex (PEC) Formation and Their Properties, The University of Akron, 2018.
(33) Gu, Y.; Huang, X.; Wiener, C. G.; Vogt, B. D.; Zacharia, N. S. Large-Scale Solvent Driven Actuation of Polyelectrolyte Multilayers Based on Modulation of Dynamic Secondary Interactions. *ACS Appl. Mater. Interfaces* **2015**, *7* (3), 1848–1858. https://doi.org/10.1021/am507573m.
(34) Gu, Y.; Ma, Y.; Vogt, B. D.; Zacharia, N. S. Contraction of Weak Polyelectrolyte Multilayers in Response to Organic Solvents. *Soft Matter* **2016**, *12* (6), 1859–1867. https://doi.org/10.1039/c5sm02313k.
(35) Gu, Y.; Zacharia, N. S. Self-Healing Actuating Adhesive Based on Polyelectrolyte Multilayers. *Adv. Funct. Mater.* **2015**, *25* (24), 3785–3792. https://doi.org/10.1002/adfm.201501055.
(36) Yildirim, E.; Zhang, Y.; Lutkenhaus, J. L.; Sammalkorpi, M. Thermal Transitions in Polyelectrolyte Assemblies Occur via a Dehydration Mechanism. *ACS Macro Lett.* **2015**, *4*, 1017–1021. https://doi.org/10.1021/acsmacrolett.5b00351.
(37) Zhang, Y.; Li, F.; Valenzuela, L. D.; Sammalkorpi, M.; Lutkenhaus, J. L. Effect of Water on the Thermal Transition Observed in Poly(Allylamine Hydrochloride)-Poly(Acrylic Acid) Complexes. *Macromolecules* **2016**, *49*, 7563–7570. https://doi.org/10.1021/acs.macromol.6b00742.
(38) Batys, P.; Zhang, Y.; Lutkenhaus, J. L.; Sammalkorpi, M. Hydration and Temperature Response of Water Mobility in Poly(Diallyldimethylammonium)–Poly(Sodium 4-Styrenesulfonate) Complexes. *Macromolecules* **2018**, *51*, 8268–8277. https://doi.org/10.1021/acs.macromol.8b01441.
(39) Meng, X.; Perry, S. L.; Schiffman, J. D. Complex Coacervation : Chemically Stable Fibers Electrospun From. *ACS Macro Lett.* **2017**, *6*, 505–511. https://doi.org/10.1021/acsmacrolett.7b00173.
(40) Sun, J.; Perry, S. L.; Schiffman, J. D. Electrospinning Nanofibers from Chitosan/Hyaluronic Acid Complex Coacervates. *Biomacromolecules* **2019**, *20* (11), 4191–4198. https://doi.org/10.1021/acs.biomac.9b01072.
(41) Ting, J. M.; Wu, H.; Herzog-Arbeitman, A.; Srivastava, S.; Tirrell, M. V. Synthesis and Assembly of Designer Styrenic Diblock Polyelectrolytes. *ACS Macro Lett.* **2018**, *7*, 726–733. https://doi.org/10.1021/acsmacrolett.8b00346.
(42) Perry, S. L.; Li, Y.; Priftis, D.; Leon, L.; Tirrell, M. The Effect of Salt on the Complex Coacervation of Vinyl Polyelectrolytes. *Polymers (Basel).* **2014**, *6*, 1756–1772. https://doi.org/10.3390/polym6061756.
(43) Dautzenberg, H.; Kriz, J. Response of Polyelectrolyte Complexes to Subsequent Addition of Salts with Different Cations. *Langmuir* **2003**, *19* (13), 5204–5211. https://doi.org/10.1021/la0209482.
(44) Properties of substance: sodium bromide http://chemister.ru/Database/properties-en.php?dbid=1&id=714 (accessed Nov 13, 2020).
(45) 1-Butyl-3-methylimidazolium bromide | 85100-77-2 https://www.chemicalbook.com/ChemicalProductProperty_EN_cb4490490.htm (accessed

Nov 13, 2020).
(46) Fukunaga, Y.; Hayashi, M.; Satoh, M. Specific Swelling Behaviors of Alkali-Metal Poly(Styrene Sulfonate) Gels in Aqueous Solvent Mixtures. *J. Polym. Sci. Part B Polym. Phys.* **2007**, *45* (10), 1166–1175. https://doi.org/10.1002/polb.21141.
(47) Volkov, E. V.; Filippova, O. E.; Khokhlov, A. R. Dual Polyelectrolyte-Ionomer Behavior of Poly(Acrylic Acid) in Methanol: 2. Salt Solutions. *Colloid J.* **2004**, *66* (6), 669–672. https://doi.org/10.1007/s10595-005-0046-z.
(48) Mauritz, K. A. Review and Critical Analyses of Theories of Aggregation in Lonomers. *J. Macromol. Sci. Part C* **1988**, *28* (1), 65–98. https://doi.org/10.1080/15583728808085375.
(49) Eisenberg, A.; Hird, B.; Moore, R. B. A New Multiplet-Cluster Model for the Morphology of Random Ionomers. *Macromolecules* **1990**, *23* (18), 4098–4107. https://doi.org/10.1021/ma00220a012.
(50) Philippova, O. E.; Sitnikova, N. L.; Demidovich, G. B.; Khokhlov, A. R. Mixed Polyelectrolyte/Ionomer Behavior of Poly(Methacrylic Acid) Gel upon Titration. *Macromolecules* **1996**, *29* (13), 4642–4645. https://doi.org/10.1021/ma951697p.

Chapter 5. Summary

Polyelectrolyte complexes, formed when two aqueous solutions of oppositely charged polyelectrolytes are mixed together, have received numerous interests because of their occurrence in biological and natural systems, as well as their broad applications in consumer products, underwater adhesives, drug delivery vehicles, etc. Depending on the chemical and physical nature of their polyelectrolyte components, the physical states of PECs can range from glassy solids to low viscosity liquids. In the past decades, most of the efforts have been devoted to probing the properties of liquid coacervates due to their resemblance to membrane-less organelles and their broad applications in plentiful industrial fields. In comparison, far less attention has been given to solid-state PECs because they were shown to be recalcitrant to common processing technique. A recent study found that the this shortcoming in solid PECs can be easily addressed by adding salt, which drives the phase transformation from solid precipitates into liquid coacervates by breaking the intrinsic ion pairs between oppositely charged chains. Even though this finding has spurred many interests in probing the properties and applications of solid PECs, the molecular details of this process still remain poorly understood. In this dissertation, the main goal is to first understand the mechanism behind this salt-driven solid-liquid transition. Next, we introduce solvent quality as an orthogonal parameter to govern the phase transition and modulate PEC phase behaviors along the complex-coacervate continuum.

In Chapter 2, we have comprehensively explored the mechanism behind solid-liquid transitions from the perspectives of dynamics, phase behavior, and internal structures. A model PEC formed by two styrenic polyelectrolytes (PVBTMA and PSS) was investigated during its solid-liquid transition driven by NaBr, The solid-state PEC under low-salt conditions (0-1.5 M NaBr) displayed a counterintuitive salt-stiffening trend that can be ascribed to dehydration and

evolution in polyelectrolyte chain conformation. Upon salt addition, osmotic deswelling expelled water from complex into the supernatant phase. From the structural aspect, salt-free PECs formed tightly coiled near-spherical aggregates that disentangled as salt concentration increased, which caused these clusters to expand and increased the frictions and collisions between chains. Together, the dehydration and change in polymer chain conformation with increasing salt translated into a higher modulus in rheological measurements. In the liquid regime at high salt (2-6.5 M NaBr), polymer chains rearranged into paired ladder-like structures. As more salt was added, the water content within the complex phase continued to drop and chains further relaxed. Eventually, at 7 M NaBr, all the intrinsic ion pairs were broken and liquid coacervates completely dissolved into a homogenous solution.

Chapter 3 reported a novel method of weakening the resistance of PVBTMA/PSS towards NaBr during the solid-liquid transition through tuning the hydrophobicity of the solvent. Microscopy was employed to qualitatively determine the physical states of PECs under different salt and solvent conditions. When we switched the solvent from water into co-solvents of ethylene glycol/water or ethanol/water and progressively increased the solvent hydrophobicity by increasing the component of organic solvent in the binary mixture, both solid-to-liquid and liquid-to-solution transitions occurred at lower NaBr concentrations. This observation implies how co-solvents can be developed into a powerful tool to govern the physical states and properties of strongly interacting PECs during salt doping.

In Chapter 4, the investigation in the joint effects of salt and solvent quality on PVBTMA/PSS was further expanded. Through preparing this PEC in four binary solvent mixtures of water with ethanol/methanol/1,3 propanediol/ethylene glycol, and then carefully comparing the

physical behaviors of this PEC with added NaBr, we found a general correlation between the salt resistance of this PEC to NaBr and solubility of NaBr in different solvents. When we explored the high salt high organic solvent domain beyond the homogenous solution state, an unexpected reverse phase transition occurred: liquid droplets reemerged from solution state and even transformed into solid aggregates as NaBr concentration continued to increase. Detailed examination in the composition of the materials emerged from this reverse phase transition revealed that this surprising behavior was caused by the collapse of PSS single chain, rather than the complexation of two oppositely charged polyelectrolytes. We hope that the findings in this study can spur more future efforts in inspecting the role that other orthogonal parameters play during the solid-liquid transition of strongly interacting PEC systems.